Dissertation

VTT PUBLICATIONS 728

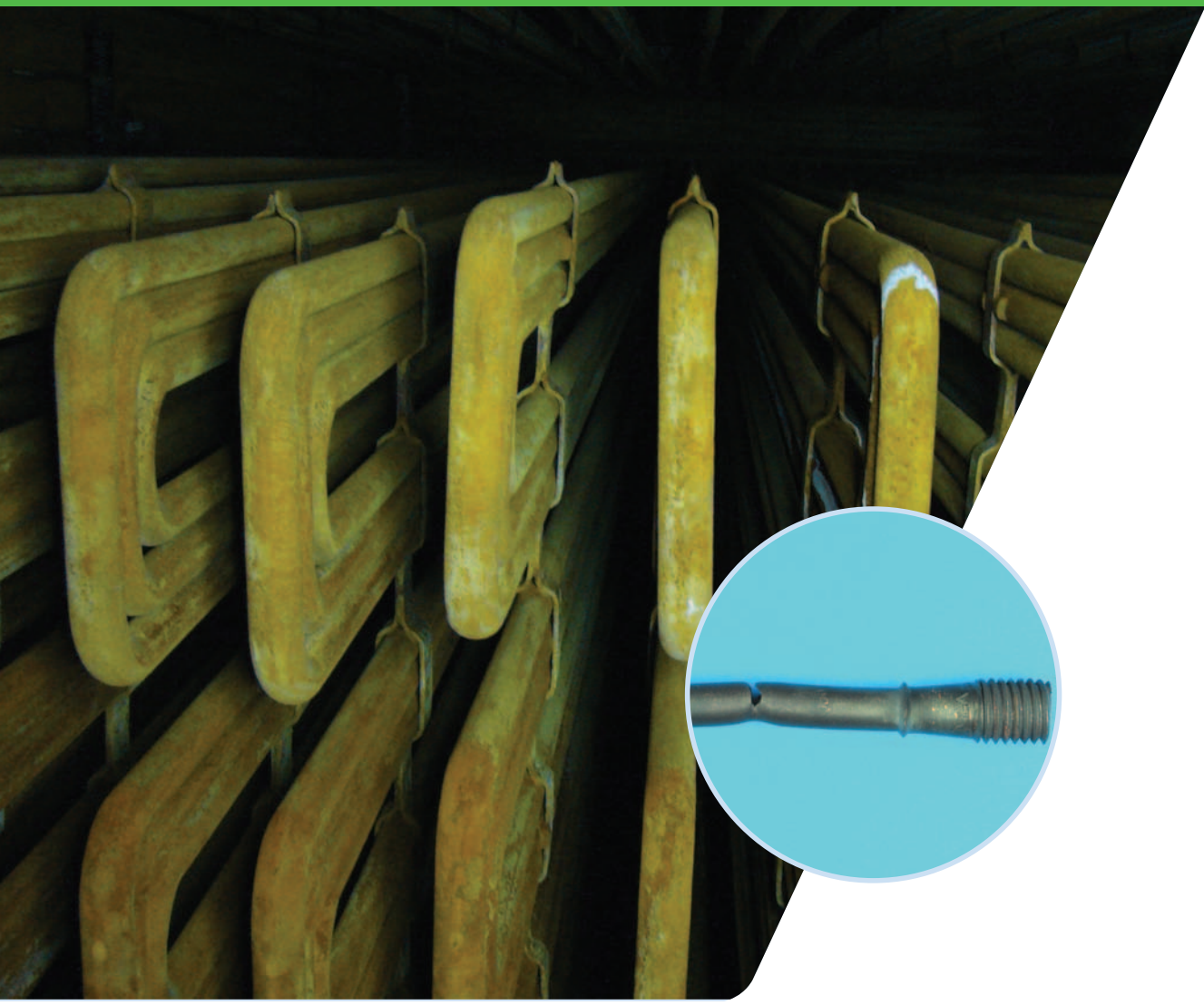

Stefan Holmström

Engineering Tools for Robust Creep Modeling

VTT PUBLICATIONS 728

Engineering Tools for Robust Creep Modeling

Stefan Holmström

Dissertation for the degree of Doctor of Science in Technology to be presented with due permission of the Faculty of Engineering and Architecture, The Aalto University School of Science and Technology, for public examination and debate in K216 at Aalto University (Otakaari 4, Espoo, Finland) on the 5th of February, 2010, at 12 noon.

ISBN 978-951-38-7378-3 (soft back ed.)
ISSN 1235-0621 (soft back ed.)

ISBN 978-951-38-7379-0 (URL: http://www.vtt.fi/publications/index.jsp)
ISSN 1455-0849 (URL: http://www.vtt.fi/publications/index.jsp)

JULKAISIJA – UTGIVARE – PUBLISHER

VTT, Vuorimiehentie 5, PL 1000, 02044 VTT
puh. vaihde 020 722 111, faksi 020 722 4374

VTT, Bergsmansvägen 5, PB 1000, 02044 VTT
tel. växel 020 722 111, fax 020 722 4374

VTT Technical Research Centre of Finland, Vuorimiehentie 5, P.O. Box 1000, FI-02044 VTT, Finland
phone internat. +358 20 722 111, fax + 358 20 722 4374

Technical editing Mirjami Pullinen

Edita Prima Oy, Helsinki 2010

Stefan Holmström. Engineering Tools for Robust Creep Modeling [Virumismallinnuksen uudet menetelmät]. Espoo 2010. VTT Publications 728. 94 p. + 53 p.

Keywords creep, strain, damage, modeling, steel, OFP copper

Abstract

High temperature creep is often dealt with simplified models to assess and predict the future behavior of materials and components. Also, for most applications the creep properties of interest require costly long-term testing that limits the available data to support design and life assessment. Such test data sets are even smaller for welded joints that are often the weakest links of structures. It is of considerable interest to be able to reliably predict and extrapolate long term creep behavior from relatively small sets of supporting creep data.

For creep strain, the current tools for model verification and quality assurance are very limited. The ECCC PATs can be adapted to some degree but the uncertainty and applicability of many models are still questionable outside the range of data. In this thesis tools for improving the model robustness have been developed. The toolkit includes creep rupture, weld strength and creep strain modeling improvements for uniaxial prediction. The applicability is shown on data set consisting of a selection of common high temperature steels and the oxygen-free phosphorous doped (OFP) copper. The steels assessed are 10CrMo9-10 (P22), 7CrWVMoNb9-6 (P23), 7CrMoVTiB10-10 (P24), 14MoV6-3 (0.5CMV), X20CrMoV11-1 (X20), X10CrMoVNb9-1 (P91) and X11CrMoWVNb9-1-1 (E911).

The work described in this thesis has provided simple yet well performing tools to predict creep strain and life for material evaluation, component design and life assessment purposes. The uncertainty related to selecting the type of material model or determining weld strength factors has been reduced by the selection procedures and by linking the weld behavior to the base material master equation. Much of the resulting improvements and benefits are related to the reduced requirements for supporting creep data. The simplicity and robustness of the new tools also makes them easy to implement for both analytical and numerical solutions.

Stefan Holmström. Engineering Tools for Robust Creep Modeling [Virumismallinnuksen uudet menetelmät]. Espoo 2010. VTT Publications 728. 94 s. + liitt. 53 s.

Keywords creep, strain, damage, modeling, steel, OFP copper

Tiivistelmä

Rakenteiden suunnitteluun ja elinikäennusteisiin käytetyt kuumalujien terästen lujuusarvot ja hitsien lujuuskertoimet pohjautuvat virumiskoetuloksiin, joita on varsinkin pitkäaikaisina käytettävissä usein vain niukasti. Sen vuoksi on erityisen tärkeää, että koetuloksiin sovitetut materiaalimallit ovat taloudellisia, tarkkoja ja luotettavia erityisesti ekstrapoloitaessa pidemmille käyttöajoille.

Tässä väitöstyössä on kehitetty uusia malleja työkaluiksi virumismurtolujuuden, hitsien lujuuskertoimien ja virumisvenymän luotettavaan määrittämiseen sekä virumiseliniän ennustamiseen erityisesti tapauksissa, joissa mallinnuksen tueksi on käytettävissä niukasti virumiskoetuloksia. Uusien mallien suorituskykyä on testattu eurooppalaisessa vertailututkimuksessa, jossa ne ennustivat yksin-kertaisesta muodostaan huolimatta venymiä tarkemmin kuin aiemmat ja huomattavasti monimutkaisemmat virumismallit. Uusia malleja on työssä sovellettu OFP-kuparille ja ferriittisille teräksille 10CrMo9-10 (P22), 7CrWVMoNb9-6 (P23), 7CrMoVTiB10-10 (P24), 14MoV6-3 (0.5CMV), X20CrMoV11-1 (X20), X10CrMoVNb9-1 (P91) ja X11CrMoWVNb9-1-1 (E911). Materiaalimalleja on myös sovitettu numeerisen suunnittelun työkaluihin (COMSOL ja ABAQUS) ja verifioitu pitkään käytössä olleen hitsatun putkiyhteen elinikätarkastelulla.

Väitöstyön tuloksena kehitettyjä malleja ja menetelmiä voivat soveltaa korkean lämpötilan rakenteiden suunnittelijat ja eliniän hallinnan asiantuntijat helpottamaan ja tarkentamaan virumiskäyttäytymisen ennustamista. Työn keskeinen anti on kehitettyjen menetelmien tarjoama vähentynyt materiaalidatan tarve ja mallien yksinkertainen rakenne, joka helpottaa niiden hyödyntämistä sekä analyyttisissä että numeerisissa ratkaisuissa.

Preface

This work has been carried out at VTT, financially supported by the Academy of Finland grant 117700 with prof. Kim Wallin acting as instructor. It has been supervised by prof. Hannu Hänninen, head of laboratory of Engineering Materials at Helsinki University of Technology (HUT). Prof. Hänninen is greatly acknowledged for his valuable input in the finalization stage of the thesis and for arranging a place at HUT to escape the hectic work surroundings of VTT.

A substantial part of the research gone into the development of the creep models and modeling tools has been done over several years within many VTT projects, both national and international. Projects like Extreme (internal VTT), Aloas (RFCS), LC-Power & Life-Power (Tekes financed), The Värmeforsk project on Creep damage development in welded X20 and P91 components and the LEIA / PIKE projects, to name a few, have contributed to this thesis.

The European Creep Collaborative Committee (ECCC) has been a valuable supply of interesting challenges, creep expertise, relevant feed-back, active support, friendship and an invaluable source of creep data that would not have been accessible without the ECCC WG1 network lead by Dr. Stuart Holdsworth. The Japanese creep data produced and freely distributed by NIMS has also been a valuable source of high quality data. The work done on the OFP copper for nuclear waste canisters has been part of the national projects LEIA / PIKE, funded by the public Nuclear Waste Management Program in Finland (KYT).

Special thanks go of course to the co-authors of the publications incorporated in this thesis. Also my team, “Materials performance for combustion systems”, has given me great support and has shown incredible patience and has not complained over sloppily done administrative tasks during the final stages of this work.

Finally, I would like to thank my wife and children for their valuable support and understanding when my eyes have glazed over at home, in the car or at some social event, brooding over some nutty creep modeling detail.

Contents

Appendices II, III, V and VI of this publication are not included in the PDF version.
Please order the printed version to get the complete publication (http://www.vtt.fi/publications/index.jsp).

Research hypothesis and original features

The hypothesis of this thesis is that there are possibilities (simple tools) for by-passing many of the difficulties in establishing creep properties for materials, especially those caused by insufficient amount of (available) data. The problem with scarce or insufficient data is encountered even for well established steels. The public domain availability of relevant models or creep strain data excluding the simplest Norton law approaches or Monkman-Grant relationships are difficult to come by. The "engineering tools" developed in this thesis (presented in Table 1) are all original contributions to the benefit of simplifying and enhancing the creep property determination (rupture, strain, multi-axial response).

Table 1. List of engineering tools developed in the scope of this thesis and their main usage.

TOOL	*USAGE*
RPC Rigidity Parameter Correction	Method for testing creep-rupture model flexibility. Determines the susceptibility of conservatism in extrapolation. Can also be used for determination of conservative weld strength factors [1], [2].
MHG Manson-Haferd-Grounes creep strain model	Simple parametric creep strain model, based on strain data only [3].
LCSP Logistic Creep Strain Prediction strain model	Robust creep strain model, based on rupture model and a curve shape function. Gaining accuracy with increasing availability of strain data [4], [5].
Λ-filter Multi-axial damage parameter	Method of visualizing creep exhaustion (consumed multi-axial creep strain factor) in FEA modeling implemented with multi-axial form of LCSP model [6], [7].

The developed tools can be utilized for the prediction of weldment creep life, creep strain and even multi-axial creep damage. The models are in themselves robust, meaning that similar reliability can be expected from the predictions as would be expected from creep rupture models. The best feature is, however, that this is accomplished utilizing a minimum amount of data. Some of the strain models presented have been verified with creep data withheld from the initial model optimization. The LCSP together with the Λ-filtering method for visualizing creep damage in FEA simulations has shown great potential in predicting creep damage evolution. The Λ-filtering tool can be used as a stand-alone feature with any FEA creep model. The special tool developed for rationalizing the weld strength factor calculation (RPC) is also (as the LCSP) based on the base material strength giving a better mathematical capability for extrapolation purposes.

The "engineering" approach and the deliberate aim of keeping the modeling tools simple will hopefully make them more attractive to the design engineer and the life management expert. The simplicity, accuracy and robustness in prediction are in itself the driving force and ultimate aim of this work.

List of publications and author's contribution

The scientific papers of this thesis are:

I Holmström, S. & Auerkari, P. Effect of short-term data on predicted creep rupture life – pivoting effect and optimized censoring. Materials at High Temperatures, Vol. 25 (2008) 3, September, pp. 103–109, Northampton, UK: Science Reviews 2000 Ltd.

II Holmström, S. & Auerkari, P. Predicting weld creep strength reduction for 9% Cr steels. International Journal of Pressure Vessels Piping, Vol. 83 (2006) 11–12, pp. 803–808.

III Holdsworth, S. R., Askins, M., Baker, A., Gariboldi, E., Holmström, S., Klenk, A., Ringel, M., Merckling, G., Sandstrom, R., Schwienheer, M. & Spigarelli, S. Factors influencing creep model equation selection. International Journal of Pressure Vessels and Piping, Vol. 85 (2008) 1–2, pp. 80–88.

IV Holmström, S. & Auerkari, P. Robust prediction of full creep curves from minimal data and time to rupture model. Energy Materials, Materials Science & Engineering for Energy Systems, Vol. 1 (2006) 4, pp. 249–255, Maney Publishing.

V Holmström, S. & Auerkari, P. Predicting creep rupture from early strain data. Materials Science and Engineering: A, Vol. 510–511 (2009), pp. 25–28.

VI Holmström, S., Laukkanen A. & Calonius, K. Finding critical damage locations by Λ-filtering in FE modeling of a girth weld. Materials Science and Engineering: A, Vol. 510–511 (2009), pp. 224–228.

VII Holmström, S., Laukkanen, A., Rantala, J., Kolari, K., Keinänen, H. & Lehtinen, O. Modeling and verification of creep strain and exhaustion in a welded steam mixer. Journal of Pressure Vessel Technology, Vol. 131 (2009), 061405 (5 pages).

Pertti Auerkari the co-author in most of the papers (I, II, IV & V) is an extremely experienced senior research scientist with over 30 years of experience in creep research. His contribution is an important one in all the papers he co-authors, namely his never-ending enthusiasm, guidance to the core questions of the creep problem at hand and especially in the noble art of formulating sound conclusions.

Paper III, with a number of authors, written by Dr. Stuart Holdsworth, is based on the round robin results of the creep strain modeling efforts of the ECCC. In this paper the work done on the Manson-Haferd-Grounes (MHG) strain model and its performance is contributed by the present author, and the rest is the excellent work of my colleagues from the ECCC network.

Paper IV is the central paper of the thesis, combining the rupture model of P22 (10CrMo9-10) steel with a creep curve shape function into a creep strain model. The results of this paper are utilized and implemented in all the rest of the thesis papers (V–VII).

In Paper V the LCSP is successfully applied to predict long-term creep behavior (strain and rupture) for oxygen-free phosphorus doped copper (OFP).

In Paper VI the LCSP is implemented in COMSOL finite element code and used for predicting creep damage (with the Λ-filter) in a simple girth weld case. My co-author Anssi Laukkanen contributed with the LCSP coding, the meshing of the weld, running the simulations and by sharing his FEA expertise. Kim Calonius made comparison runs for the same structure using the Norton law strain model in ABAQUS.

In Paper VII a more complicated welded component is assessed with LCSP and the Λ-filter. For this paper my co-author Kari Kolari made the ABAQUS implementation with input from both Anssi Laukkanen and me. The mesh and simulation runs were made by Kari Kolari and Heikki Keinänen. Juhani Rantala coordinated the work and Olli Lehtinen was the utility contact person contributing with all the needed background information.

List of abbreviations and symbols

MCM	Minimum commitment method (nonlinear with instability parameter A)
MC	Minimum commitment method (multi-linear without instability parameter)
PLM	Larson-Miller model
MH	Manson-Haferd model
A	Instability parameter of the nonlinear Minimum commitment method
A	Norton law constant (considered temperature dependent)
K	Intercept of the Monkman-Grant relationship
r	Slope of the Monkman-Grant relationship
OFP	Phosphorus doped oxygen-free copper
WSF	Weld strength factor
SRF	Stress reduction factor
TRF	Time reduction factor
t_r	Time to rupture
t_{rd}	Time to rupture (data)
t_{rm}	Time to rupture (model)
t_ε	Time to strain
ε	Strain
ε_c	Creep strain
$\dot{\varepsilon}$	Strain rate (1/h)

$\dot{\varepsilon}_m$	Minimum (or "steady state") creep rate (1/h)
ε_0	Initial strain (strain after loading of a creep test)
ε_f	Creep failure strain
ε_{fu}	Uniaxial creep failure strain
ε_{fm}	Multi-axial creep failure strain
$\dot{\varepsilon}_s$	Strain rate in strain control (SSRT testing)
$\dot{\varepsilon}_t$	Strain rate in stress control (SSRT testing)
A	Dimensionless factor (Norton law)
B	Rate coefficient
D	Diffusion coefficient
E	Elastic modulus
b	Burgers vector
d	Grain size
p	Exponent for grain size dependence (Norton law)
p	LCSP parameter
σ	Stress (in MPa)
σ_{UTS}	Ultimate tensile stress
Q_c	Activation energy for creep
Q_c*	Activation energy for creep (Wilshire)
n	Norton stress exponent
T(K)	Temperature (in Kelvin)
k	Constant in Wilshire equation
u	Constant in Wilshire equation
t_r	Time to rupture
R	Gas constant
$d\sigma / dt$	Rate of stress relaxation
α	Parameter for SSRT testing (approx. 0.75)
η	Reference parameter in indentation creep testing
P	Mean pressure under indenter (indentation creep)

Δ	Displacement (indentation creep test)
d	Indenter width (indentation creep test)
β	Reference parameter (indentation creep test)
F_{SP}	Test load (small punch testing)
K_{SP}	Material constant (small punch testing)
h	Thickness of specimen (small punch testing)
r_{SP}	Radius of the punch indenter (small punch testing)
R_{SP}	Radius of the receiving hole (small punch testing)
C	Larson-Miller and LCSP constant
Z	Data scatter parameter
RMS	Root mean square
SSE	Standard error of estimate
PAT	Post assessment test
$f(\sigma)$	Stress function ($\log(\sigma)$ or σ^x)
$P(\sigma)$	Manson-Brown stress function
$R_{u/t/T}$	Rupture strength, time *t* and temperature *T*
$R_{u(W)/t/T}$	Rupture strength for weld, time *t* and temperature *T*
LF	Life fraction
HAZ	Heat affected zone
t_{rR}	RCP corrected rupture time
t_{rm}	Model rupture time
t_p	Pivot point for RPC model
R	Rigidity parameter
x_o and p	Fitting parameters in LCSP
Λ	Lambda filter designation
h	Hydrostatic stress

1. Introduction

Creep is often dealt with using properties and models based on small data set or by using old classical approaches. The shortcomings related to the determination of creep strength or creep strain are mainly due to the nature of creep. Since it is a time-dependent damage mechanism it naturally requires long-term testing to give reliable strength values. For instance the reliable extrapolation range is considered to be a factor of three times the longest test duration in the data set representing the material. This leads to a requirement for testing beyond 30 000 h to cover a design life of 100 000 h. Most conventional power plants are designed for 200 000 h of service. Creep is also an expensive property to determine. Alternative shorter term tests have of course been proposed, but the classical long-term constant load creep test is still considered by most materials experts to be the only test incorporating time-dependent material degradation needed for reliable long term life management. The creep properties (mainly rupture strength) used in design of high temperature components are based on standardized strength values given in standards such as the EN10216-2 [8]. These standardized values are mean material values and material scatter of ±20% in stress can be expected. It is to be remembered that the final strength values (published in standards) are average values from several assessments performed by experts using different modeling tools, not always in agreement with each other. In the end, the values are agreed on by the expert group preparing the standard. As a consequence the strength values are seldom directly retrievable from any specific creep model. Also, it has happened quite frequently that the standard strength values, especially for new steel grades, have had to be corrected downward after obtaining more long-term test data or severe damage has been found in service, as was the case for P122 steel in Japan.

For a new steel to become standardized is a long process. The first-time qualifications may include a minimum of 2 to 3 isotherms with 3–5 rupture points not

less than 10–30 kh. The PED directive (EU 1997) allows the use of any internationally recognized standard for dimensioning and safety factors of components operating in the creep regime. If a material intended for a component design cannot be selected from a standard it has to pass acceptance or material appraisal. The final strength values (in standards) are, as previously stated, the result of many assessments reaching consensus.

When looking for material creep properties the designer or life management researcher is usually confronted with the dilemma of lacking data. For some materials the only easily accessible data available might be the standard (mean) creep strength values such as rupture stress for 10 000, 100 000 or 200 000 hours at specified temperatures,. These are in themselves usually already extrapolated values (in time) by a factor of close to three. Sometimes, in rare cases, both rupture and creep strain data can be found but then again it seems that the data from different sources inevitably leads to a situation showing wide scatter in the data between different material batches and testing laboratories. The problem of creep design and creep life prediction and management seems to always return to the critical question of available data and what can be derived from it. In conclusion it is nearly always a challenging task to produce robust predictions (or models) for creep strain or creep rupture for arbitrary high temperature conditions.

The ECCC has with its work on harmonization of creep rupture assessments developed an evaluation method (Post assessment testing or PATs) that enables the assessor to understand and to weigh the quality of the result of the model fit. It also allows the assessor to produce reliable and credible creep strength predictions, suitable for inclusion into European standards. Some of these tests are also suited for testing the creep strain model fits. The tools of this thesis are extensions and model improvements meant to be used in addition to the ECCC PATs for optimal benefit in material creep modeling.

In literature there is a multitude of creep strain and creep rupture models for creep life and creep strain prediction [9]. However, in most cases the data used for the models is not published and the resulting models require many, in some cases as much as 26 fitting parameters to describe the creep response [10], [11]. In these cases it is almost impossible to validate the models and the resulting possible error in extrapolation. Though it is common sense to avoid using models where the range of data or the accuracy of the models is unknown, it might be the only one available.

By finding simple robust modeling alternatives that require a minimum amount of data (and that can easily be verified) will make structural integrity

calculations more accurate, especially for new materials at an early stage of their development. The same applies for less known or materials where the material data has been kept unpublished due to business reasons. For instance, state-of-the-art gas turbine blading material data seems to be especially difficult to access. Simplicity and robustness of the creep strength and strain models will contribute to safe design and life management of new and existing high temperature components.

In this thesis tools for creep data set structure optimization, creep modeling and implementation techniques for creep life assessment have been developed. The creep response (rupture and/or strain) of high temperature steels such as P22 [12], [13], [14], P23 [15], 0.5CMV [16], X20 [17], P91 [18] and E911 [1], [2] have been studied.

The selected materials represents well the historic development of the heat resistant steels from the 530–550°C temperature range materials (low alloy steels P22 and 0.5CMV) to those suitable for the intermediate range 550–580°C (9–11Cr steels P91 and X20). Also, a material intended for the higher steam values in the temperature range 580–620°C has been assessed (E911, the European not so successful version of the grade 92 steel).

Model development has also been successfully done for oxygen-free phosphorus doped copper (OFP) [19] to be used in nuclear waste disposal canisters. This material is obviously not a fossil fuel high temperature material but shows the applicability of the thesis engineering tools on a highly complicated modeling case with an extreme extrapolation need for the range of service life.

The binding link between the articles in this thesis is the clear path from simple uniaxial rupture modeling towards more complex structures such as welds and creep strain modeling, culminating in the creep life assessment of a creep damaged weld region of a power plant mixing tank (thesis Paper VII and [20]). The main steps and the papers included in this thesis are presented in the order of increasing modeling complexity, towards the goal of large complex component creep life multi-axial FEA modeling.

2. General aspects on creep data, modeling and design

Creep is commonly encountered for metals (and alloys) at temperatures roughly above half of the melting point. In general, creep refers to time-dependent deformation (strain) accumulated under load. From a macroscopic (and engineering) point of view creep is often treated as time-dependent plastic deformation and both elastic and viscous strain components are usually neglected. Ashby [21] proposed that there are six independent deformation mechanisms: defect-free flow, dislocation glide, dislocation creep, volume diffusion flow and twinning. The contribution to deformation is very limited for twinning and it is usually not represented in deformation mechanism maps. The deformation maps describe the steady state flow (strain rates) at specified temperature and stress (see Fig. 1). This means that they are representing the mean (model) interpolated or extrapolated minimum strain rates based on measured creep strain data.

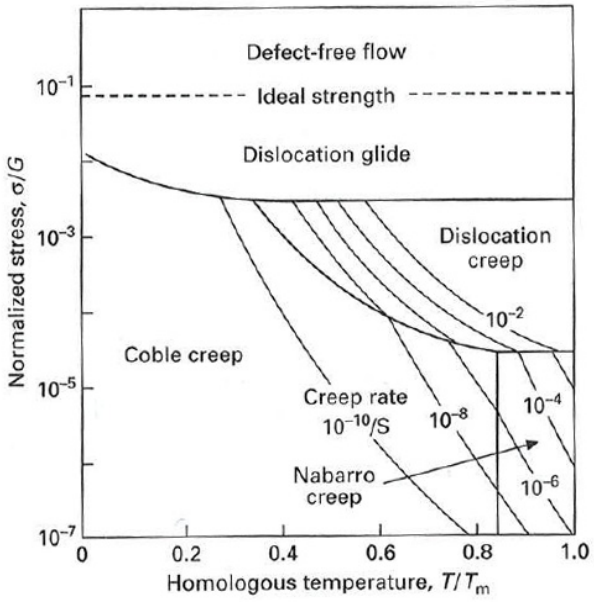

Fig. 1. Schematic deformation mechanism map (no actual material) with minimum creep rates [9].

The strain data acquired from the most common creep tests, the constant load (or stress) tests, is classically divided into three characteristic stages (see Figs 2–3).

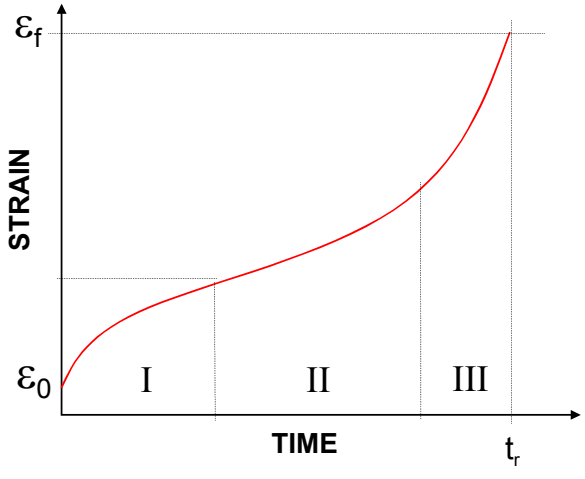

Fig. 2. Classical creep curve with primary (I) creep stage starting at loading with instantaneous strain (ε_0), secondary (II) stage with the minimum creep rate and tertiary (III) stage ending in rupture (at time t_r with a fracture strain ε_f).

In the first stage, primary or transient creep, the curve has a concave shape starting with an initial strain addition (ε_0) right after loading. This stage can be considered as a hardening stage. In the next stage, secondary creep, the strain is evolving roughly linearly as a function of time. In the third stage, tertiary creep, the curve takes a convex form that ends with rupture (damage accumulation and necking). The duration and extent of strain accumulated in the different stages naturally depends on temperature and stress.

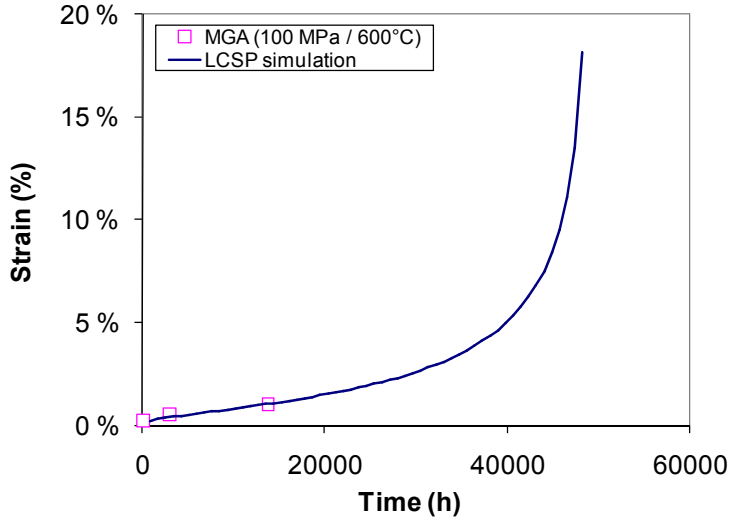

Fig. 3. Simulated creep curve and recorded time to strain data for P91 steel at 100 MPa, 600ºC.

Taking the derivative of the creep curve with respect to time, one usually ends up with a "bath tub" shaped curve, where the minimum of the curve is the minimum creep rate (see Fig. 4), or the "steady state" strain rate of the deformation maps. There is a close relationship between minimum creep rate and the time to rupture, the Monkman-Grant relationship.

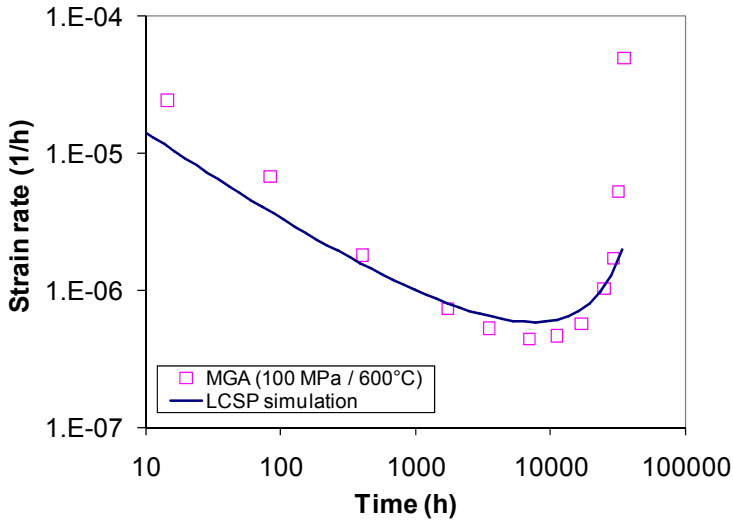

Fig. 4. Simulated creep strain rate curve in comparison with measured strain rates for P91 steel at 100 MPa, 600ºC.

The Monkman-Grant relationship is defined as

$$t_r = K \cdot \dot{\varepsilon}_m^{-r} \text{ or } \ln(t_r) = \ln(K) - r\ln(\dot{\varepsilon}_m) \qquad \textit{Eq. 1}$$

where t_r is the time to rupture and K and r are material constants. Note that the constants may well be sensitive to both temperature and stress.

At stress levels above approximately 1/20 of the shear modulus (G), dislocation glide is the dominant mechanism. When the stress is lower, the deformation is either dislocation creep (at higher temperatures) or diffusion flow driven creep (at lower temperatures).

The dislocation creep range, also called the “power law” creep range, is a combination of diffusion mechanisms and dislocation glide. The stress state will cause dislocation glide until the dislocation hits an obstacle with too high activation energy for it to pass, the dislocation then remains immobile while diffusion occurs, allowing the dislocation to pass by climb. The interfacing region towards the dislocation glide range is by some referred to as the “power law break down” region. At the high stress state end (of the power law range) the fracture caused by creep is in most cases transgranular with high ductility (large fracture strain). The lower the strain rates become (at the lower stress end) the more likely the fracture becomes intergranular and the creep ductility diminishes (low fracture strain).

For a creep model to produce accurate results in extrapolation the macroscopic (modeled) strain response should be based on physical simplified functions able to cover the complex interplay of microstructural and sub-microstructural changes interpreted by the micro-mechanisms controlling the creep rate and thereby the measured strain accumulation. However, even though the materials science has been able to produce sufficiently accurate models linking the high temperature microstructural and macroscopical materials response for pure metals, the more complex high temperature materials still seem to be beyond reach.

The modeling tools developed and all the data assessed within the scope of this thesis are targeted at solving the challenges of the dislocation creep range. Also, most high temperature engineering structures such as steam lines, boilers, turbines operate in this. However, some extrapolations, such as the low stress service conditions of the high temperature steam mixer assessed is approaching diffusion flow dominated conditions and the data assessed at high stress for the nuclear spent fuel copper canister is again crossing over into the power law break down range.

The diffusion flow range, usually divided into Nabarro-Herring creep at higher temperatures and Coble creep at lower temperatures has not been studied in closer detail in this thesis. The Nabarro-Herring creep deformation progresses through the diffusion of atoms and vacancies. Coble creep again progresses through mass and vacancy diffusion along grain boundaries where diffusion can occur at lower energy levels. This is also a reason why Coble creep is more pronounced for fine grain size materials than in coarse grain ones. Both Coble creep and Nabarro-Herring creep produce voids (creep cavitation) or cracks at grain boundaries. For all the mechanisms, the creep rate is controlled by activation energy.

A number of models taking dislocation theory as a basis have been proposed, but they are in most cases better suited for pure metals and not for complex high temperature steels that are highly dynamic and not in thermodynamic equilibrium. For pure (OFHC) copper a model has recently been introduced, stating no fitting parameters. Though, already when very small amounts of phosphorus are added to the material (<60 ppm), the model shows inconsistencies, that seem difficult to overcome with the attempted scaling factors only [22].

Traditionally the minimum strain rate in the dislocation creep range is described by the extended Norton law expression of Eq. 2. The stress exponent n for minimum creep rate $\dot{\varepsilon}_m$ will normally range within 3–5 for high temperature power law creep and within 5–7 for low temperature power law creep in the classical expression for polycrystalline metals:

$$\dot{\varepsilon}_m = A \cdot (DEb/kT) \cdot (b/d)^p \cdot (\sigma/E)^n \exp(-Q_c/kT), \qquad \textit{Eq. 2}$$

where A is a dimensionless factor, D the diffusion coefficient, E the elastic modulus, b the Burgers vector, d the grain size, p the exponent for grain size dependence, σ is the applied stress, k the Boltzmann's constant and Q_c the activation energy for creep.

For Coble (grain boundary diffusion) and Nabarro-Herring (volume diffusion) creep the corresponding stress exponent n is 1. However the grain size exponent p changes from 3 to 2 when moving towards volume diffusion.

The mechanism related diffusion coefficients for high temperature power law creep and Nabarro-Herring creep are lattice diffusion and for the lower temperature power law creep and Coble creep it is pipe diffusion and grain boundary diffusion, respectively.

The main difficulty in utilizing the above equation in modeling complex high temperature steels, and especially in extrapolation, is that the stress exponent n and the activation energy Q_c tend to change at stress levels and temperatures relevant for service conditions. The stress and temperature dependence of n and Q_c is shown in Fig. 5 for the grade 91 steel (P91) assessed in this thesis.

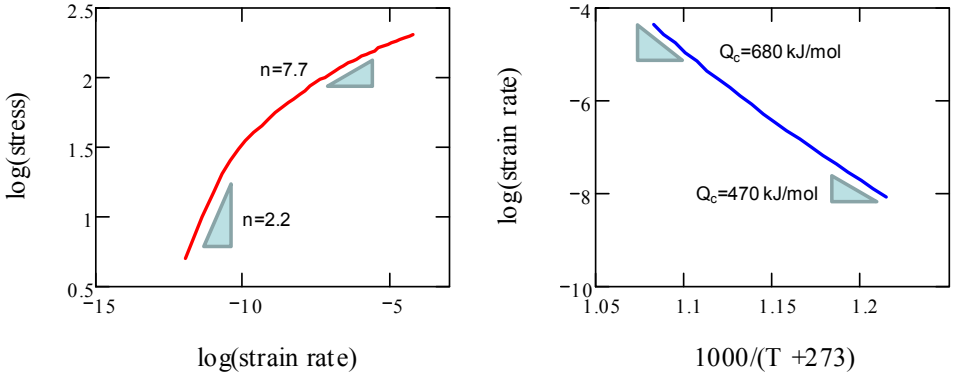

Fig. 5. Presentation of the changing nature of the stress exponent n (at 575°C) and the apparent activation energy Q_c (at 100 MPa) for P91 steel (LCSP simulated).

Modifications of the classical power law stress dependency have been proposed in the threshold stress concept and the internal stress concept. These methods rationalize the "oversized" stress exponents common for the complex high temperature steels. The determination of the additional stress variable though requires iterative exponent data fitting or sudden short term force reductions dur-

ing creep testing. The increased uncertainty in parameter determination and the increased complexity of the creep testing has not encouraged the usage of these methodologies in greater extent.

The recent introduction of the Wilshire equations [23] has provided a simple effective competitive methodology for strain rate, time to strain and time to rupture assessments. The method though needs additional tensile test data to accompany the constant load tests. The method is normalizing the creep test stress with yield or ultimate tensile strength at the temperature in question and plotting against either $\dot{\varepsilon}_m \cdot \exp(-Q^*_c/RT)$ for minimum strain rate data or $t_r \cdot \exp(-Q^*_c/RT)$ for rupture data. The model avoids the varying stress exponent n and the activation energy is definable in a straight forward, simple way. Note, however, that that $Q^*_c \neq Q_c$ of Eq. 2.

The Wilshire equation for time to rupture t_r (note in seconds) at stress σ (MPa) and temperature T (K) is expressed as:

$$\ln(\sigma / \sigma_{TS}) = -k[t_r \exp(-Q_c^* / RT)]^u, \qquad \textit{Eq. 3}$$

where k and u are constants obtained by fitting to the test data, Q_c^* is the apparent activation energy and σ_{UTS} is the tensile strength at the specified temperature. The equation for strain rate is identical to Eq. 3 with t_r replaced by $\dot{\varepsilon}_m$.

Application of this model obviously requires data from both creep rupture testing and tensile testing. An example of a Wilshire model assessment for time to rupture is presented for P91 steel with data from NIMS [24] in Figs. 6–8.

The Wilshire equation has been thoroughly tested for several materials including bainitic rotor forgings of 1Cr-1Mo-0.25V steel [25], martensitic steels P91, P92 and P122, Waspalloy, aluminum alloys and for OFP copper (thesis Paper V).

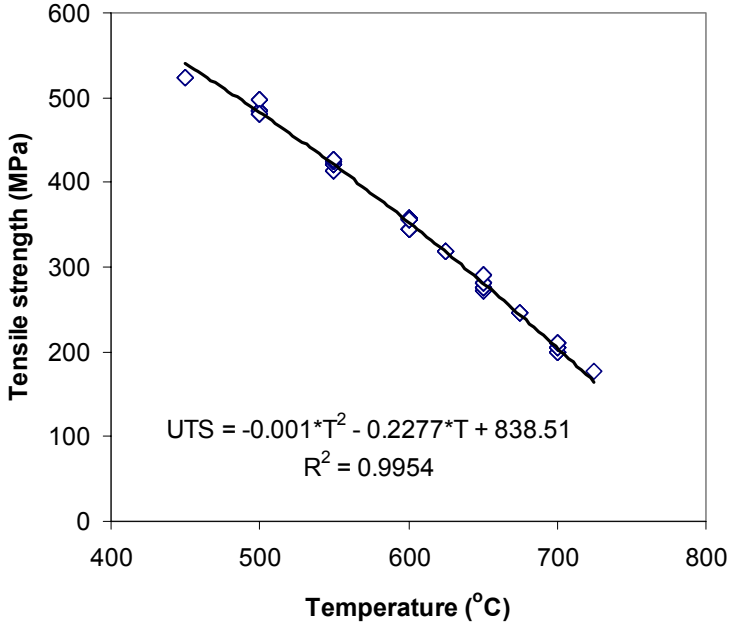

Fig. 6. Temperature dependence of the tensile strength for the 4 NIMS P91 steel heats.

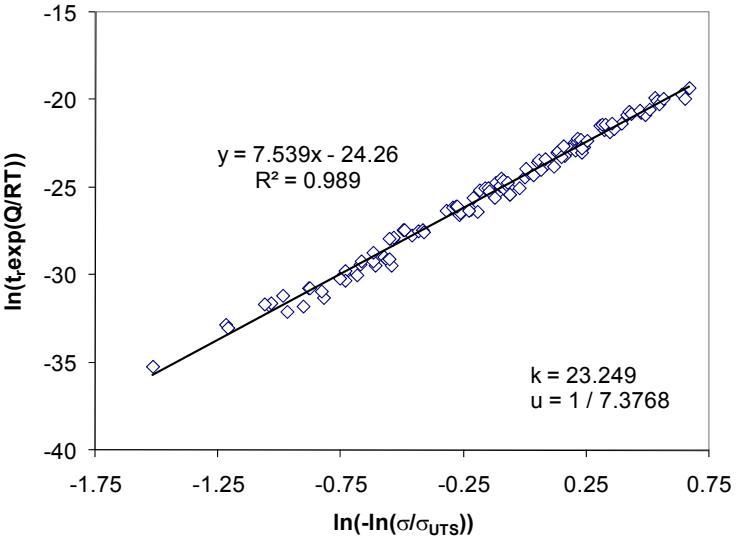

Fig. 7. Determination of the constants k and u for P91 steel. Note that this data set produces a linear relationship over the whole stress range.

The main benefit found for the model is that “heat to heat” data scatter is reduced by the normalization. The heat to heat data scatter is related to differences in the creep properties due to alloying, heat treatments, product forms and manufacturing routes for the tested material heats. Also, the mathematical form is inherently more stable at lower stress levels than for traditional time to rupture models with polynomial stress dependence. The equation also gives rupture times that tend to zero when approaching the ultimate tensile strength and values that tend to infinity when the stress approaches zero. The data scatter reduction in the above presented P91 assessment is shown in Figs. 9–10.

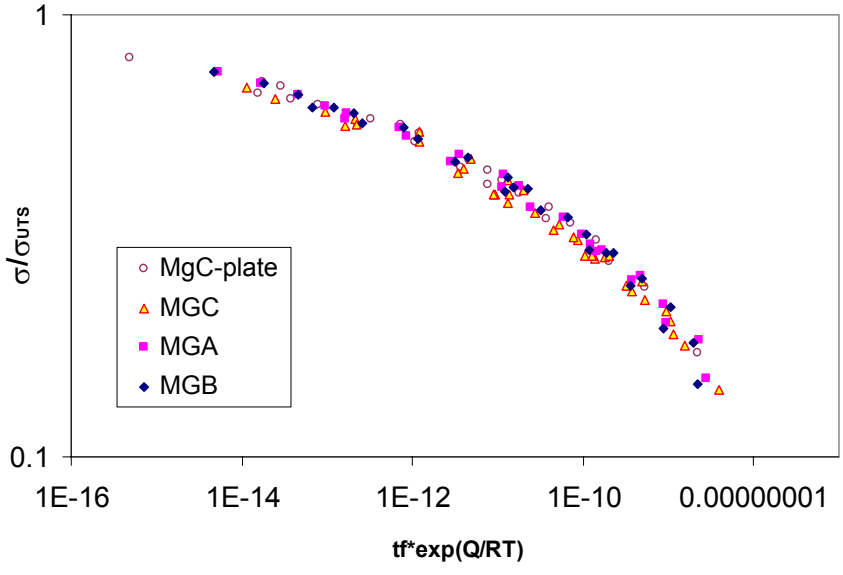

Fig. 8. The Wilshire master curve for P91 steel with Q^*_c= 300 kJ/mol. The designations MGA, MGB and MGC are pipe, tube and plate heats.

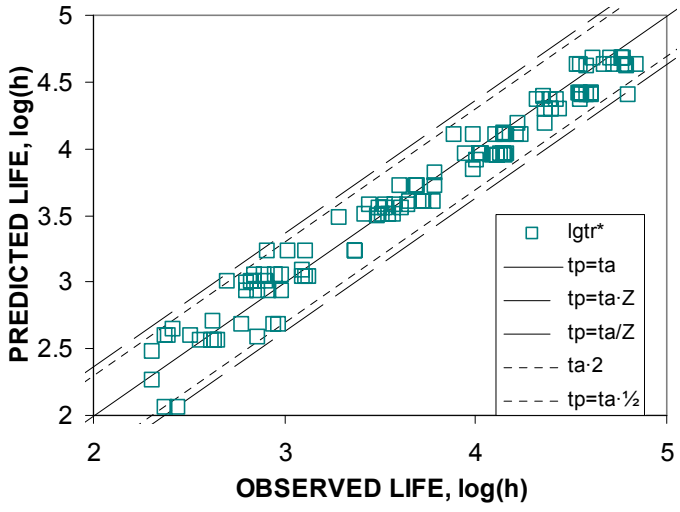

Fig. 9. Predicted times to rupture against the observed rupture times using the Wilshire equation with calculated tensile strength. The scatter is low (scatter factor Z=2.34, see *Eq. 18* for definition).

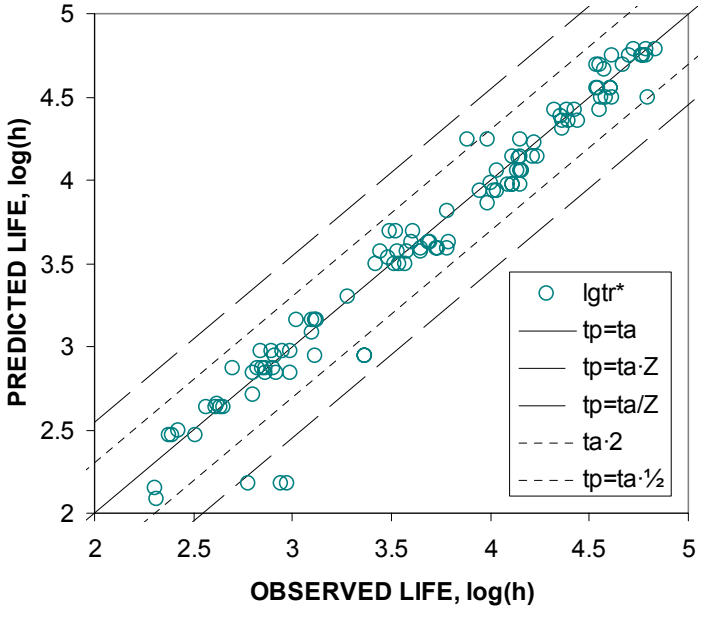

Fig. 10. Predicted times to rupture against the observed rupture times using the best parametric equation, in this case Manson-Brown 4th degree stress function f(σ)= $\sigma^{0.75}$. The scatter factor is larger than in Fig. 9, Z=3.59 mainly due to badly fitting short term data.

2.1 Creep testing

The most common type of creep data is the constant load rupture data. The data consists of time to rupture values at specified applied loads at specified temperatures. Another “common” creep data type is closely related to the rupture data, namely the same constant load test including strain measurement (continuous or interrupted test). The constant load creep test is specified in EN 10291 [26]. In the Annex C of the same document the method of estimating the uncertainty of the measurement in accordance with the ISO "Guide to the expression of uncertainty in measurement" is presented. The EN ISO 7500-2 [27] specifies the criteria for the measurement and calibration of static uniaxial creep testing machines.

Today most constant load creep tests are performed in single specimen dead weight lever machines with continuous displacement measurement (see Fig. 11). However, in Germany rupture and interrupted creep strain tests are still performed in multi-specimen creep furnaces. This method produces large amounts of data, but the quality of temperature control and the acquired strain curves are somewhat inferior to the ones acquired by single specimen machines.

In the test type comparison work done in Germany [28] it was shown that the influence of interruptions is weak, always inside the scatter band of uninterrupted testing. For the steel P22 it was shown that the interrupted tests had a strain factor of around 1.055 in comparison to the uninterrupted tests.

The assessments and models presented in this thesis are solely based on the creep strain and time to rupture data produced with single or multi specimen constant load testing machines.

To get an impression on the data scatter expected in creep data assessments, raw creep rupture data and standard table data (EN 10216-2 [29]) are plotted together with two rupture master curves optimized on the standard in Fig. 12.

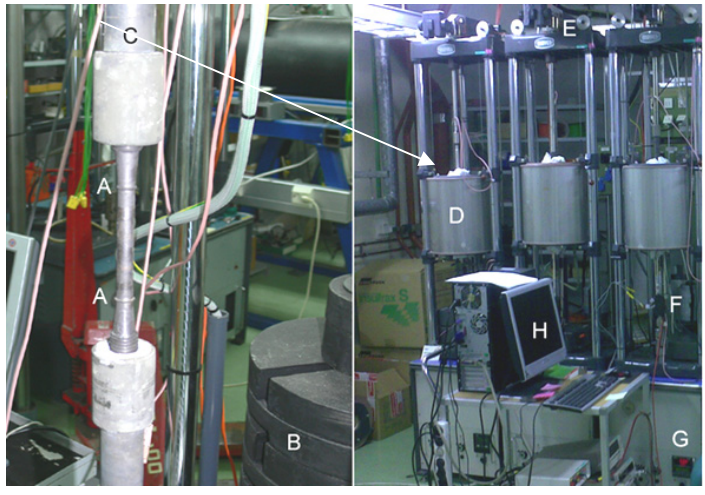

Fig. 11. Constant load creep testing machine assembly. A) Creep specimen ridges for extensometers (displacement measurement), B) Loading weights, C) Upper pull rod, D) Furnace, E) Lever mechanism (1:10), F) Displacement transducer, G) Temperature controller, H) Data acquisition computer.

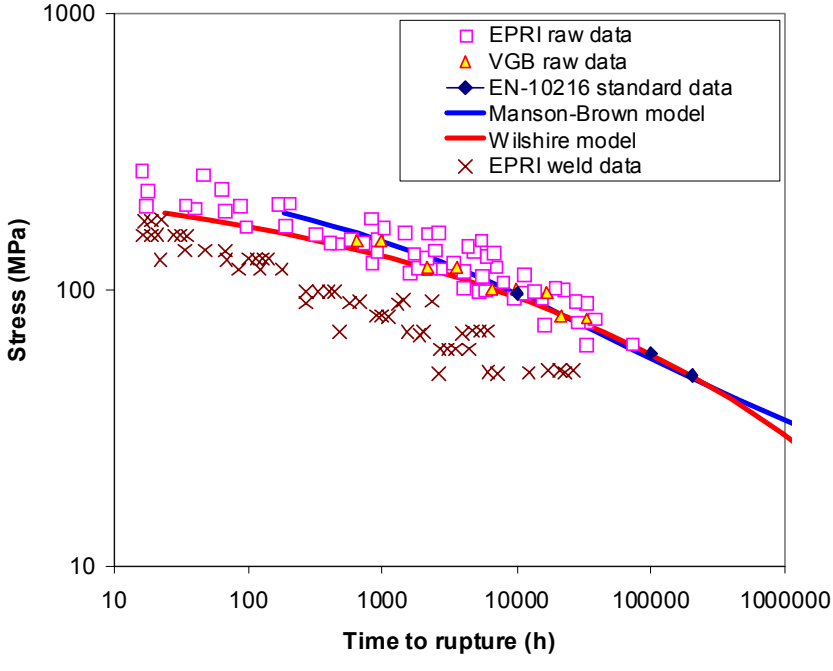

Fig. 12. EPRI and VGB data for X20 steel at 600°C with time to rupture models (classical Manson-Brown and Wilshire) optimized on EN-10216 creep strength data.

Data scatter, encountered in different magnitude for all creep test data, is mostly caused by material specific differences such as heat specific differences in composition, product form or heat treatment. The data scatter will of course play a significant role in the modeling, adding to the uncertainty of the extrapolations done.

When dealing with creep strain curves one should keep in mind that in some reports the creep curves are given with and in others without the instantaneous strain. Looking at creep rupture data, for instance isothermally plotted, the behavior can be divided into three different types. The pure materials normally behave quite linearly in a log-log plot. The creep mechanism might, however, quite suddenly change (the slope changes) at low stress levels. Most ferritic high temperature steels show gradual creep mechanism change over the whole stress range giving the isothermal curves a bent shape. The high temperature steels assessed in this thesis belong mainly to this group (see Fig. 13, for example).

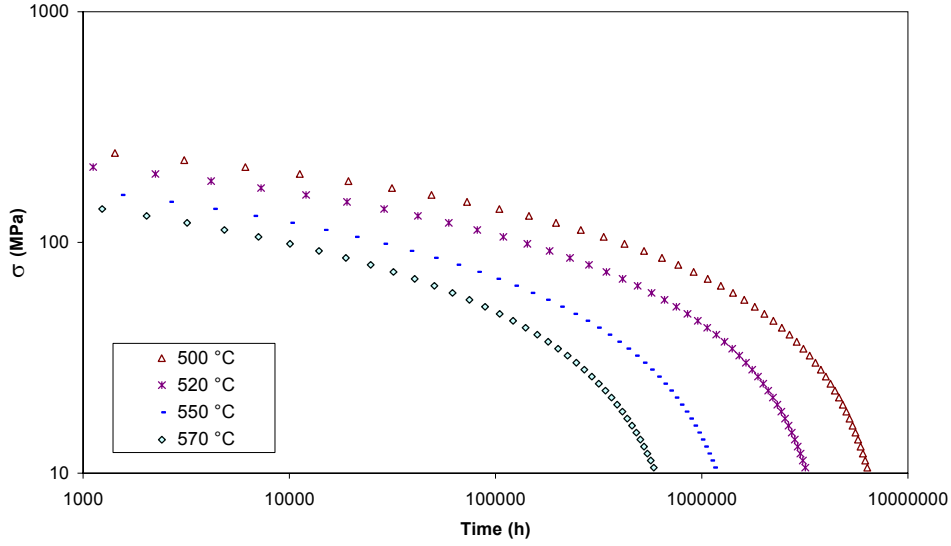

Fig. 13. Rupture model isotherms 500–570 ºC for 0.5CMV steel based on stress to specified rupture time tables [30].

Some martensitic steels show sigmoidal behavior, the strength gradually decreasing in a limited stress range and then stabilizing again. The sigmoidal behavior is especially conspicuous for the 11CrMoVNb steel assessed in an ECCC round robin yet to be published but shortly presented in the 2009 ECCC conference in Switzerland. These kinds of material data sets are especially difficult for

both time to rupture and strain modeling. The pre-assessed 11CrMoVNb steel rupture model is presented in Fig. 14.

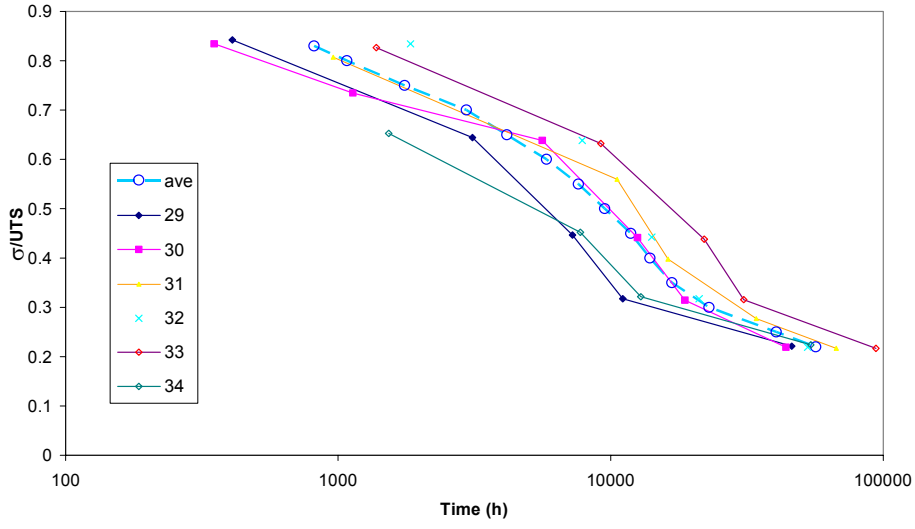

Fig. 14. Sigmoidal rupture model (open points) for 600ºC isotherm based on normalized stress for 6 heats of 11CrMoVNb steel.

The most common creep test types are presented in Table 2 together with some comments on data availability. The short descriptions of the different testing types are included in the thesis, though not utilized as data sources, for the purpose of determining the possibility of withdrawing uniaxial creep parameters from them.

The stress relaxation tests are performed at constant total strain and as creep strain accumulates, the elastic strain component of the total strain decreases, leading to a decreasing stress [31]. The relaxing stress is monitored on-line until it stabilizes and the rate of change becomes insignificant. An example of a relaxation sequence in a low cycle fatigue test is presented in Fig. 15.

An estimate of the (constant load) secondary creep rate can theoretically be determined from the relaxation test, as a function of stress, when initially loading the sample sufficiently to pass the region of primary creep.

Table 2. Creep test types.

Test type	*Data type and availability*
Constant load / Time to rupture	- The most common data type - Standard data tables / standards - Full raw data creep curves are rare
Constant load / Creep strain (+rupture)	- For some steels data tables for specified stress, strain and time are available
Constant stress / Creep strain (+rupture)	- As above but even more rare
Relaxation test	- Data mainly for bolting steels - Difficult to relate to standard creep properties
Slow strain rate test - SSRT (= Constant strain rate test - CSRT)	- Often used for combined creep / environment testing - Usually not very long durations - Offset in strain rate comp. to creep strain data
Notched bar creep test	- Notch sensitivity tests (limited) - For determining notch weakening/ strengthening - For defining skeletal point multi-axial representative rupture stress
Small punch creep test	- Made in increasing amount - Small samples from service exposed components - Weld zone testing - Relationship to standard creep data not well defined (requires FEA)
Impression creep test	- Limited data published - Mainly used in UK - Gives primary / secondary creep
Component testing: - internal pressure - internal pressure + tensile load	- Very limited - Interaction and combined damage

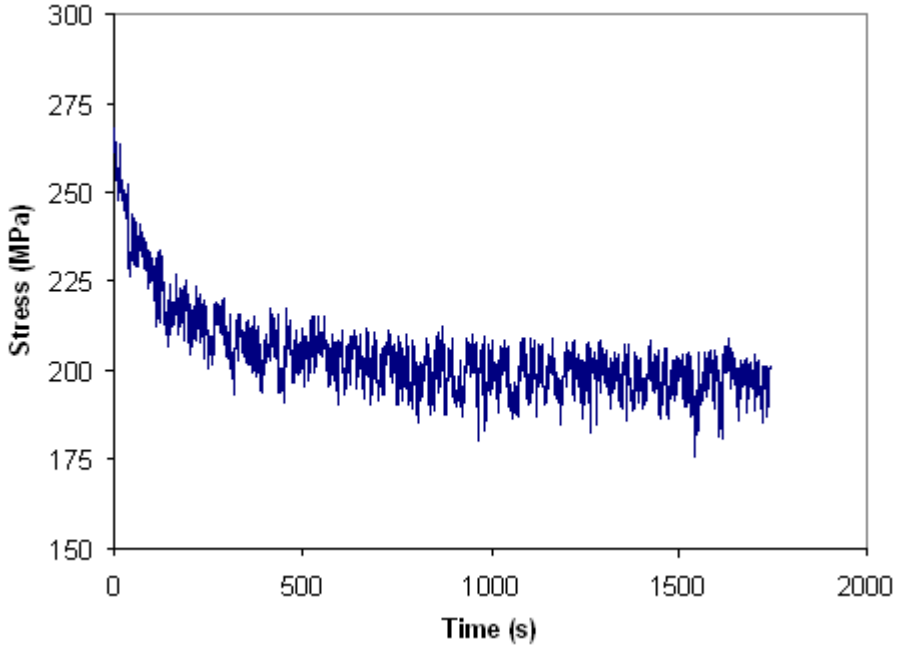

Fig. 15. Creep relaxation curve extracted from a hold period in a low cycle fatigue (LCF) test for low alloy steel P23 (creep resistant modification of P22) strained to 0.2% at 575ºC [32].

The plastic (creep) strain rate $\dot{\varepsilon}_p$ can then be determined from the equation:

$$\dot{\varepsilon}_p = -1/E(d\sigma/dt), \qquad \textit{Eq. 4}$$

where E is the Young's modulus and $d\sigma/dt$ the measured rate of stress relaxation. It is, however, to be noted that for some materials, in the later stages of relaxation, recovery might become significant leading to lower calculated strain rates than would be measured from corresponding conventional creep tests. An alternative practice of stress relaxation testing is the multi-specimen model-bolt test, where the relaxed stress is measured by means of strain gauges during unloading after long-term creep exposure. Guidelines are found in the ECCC recommendations (2005, Vol. 3) and in the European standards EN 10319-1 [33] and 2 [34]. To date there are no formally recognized procedures for assessing the stress relaxation data, but it is used by some assessors as a "fast" method for comparing of service exposed materials [35] to virgin material properties. To accurately determine the creep strain exhaustion level, or consumed creep life fraction from these tests would be beneficial for assessing creep fatigue tests

with holding times. The LCSP model developed will in the near future be used for this purpose.

The slow strain rate test (SSRT) or as others call it the constant strain rate test (CSRT) is also an accelerated experimental procedure to determine basic creep properties [36]. In this test the "internal stress" under the "stationary" creep stage in a slow tensile test is measured. Some SSRT curves from tests in super-critical steam are shown in Fig. 16.

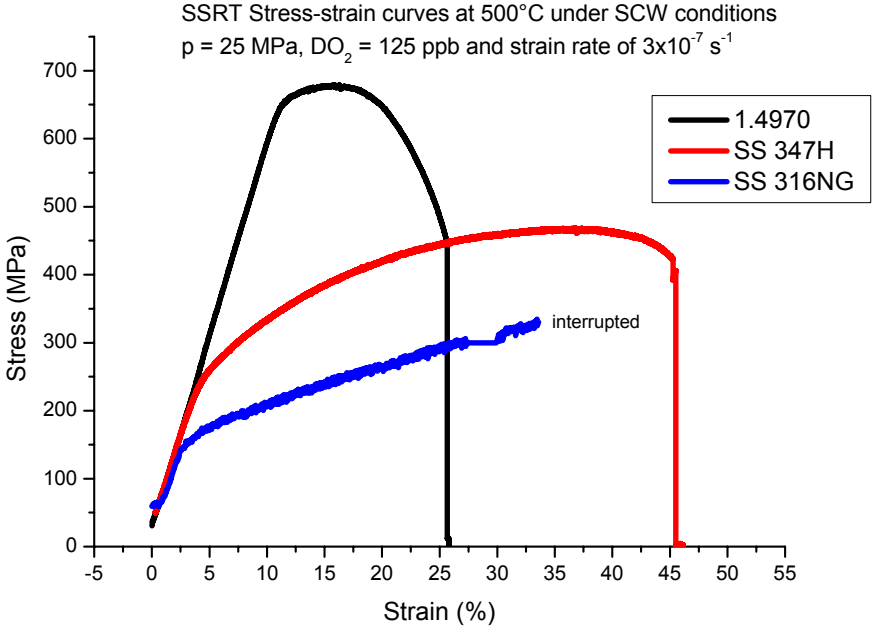

Fig. 16. SSRT test data for HPLWR materials in supercritical steam conditions [37].

The creep deformation is imposed on the specimen at a constant displacement rate (or strain rate) and the material will build up a resistance against deformation. The steady state, where the stress is no longer increasing, identifies the internal stress, i.e. the materials resistance against (creep) deformation. The stress value obtained will be dependent on the imposed strain rate. The strain rate and temperature dependence of the internal stress is the basis of the CSR concept. To translate the imposed strain rates to conventional strain controlled (creep strain tests) strain rates the following formula has been derived from *Eq. 2* by assuming n = 3:

$$\dot{\varepsilon}_s = \alpha^3 \cdot \dot{\varepsilon}_t \,, \qquad \textit{Eq. 5}$$

where $\dot{\varepsilon}_s$ is the strain rate in strain control and $\dot{\varepsilon}_t$ in stress control. The difficulty in determining the true value of the α-parameter (usually approximately 0.75) has been a drawback of this testing type, and has therefore not acquired high popularity among creep experts. An increased use of this creep testing type is foreseen for extreme environments where time is essential for the cost of testing, such as supercritical steam autoclave testing, in-core nuclear test reactor testing or material screening for Generation IV nuclear test reactor coolant environments. The most promising materials could then be tested for long-term creep under constant load. Also for this testing type the LCSP creep strain model will be attempted for improving the determination of the α-parameter.

Impression creep [38][39][40] is a relatively new testing technique developed for local (micro-region) creep properties such as weld zones. The impression creep testing technique involves the application of a steady load to a flat-ended rectangular indenter placed on the surface of a material at the required test temperature. Creep allows the indenter to push its way into the surface of the material. The displacement-time plot is related to the creep properties of the small volume of material in the immediate vicinity of the indenter.

The stress σ related to the creep properties sought is calculated from:

$$\sigma = \eta \cdot P \,, \qquad \textit{Eq. 6}$$

where P is the mean pressure under the indenter and η reference parameter. The accumulating creep strain ε from the displacement of the indenter follows the equation;

$$\varepsilon = \frac{\Delta}{\beta \cdot d} \,, \qquad \textit{Eq. 7}$$

where Δ is the displacement, d the indenter width and β a reference parameter. In [41] the equivalent uniaxial stress was determined to be 0.296 times the mean indenter pressure (= η) and the effective gauge length 0.755 times the indenter width (= β). The creep strain rates in the primary and secondary creep can be obtained with this method. The primary and secondary creep properties determined with the indenter will be utilized for determining the shape functions (LCSP) for in service materials and material zones difficult to test due to re-

stricted size (such as heat affected zones). These can then be transferred to FEA simulations of complex structures.

The small punch creep test (SP) [42] is like the impression creep test based on small or miniature specimens. The SP specimens are discs 0.25–0.5 mm thick and 8–10 mm in diameter. The SP technique was first introduced in the USA and Japan in the 80s. In recent years it has become more widely used also in Europe. The drawback of the method is that the results have to be correlated between the puncher load and the corresponding uniaxial creep test stress.

This relationship is dependent on the radius of the punch indenter, the thickness of the test disc, the radius of the receiving hole, and the material under test. A standardization initiative for the SP test method has been put forward in a Code of Practice (CoP) or CEN Workshop Agreement, CWA 15627 [43] published in December 2006.

In the CoP the ratio of SP test load F_{SP} to the uniaxial creep stress σ is:

$$\frac{F_{SP}}{\sigma} = 3.33 \cdot K_{SP} \cdot R_{SP}^{-0.2} \cdot r_{SP}^{1.2} \cdot h, \qquad \textit{Eq. 8}$$

where r is the radius of the punch indenter, h is the thickness, R is the radius of the receiving hole, and K_{SP} is a material constant. The LCSP strain model implementation for FEA could readily be utilized for the "decoding" of the SP indenter movement towards better compliance with standard uniaxial creep curves.

Notched bar creep test [44] is also covered by a CoP, issued in 1991. The test was developed for establishing the multi-axial creep stress-rupture properties. The CoP was updated in 2001, to enable the extraction of multi-axial creep strain response. The notched bar test can also be implemented for the determination of local creep strain properties in a weld [45]. The thesis tools such as the FEA implemented LCSP model together with the multiaxial creep exhaustion parameter could improve the understanding of notch sensitivity and creep damage accumulation.

3. Creep rupture modeling

Since creep is time dependent the determination of creep properties is time consuming and therefore also expensive, even though the machines used for testing are in most cases simple dead weight machines (constant load). The design stresses and/or temperatures in most high temperature engineering structures are low compared to the test conditions giving test results within a reasonable time frame. This makes the reliable extrapolation of these properties a necessity for the use in design and life management of high temperature components.

From the engineering point of view the most important (and challenging) aspect of creep research is how to accurately and reliably, with minimal data and cost, determine the creep properties in the relevant service conditions. Much effort has been invested into developing reliable methods to establish optimal creep testing matrices and methodologies for creep rupture extrapolation. One active player in Europe is the European Creep Collaborative Committee (ECCC) that has done extensive work in developing common rules for the assessment of creep data, arranging intercomparison round robins among creep assessors and most importantly developing post assessment tests, for finding and validating the suitable models [46], [47]. These PATs are now widely accepted and form an integral part of modern creep-rupture data assessment procedures such as the PD 6605 [48] or DESA [49]. The flow chart of an ECCC creep rupture data assessment (CRDA) is shown in Fig. 17.

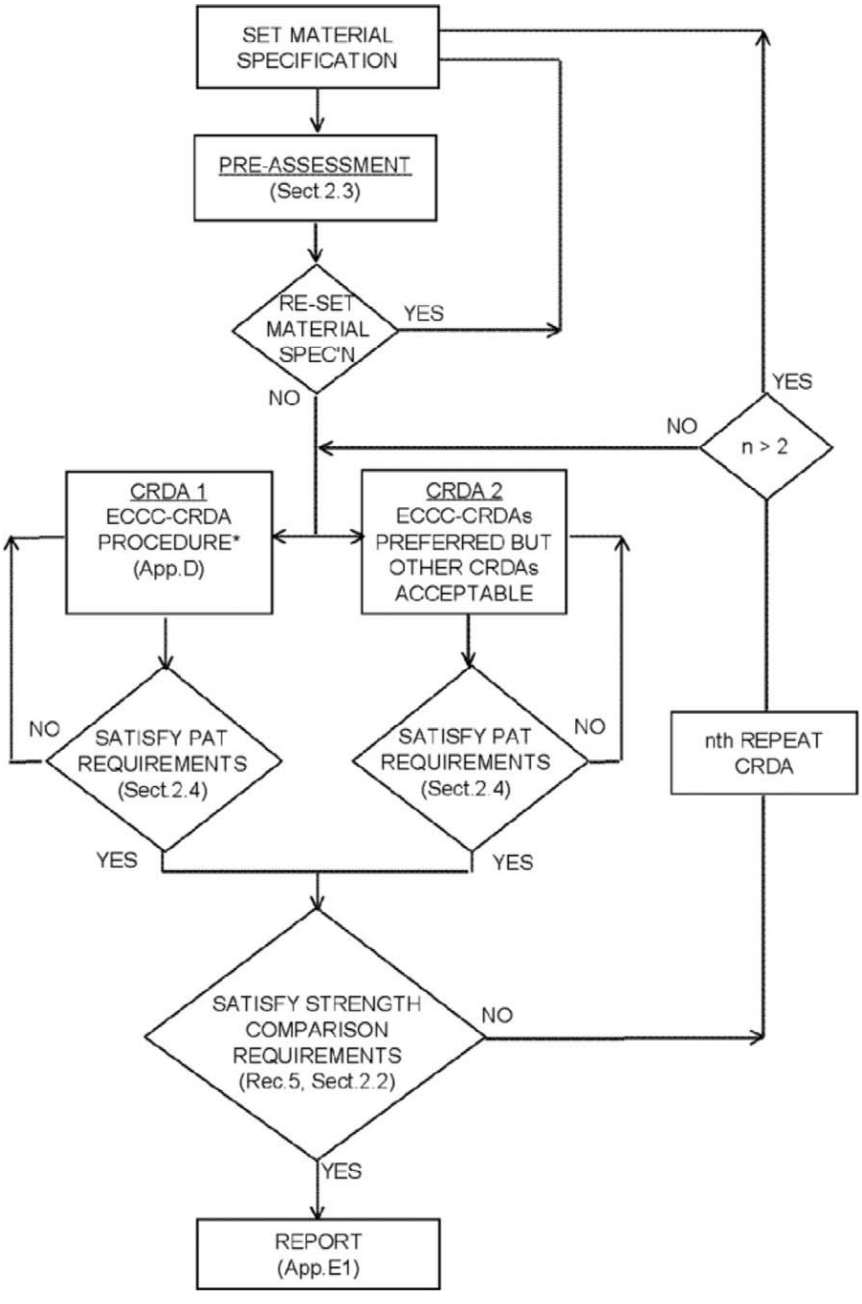

Fig. 17. The ECCC creep rupture data assessment procedure. The references in parentheses refer to sections in the ECCC Recommendations Vol. 5, Part Ia.

The creep data readily available is for many engineering steels limited to standard values such as the EN-10216 or to rather short-term data found in the public domain. Short-term data found in the literature are in most cases reported with inadequate background information of the tested material (pedigree data such as tensile strength, material batch information, chemical composition and heat treatments). The results of assessments for use in standards are usually presented as the stress required to cause rupture in 10 000, 100 000 and 200 000 hours. To acquire these values, interpolation and extrapolation has to be done in most cases. The ECCC recommendations limit the extrapolation in time to three times the longest test duration.

The state-of-the-art software tools for modeling creep rupture (or time to specified strain) utilize least squares (DESA) or maximum likelihood (PD 6605) data fitting. The benefit of the maximum likelihood fitting is that also unfailed tests (running of interrupted tests) can be utilized in the master equation fitting.

The main bulk of the creep rupture models presented in the assessment software are the classical time temperature parameters (TTPs). In TTPs the temperature and rupture time is combined into a "temperature compensated time" parameter. The data can then be plotted in two dimensions (TTP vs stress). The data is then fitted to a suitable polynomial stress function. One main problem with this approach is that the polynomial characteristics of the model can lead to turn-back or sigmoidal behavior when predicting outside the data range. From the TTPs mentioned above the most commonly used ones are the Larson-Miller and the Manson-Haferd models [50]. Also three generalized models are supported in both DESA and PD 6605 software, namely the Minimum Commitment model (MCM or MC [51]) and two "Soviet Models" (SM1 [52] and SM2). These models are in character more stable than the polynomial TTPs and do not easily produce turn-back and sigmoidal behavior. The MC model used in the software is though the simplified form of the Manson's minimum commitment method (MCM). In the MC model the instability factor A (making the model non-linear) has been set to zero (A=0).

As an example of how the physical basis of creep is related to a classical rupture model, a closer look at one of most used ones, the Larson-Miller, is given below.

The Larson-Miller parameter

The temperature dependence of the TTPs is based on the Arrhenius law for the thermally activated process rate (in this concept minimum strain rate).

$$\dot{\varepsilon}_m = A \cdot \exp(-Q/kT), \qquad \textit{Eq. 9}$$

and for the stress dependence the Norton law [53] is used:

$$\dot{\varepsilon}_m = B \cdot \sigma^n, \qquad \textit{Eq. 10}$$

where B is the rate coefficient (considered temperature dependent) and n the creep exponent. Integration of the combination of *Eq. 9* and *Eq. 10* gives the inverted Norton law:

$$\varepsilon = -\frac{1}{n} \cdot \ln(1 - nB) \cdot \exp(\frac{-Q}{kT}) \cdot \sigma^n \cdot t, \qquad \textit{Eq. 11}$$

from which at high values of n and/or failure strain ε_f, the basic TPP formulation (r ~ n) for rupture is obtained:

$$t_r = \frac{1}{rB \cdot \exp(\frac{-Q}{kT}) \cdot \sigma^r}. \qquad \textit{Eq. 12}$$

In the case of Larson-Miller parameter we take the logarithms of both sides and manipulate:

$$T(\log(t_r) + \log(rB)) = M - rT \cdot \log(\sigma), \qquad \textit{Eq. 13}$$

where $M = Q \cdot \log(e)/k$ and then assuming log(r·B) and r·T ~ constant gives the Larson-Miller (P_{LM}) equation:

$$P_{LM}(\sigma) = T[\log(t_r) + C] = M - N \cdot \log(\sigma), \qquad \textit{Eq. 14}$$

where M and N are material dependent factors and $C = \log(r \cdot B)$.

The equation above indicates that the Larson-Miller parameter in its basic form is linear against logarithmic time. However, it is commonly known that all TTPs are fitted as polynomial stress functions such as:

$$P_{LM} = T[\log(t_r) + C] = a + b \cdot \log(\sigma) + c \cdot \log(\sigma)^2 + d \cdot \log(\sigma)^3 + .. \qquad \textit{Eq. 15}$$

The apparent activation energy Q for creep rupture life is known to decrease (see Fig. 5) when moving from short duration test data to long-term results. This is

ignored in the Larson-Miller parameter definition which leads to the tendency of rupture life overestimation.

As a retrospective the experience is from materials such as P91, E911 and HCM12A (P122), that the initial evaluations of creep life were overestimated with far reaching consequences in the last case. The long-term creep life of E911 steel has fallen to a level very close to that of P91steel. The E911 steel rupture strength for 100 000 h at 600°C is 98 MPa ([54] assessed in 2005) against 94 MPa for P91 ([55] assessed in 1995). The newest assessment for P91 ([56] assessed in 2009) has though dropped the value to 90 MPa. It is clear that when the actual long-term data starts to appear, the strength values acquired from the new assessments call in most cases for value reductions. For P122 steel not only was the base material strength overestimated [57], but the weld strength reduction factor was also severely underestimated. Catastrophical failures in seam welded steam lines in Japan have, being a touchy subject, only been reported orally in some recent high temperature conferences. These are only a few examples of steels that have suffered from the short term data abundance and the rigid nature of the selected model used. The Japanese have now started to adopt a methodology of dividing the data (and the prediction) into two separate ranges [58]. This methodology, the region splitting method, is not a new idea but the method of separating the regions and the further modifications makes it an improvement to the classical Japanese Larson-Miller assessments. The data is divided with a boundary condition of $0.5 \cdot \sigma_{yield}$ or through separating the data according to "high" and "low" activation energy calculated for time to rupture [59]. The selection of a best fitting model is of less importance in this kind of assessment and for instance NIMS assessors continue to use the Larson-Miller (usually with 2^{nd} degree stress function) model. The draw-back of the multiregion approach is that the data relevant for the long-term life is decreased especially for the lower temperatures (closer to service temperatures). The region splitting analysis of creep rupture data is not at least yet) implemented by the ECCC assessors but is under investigation.

3.1 Post assessment testing

The post assessment acceptability criteria (PATs) for creep rupture data assessment (CRDA) can be categorized in three main groups, PAT1, 2 and 3. PAT1 evaluates the physical realism of predicted isothermal lines, PAT2 the effective-

ness of the model prediction and finally PAT3 tests the repeatability and stability in extrapolation. The PATs are shortly presented below.

PAT1 – Physical realism of predicted isothermal lines

In PAT1 the credibility of the model is first checked visually in a log-log stress versus rupture time plot for each isotherm (PAT1.1). For the predicted times between 10 and 10^6 h and above 80% of the minimum stress represented, the isotherms are not allowed to cross over, come-together or turn-back (PAT1.2). The derivative $\partial \log(t_r) / \partial \log(\sigma_0)$ is then plotted against log(σ) to show whether the predicted lines decrease "too quickly" at low stresses. The $\partial \log(t_r) / \partial \log(\sigma)$ should not fall below 2 (ECCC recommendation). The PD 6605 has the rejection criteria of 1.5 for the same test.

PAT2 – Effectiveness of model prediction within range of input data

There are two categories of PAT2 tests. The first tests all data and the other isotherms individually. Each category has 2 criteria parameters, namely the root mean square error (RMS) and the slope. The calculation of these parameters is not supported in PD 6605. The RMS criterion is describing the error in logarithmic time between the predicted and measured rupture times. The better the RMS the better the model fits the data. No actual limits have been set for the RMS but the scatter factor (Z, see Eq. 16) calculated from the RMS should be below a value of 4 to be considered acceptable. The amount of data falling outside these limits set by the Z value is restricted to 1.5%. The slope of the PAT 2, i.e. the linear regression line fitted through logarithmic actual rupture time versus modeled rupture time is acceptable when falling between 0.78 and 1.22. An additional criterion for regression line is that it should be contained within unity line plus/minus logarithm of 2 (equaling a factor of 2 in time) between the rime of 100 to 100 000 h.

PAT3 – Repeatability and stability of extrapolations

The PAT3 tests are concentrating on the repeatability and stability of the models in extrapolation. There are two PAT3 tests, both measuring the stability of the 300 000 h prediction. If the longest test is shorter than 100 000 h the prediction should be made to three times the longest test. The PAT3.1 is culling the data randomly by 50% between 10 and 100% of the maximum rupture time. The PAT3.2 requires culling 10% of the data having the lowest stress values. This

test is not considered mandatory, if there is knowledge of sigmoidal behavior in the material response.

In the unlikely event that all the PATs would give identical results for contending models the one with less fitting parameters should be selected. The ECCC recommendations as such do not limit the method or models used for the creep rupture predictions itself, but the quality aspects given by the post assessment tests (PATs) have to be met.

3.2 Non-conservatism in creep rupture modeling

The causes for the overestimation of creep strength values, such as for the high temperature 9–12 Cr ferritic steels, are naturally not only caused by choosing the wrong model or methodology. It is obvious that a model cannot predict something that is not in the data, i.e. transition from ductile (short-term) to brittle fracture (long-term) for the lower temperatures might not be present. In addition the data from the higher temperatures might due to model restrictions or lack of data in other isothermals produce incorrect temperature dependences as described earlier for the Larson-Miller case.

Additional non-conservatism in a creep rupture model can be introduced by the following:

- the data set is not balanced, it has too much short-term data or the heats represented are in unbalance
- the assessment is based on too few heats (mainly strong ones)
- the assessment is based on thin-walled product forms only (also tend to be stronger)
- the “best” model has not been used (some assessors use only a particular model)
- the selected model is “rigid” and does not accommodate to the changing stress dependence
- isothermal behavior has been neglected (isothermal fits not properly checked).

As the above indicated, the quality of the data assessed is of the utmost importance. If, however, the data structure and the coverage of strong and weak heats are in order, the data handling (like culling the short term data and clear out-

liers), assessment tools (numerical or graphical methods) and model selection become influential on the strength prediction.

The impact of selected model has been briefly shown in the introduction to creep modeling. Numerous fitting parameters give more flexibility to the function, but it is clear that a good fit in interpolation does not necessarily guarantee good performance in extrapolation. The number of fitting constants involves a part of the inherent rigidity, and conventional fitting efficiency is therefore better described by the Z_{SEE} than the Z_{RMS} as defined in Eq. 16 and Eq. 17. The RMS, SEE and the scatter factor Z are calculated from the raw time to rupture (t_{rd}) data and the model prediction (t_{rm}) at specified stress and temperature.

$$RMS = \sqrt{\frac{\Sigma(\log(t_{rd}) - \log(t_{rm}))^2}{n-1}}\ , \qquad \textit{Eq. 16}$$

$$SSE = \sqrt{\frac{\Sigma(\log(t_{r}) - \log(t_{rm}))^2}{n-k-m-1}}, \qquad \textit{Eq. 17}$$

$$Z_{PARAM} = 10^{2.5 \cdot PARAM}\ , \qquad \textit{Eq. 18}$$

$$\log(t_r) = \log(t_{rm}) \pm \log(Z), \qquad \textit{Eq. 19}$$

where for a normal distribution the true time to rupture t_r would lie in almost 99% of the observed times within the boundary lines defined by the scatter factor Z (Eq. 18). The same equations are later also used for determining the "goodness of fit" for both time to strain and minimum strain rates. A perfect prediction, by the master-equation would be represented by Z equal to unity.

For rupture data a good fit gives *Z* values around 2. A fit giving Z values of > 4 is according to ECCC recommendations unacceptable, whereas values of 3–4 are marginal, but may be regarded as practically acceptable.

The different creep rupture data assessment routes are:

Manual assessments:

- ISO 6303 (especially good for materials showing sigmoidal behavior)
- Wilshire equation (normalized model with optimized activation energy - applied successfully for P91 steel and OFP copper in this thesis)

- the German graphical method (almost all older German assessments have been done with this method).

Specialized creep data software assessment:

- PD 6605 assessment (maximum likelihood fitting instead of minimum least squares fitting)
- DESA assessment (automated assessment and model selection tool)
- Other software or online data bases, like the JRC data bank Alloys-DB, Alias by MPA Stuttgart or Iris by R-tech.

Most specialized software packages lack some important features, such as the implementation of the full non-linear Minimum Commitment Method with instability factor optimization and the new Wilshire equations.

Any of the above assessment routes are acceptable as long as the resulting model fulfils the PATs.

3.3 Creep rupture models for ferritic steels

The rupture master curves for the materials assessed in the thesis are given in Tables 3–8. The time to rupture curves for the corresponding steels are plotted for the 575°C isotherm in Figs. 18–20.

Table 3. Creep rupture model for P22 (10CrMo9-10) steel.

P22 (EN 10216-2), Manson-Brown 4th degree (Stress in MPa, T in K)
$P(\sigma) = -725.3813 + 1730.2198 f(\sigma) - 1575.0618 f(\sigma)^2 + 632.4288 f(\sigma)^3 - 96.5729 f(\sigma)^4$ $f(\sigma) = \log(\sigma)$ $\log(t_r) = P(\sigma) \cdot (\frac{T-600}{1000})^{1.7} + 8.27$

Table 4. Creep rupture model for P23 (7CrWVMoNb9-6) steel.

P23 (in house data), Minimum Commitment Model (Stress in MPa, T in K)
$\log(t_r) = 24.6826 + 2.0101\log(\sigma) - 0.04125\sigma + 2.223 \cdot 10^{-5}\sigma^2 - 0.02622T + \frac{1850.03}{T}$

Table 5. Creep rupture model for P24 (7CrMoVTiB10-10) steel.

P24 [62], Soviet Model 1 (as in PD 6605) (Stress in MPa, T in K)
$\log(t_r) = 672.9808 - 205.831 \cdot \log(T) - 0.5432 \cdot \log(\sigma) + \frac{(-53231 - 13.6873 \cdot \sigma)}{T}$

Table 6. Creep rupture model for 0.5CMV (14MoV63) steel.

05CMV / EN 10216-2, British Energy data[60], Manson-Brown 4th degree
$P(\sigma) = -12.6179 - 0.1424 f(\sigma) - 0.00592 f(\sigma)^2 + 6.95 \cdot 10^{-5} f(\sigma)^3 - 6.9 \cdot 10^{-7} f(\sigma)^4$ $f(\sigma) = \sigma^{0.75}$ $\log(t_r) = P(\sigma) \cdot (\frac{T - 650}{1000})^{0.9} + 8.87$

Table 7. Creep rupture models for P91 (X10CrMoVNb9-1) steel.

P91 / EN 10216-2, Manson-Brown 4th degree
$P(\sigma) = -36.293 - 0.239 f(\sigma) - 0.073 f(\sigma)^2 + 1.367 \cdot 10^{-3} f(\sigma)^3 - 1.262 \cdot 10^{-5} f(\sigma)^4$ $f(\sigma) = \sigma^{0.75}$ $\log(t_r) = P(\sigma) \cdot (\frac{T - 545}{1000})^{2.5} + 10.12$
P91 steel / NIMS data[24], Manson-Brown 4th degree
$P(\sigma) = -22.907 - 0.801 f(\sigma) - 0.022 f(\sigma)^2 + 5.146 \cdot 10^{-4} f(\sigma)^3 - 5.857 \cdot 10^{-6} f(\sigma)^4$ $f(\sigma) = \sigma^{0.75}$ $\log(t_r) = P(\sigma) \cdot (\frac{T - 505}{1000})^{2.5} + 9.62$
P91 steel / NIMS data [24], Wilshire equation, T in K, σ in MPa
$\log(t_r) = (\frac{\ln(\frac{\sigma}{\sigma_{UTS}})}{-k})^{\frac{1}{u}} \cdot \frac{1}{\exp(\frac{-Q_c^*}{8.314 \cdot T}) \cdot 3600}$ $Q_c^* = 300$ kJ/mol, $k = 24.264477$, $u = 0.1326304$

Table 8. Creep rupture model for X20 (X20CrMoV11-1) steel.

X20 / EN 10216-2, VGB report [61], Manson-Brown 4th degree
$P(\sigma) = -13.564 - 2.297 f(\sigma) + 0.115 f(\sigma)^2 - 3.534 \cdot 10^{-3} f(\sigma)^3 + 3.343 \cdot 10^{-5} f(\sigma)^4$ $f(\sigma) = \sigma^{0.6}$ $\log(t_r) = P(\sigma) \cdot (\frac{T - 420}{1000})^{1.5} + 13.99$

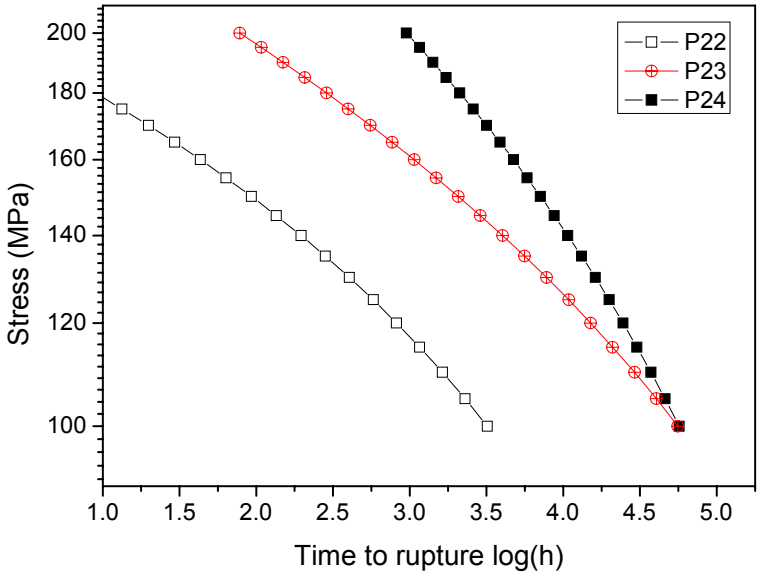

Fig. 18. Creep rupture curves for P22, P23 and P24 steels as a function of stress at 575°C.

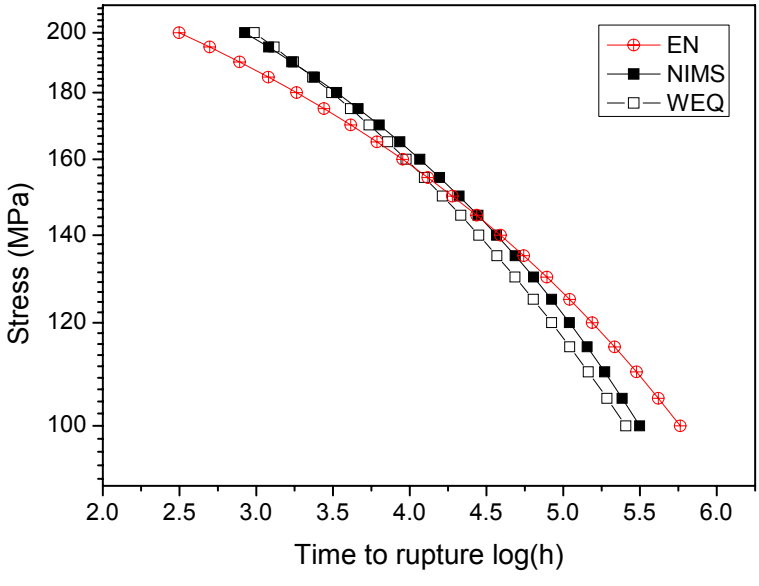

Fig. 19. Comparison of the P91 steel creep rupture models in Table 3. The predicted rupture time is given as a function of stress at 575°C.

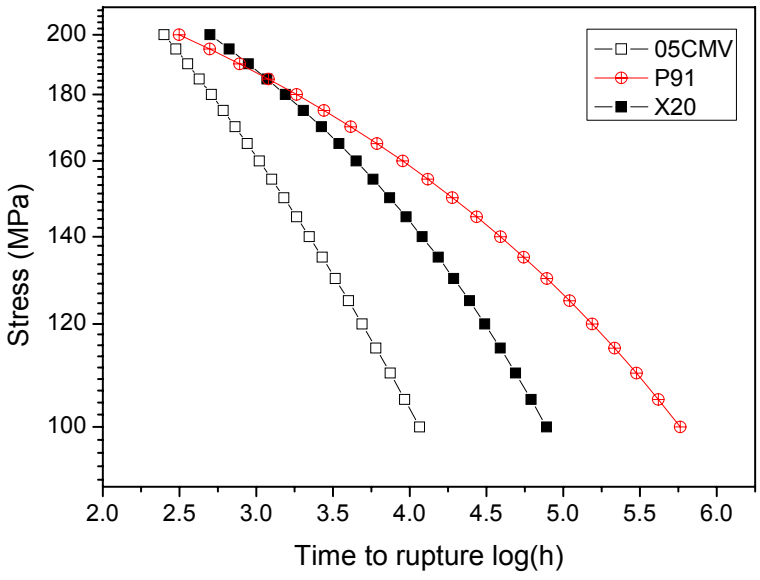

Fig. 20. Creep rupture curves for 0.5CMV, P91 (EN 10261-2) and X20 steels as a function of stress at 575°C.

3.4 Creep rupture model for oxygen-free phosphorus doped copper

For the phosphorus doped oxygen-free copper (see Table 9 for chemical compositions of heats tested at VTT) the preferred model is the Wilshire equation (see Eq. 3). The data used for the assessment consists mainly of Swedish creep rupture data sets from [22], [63], [64], [65], [66] and [67]. The VTT in-house long-term data from [68], [69]and [70] has been incorporated. The predicted isotherms 100–175°C are presented in Fig. 21 and the rupture model in Table 10.

Table 9. Chemical composition of OFP copper tested at VTT. The composition is given in ppm if not stated otherwise[1)].

Cast	*Cu%*	*P*	*Ag*	*Al*	*As*	*Bi*	*Pb*	*Fe*	*Ni*	*Cr*	*S*	*Si*	*O*
T17	99.992	54	12.4	0.3	0.5	0.2	1.4	1.6	0.5	0.93	4.9	2	2.6
T31	99.993	42	12.4	0.1	1.5	0.36	0.6	1.4	0.9	0.16	6.8	<0.2	2.6

1) T17: Cd, Co, Hg, Mn, Sb, Se, Sn, Te, Zn, Zr below the level of measuring uncertainty
T31: Cd, Co, Hg, Mn, Zn, Zr below uncertainty limit (1σ); Sb 0.3, Se 0.6, Te 0.49, Sn 0.23, H < 0.2 ppm

Table 10. Creep rupture model for OFP copper.

OFP copper, Swedish + VTT in- house data, Wilshire equation (T in K, σ in MPa)
$\log(t_r) = \left(\frac{\ln(\frac{\sigma}{\sigma_{UTS}})}{-k}\right)^{\frac{1}{u}} \cdot \frac{1}{\exp(\frac{-Q_c^*}{8.314 \cdot T}) \cdot 3600}$
Q_c^* = 89.2 kJ/mol, k = 1.629, u = 0.297

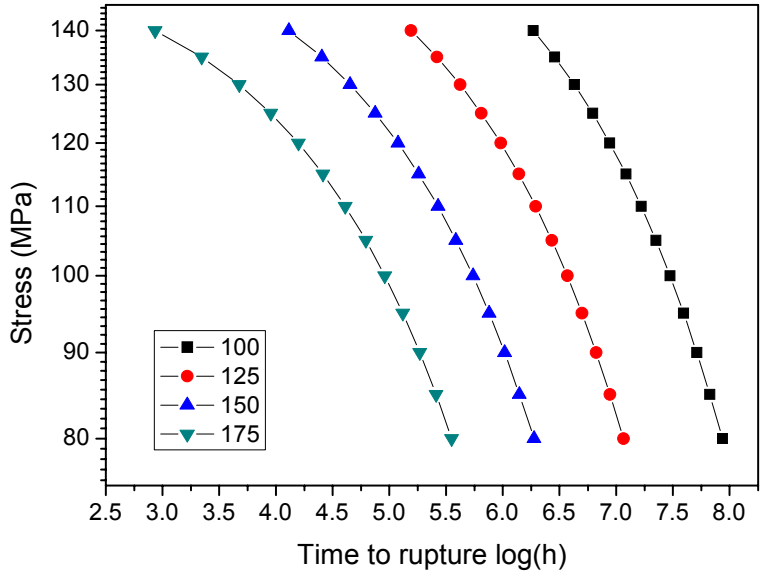

Fig. 21. OFP creep rupture curves as a function of stress at 100–75°C.

Conservative creep rupture or creep strain predictions are traditionally gained by applying safety or reserve factors into the calculations, such as the 80% in stress "rule of thumb" for rupture. However, with the application of particular numerical factors the analyses can be misleading because of the inherent but variable inter-dependence of the parameters contributing.

Confidence in the predictions is gained by investigating the sensitivity of the predictions to variations of appropriate input parameters. For example, the sensitivity analysis may consider uncertainties in the stress level, temperature and

other model calculation inputs. The Monte-Carlo simulation performed here is using the best-estimate mean data fit for the "Wilshire model" presented earlier.

The probabilistic method is directly determining the distribution of outcomes by statistical variation of the input parameters, rather than assuming that the parameters are single-valued, as in the deterministic approach. The simulation requires the estimates of the statistical distributions of the variable input parameters. Confidence in a prediction is gained when it is possible to demonstrate that realistic changes in the input parameters do not lead to dramatic changes in the predictions. In this exercise the prediction of rupture has been simulated at a temperature of 100ºC for relevant stress levels. The sensitivity of the extrapolated rupture time is checked by the random variation of the main constants in the OFP preferred model. The main parameters influencing the rupture prediction are the value for activation energy (see Fig. 21), the assumed variation in tensile properties (±2.5%) and the temperature (±2 ºC). The sensitivity of each of these parameters is determined by randomly inducing the above mentioned amount of data scatter to the OFP copper data set. The changing data of course changes the parameters of the fit. The sensitivity to the forced inaccuracies of the data and the assumed activation energy variation is transferred to the long term prediction as given in Table 11. The impact of each source of uncertainty is presented one-by-one and then combined. The activation energy is normally distributed in the range of 90 ± 3 kJ/mol, beyond which the model fit is too bad to be considered valid for the input data. The simulation result for 100°C / 50 MPa case is presented in Fig. 22. The error in the tensile properties (ultimate tensile strength) is considered to show a normal distribution with ±2.5% standard deviation. The temperature is varied randomly ±2 ºC around the test temperature. It is to be noted that the optimal activation energy is somewhat lower than the physical values for grain boundary and pipe diffusion for pure copper (104 kJ/mol). In [71] the tabled activation energies for the reduction of activation energy due to phosphorus addition indicate lower values than for pure copper.

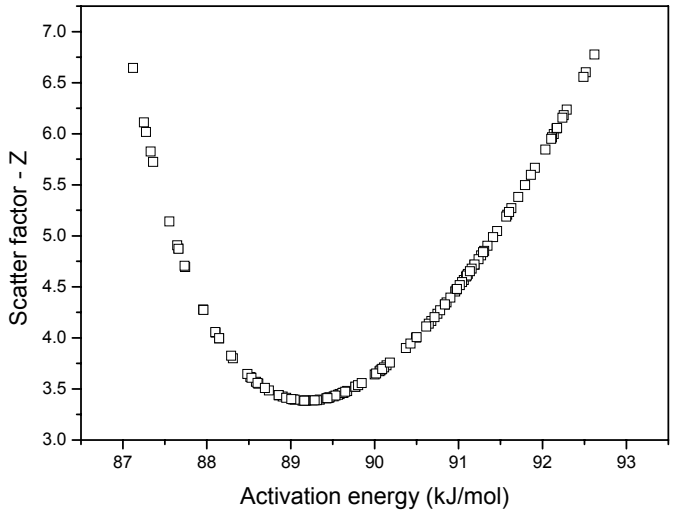

Fig. 22. Scatter factor Z of the model fit as a function of selected activation energy for the OFP rupture data set.

Table 11. Sensitivity calculation for mean, standard deviation and in brackets the minimum time to rupture in years at specified temperature and stress conditions (200 simulations) when inaccuracies are induced in the data .

Temp. / Stress	Q_c^* *90±3 kJ/mol*	σ_{UTS}*±2.5%*	*T±2ºC*	**Combined** ($Q_c^*+\sigma_{UTS}+T$)
100ºC / 50 MPa	46000 ± 6000 (40000)	42000 ± 6500 (22000)	45000 ± 2000 (40000)	43000 ± 9000 (24000)
100ºC / 80 MPa	10000 ± 1500 (8300)	9400 ± 1000 (6300)	9900 ± 260 (9100)	9900 ± 2300 (7000)
100ºC / 100 MPa	3400 ± 600 (2800)	3300 ± 300 (2400)	3400 ± 100 (3100)	3400 ± 700 (2500)
100ºC / 120 MPa	1000 ± 200 (790)	980 ± 46 (770)	1010 ± 20 (930)	1020 ± 200 (700)
150ºC / 120 MPa	12 ± 3 (7.7)	12 ± 1 (8.8)	12 ± 0.2 (11)	12 ± 3 (8)

The OFP model has been used for predicting the life fraction (LF) consumed according to the nuclear waste canister temperature profile presented in [72]. The highest predicted temperature profile is used. The canister temperature profile and the simplification used in the calculations are presented in Fig. 24.

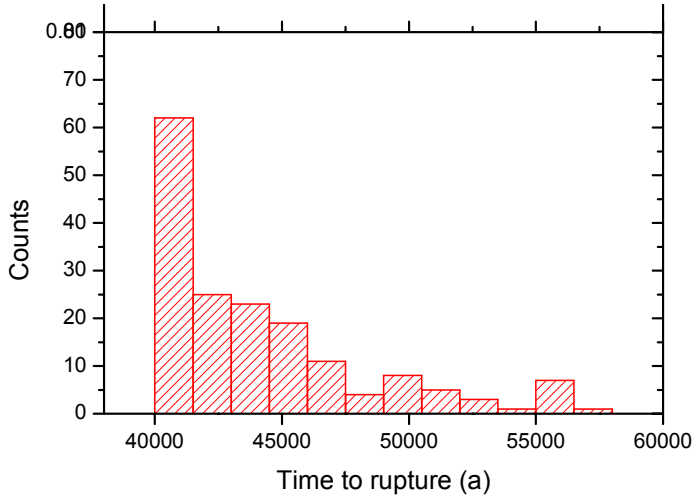

Fig. 23. Statistical presentation of time to rupture (in years) based on 200 Monte-Carlo simulations at 100°C / 50 MPa with normally distributed activation energy (90 ± 3 kJ/mol).

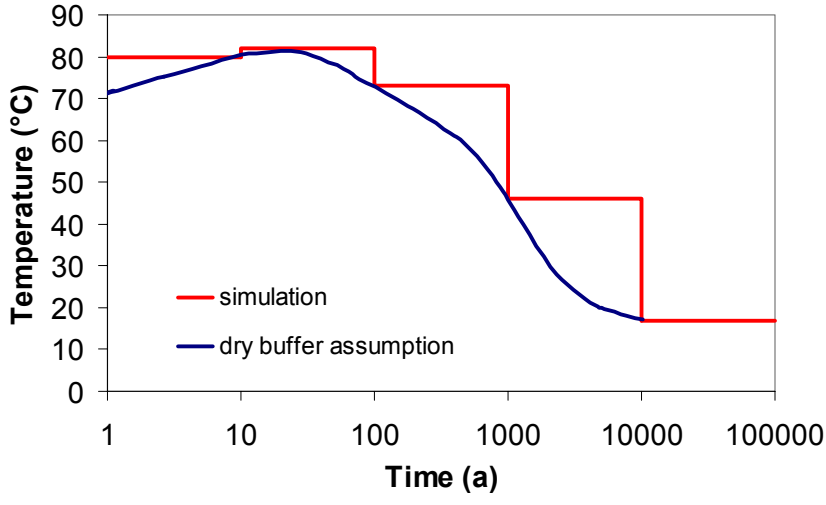

Fig. 24. Temperature profile by [74] and the simplified profile used for life fraction calculation.

To analyze the life fraction consumed (LF) and the impact of higher temperatures and strength reduction (such as required for weldments) after 1000 and 10 000 years of waste disposal Monte-Carlo simulations were performed assuming a triangular distributed overheating to temperatures between 100–120°C and a strength reduction factor (SRF) of 0.8 ± 0.2. The results are tabulated in Table 12. The simulations were performed at stress levels 50, 80 and 100 MPa. The statistics are calculated on 1000 simulations using triangle distributions for the stress and temperature variation. For comparison the deterministic life fraction at 10 000 years calculated with no alterations in temperature and with SRF = 1 is also given.

Table 12. Sensitivity calculation of consumed LF up to 10 000 years of canister service with profile according to [72]. LF = 100% is end of creep life. The LF at 10 000 years with SRF = 1 and no assumed temperature increase is given in parenthesis below the stress value. The LF distribution is log-normal.

Simulated stress (LF)	***Statistic LF***	***Incr. Temp (dry buffer+ΔT) 10 000 a***	***Incl. SRF (SRF=0.8 ± 0.2) 10 000 a***	***Combined (T+SRF) 10 000 a***
50 MPa (0.4%)	Max.	1.8%	2.0%	8.0%
	Min.	1.0%	0.4%	1.3%
	Mean	1.4%	0.8%	2.8%
	95% conf. band	1.1–1.7%	0.4–1.4%	1.4–5.7%
80 MPa (1.9%)	Max.	8.7%	38.7%	> 100%
	Min.	4.7%	1.8%	5.4%
	Mean	6.4%	5.5%	20.6%
	95% conf. band	5.0–8.2%	1.7–17.6%	5.8–73.4%
100 MPa (5.4%)	Max.	26.2%	rupt.[1)]	rupt.[1)]
	Min.	14.0%	5.1%	17.4%
	Mean	19.2%	26.9%	rupt.
	95% conf. band	14.8–24.9%	3.7–rupt.	12.2–rupt.[1)]

[1)] LF exceeds a value of 10.

The sensitivity analysis for the copper canister case reveals that with nominal values for temperature and assuming no material reduction factors, such as weld strength reduction, the canister has consumed only little more than 5% of its life at a stress level of 100 MPa. However, if the temperature is raised or a strength reduction is considered the life fraction used at 10 000 years is increased at an alarming rate. At the lowest stress levels (50 MPa) the consumed life is more sensitive to the temperature increase than to the set SRF. At 50 MPa the combined impact of a higher temperature and a reduction in material strength gives a LF = 2.8%. The corresponding LF at 80 MPa is increasing to a mean level of 20.6 % and at 100 MPa creep failure is expected already before 1000 years has passed. The higher the stress level the more sensitive the life fraction is to the SRF.

3.5 Rupture models for welds and weld strength factor

The availability of creep data is especially poor for weldments. In most cases the available creep data for welds are limited to insufficient amounts of cross weld data with lacking information of the corresponding base material. It is rather surprising that the welds are given such a low priority since the welds are in fact the most potential location of creep damage in the high temperature range. The dominant creep damage type in welded structures for high temperature ferritic steels is the Type IV cracking of the heat affected zone (HAZ fine-grain / base material interface) [73].

The amount and quality of available weld creep data has of course a direct impact on the creep models chosen to represent the weld properties. This makes the assessment even more challenging since the results are often to be combined with corresponding parent material models for determination of the weld strength factor (WSF).

The weld strength factor is defined as:

$$WSF = \frac{R_{u(W)/t/T}}{R_{u/t/T}}, \qquad \textit{Eq. 20}$$

where $R_{u(W)/t/T}$ is the predicted strength of the weld at specified time and temperature and the $R_{u/t/T}$ is the corresponding strength of the parent material.

In welds there are several “material zones” with reduced creep properties in relation to the unaffected base material. The heat affected zone (fine grained, coarse grained and intercritical zone) and the weld metal itself interact in a complex way causing creep damage, cracking and eventually rupture to develop prematurely. A weld in P24 steel is shown in Fig. 25 with the corresponding hardness measurement values plotted in Fig. 26. In addition to the mismatch in local material properties, the 3-D shape of the structure induces different amounts of constraint (multi-axiality) also influencing the creep life and expected ductility of both parent and weld metals as well as the heat affected zone [74], [75], [76].

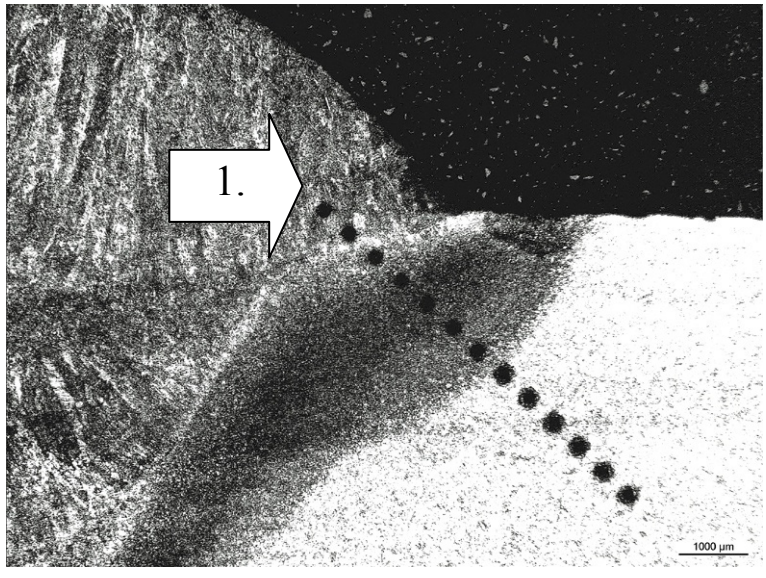

Fig. 25. Steel P24 weldment with hardness measurement marks. The starting position of the HV5 results of Fig. 26 is indicated with an arrow.

For uniaxial creep the WSF is time dependent for many steels, the longer the test the lower the creep ductility and the larger the weld strength reduction. Fundamentally tempered martensitic steels (such as P91 steel), precipitation hardened with MX and $M_{23}C_6$ particles, suffer from the loss of this strengthening as an extreme drop in creep strength which shows creep damage in service conditions. The observed creep damage in service should of course not be taken to discourage the use of P91 steel, but rather that caution is due to achieve the intended creep properties.

The classical assumption (rule of thumb) for life assessment (and design) with welds is the 20% reduction of strength from that of corresponding base material. In principle, more extensive strength loss is reported for many high temperature steels (see Fig. 27). The weld strength reduction factors (WSF) are well below 0.8 for the intended service temperatures of the steels at a duration of 100 000 h.

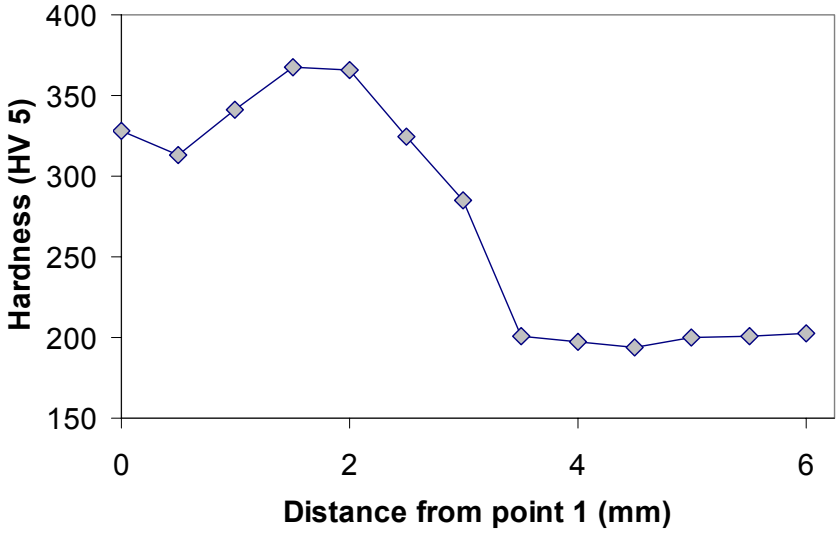

Fig. 26. Hardness results (HV 5) from measurements through weld, HAZ and into the base metal with 0.5 mm measurement intervals.

To acquire "well behaving" WSF curves, a reasonable relationship between the weld behaviour and the parent material master curve is needed. A mismatch of selected weld and parent material models can produce e.g. unrealistic cross-over or turn-back in the extrapolation as has been the case in ECCC round robin assessments on E911 and P91 steels. To avoid the problems related to mathematical incompatibility, the need for procedure development relating the WSF calculation to the parent material master curve is obvious. The simplest of the procedures developed by the current author is the implementation of the Rigidity Parameter Correction (RPC) described in Paper I of this thesis and further developed in Paper II for WSF determination.

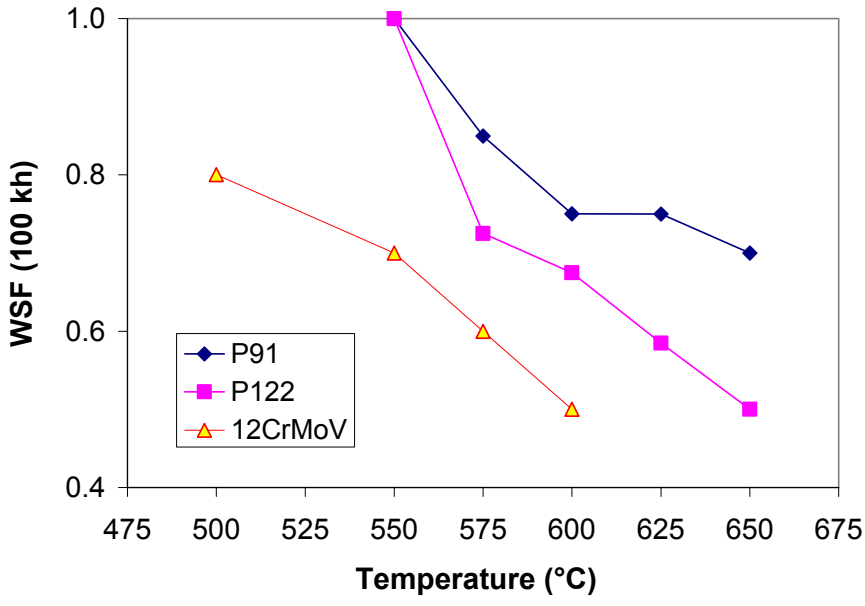

Fig. 27. Reduction of WSF at 100 000 h for some high temperature steels [9].

3.5.1 Rigidity Parameter Correction – engineering tool for improved WSF calculation

The Rigidity Parameter Correction (RPC) model was originally developed for testing the stability (rigidity) of creep rupture models in extrapolation. The RPC is based on the non-linearity formulation of the Minimum Commitment Method (MCM) by Manson [51] applying a similar curve equation and is thoroughly described in the thesis Paper I and used for WSF calculation in Paper II.

The RPC is defined as:

$$\log(t_{rR}) = \frac{\log(t_{rm}) - \log(t_p)}{1 + R \cdot (\log(t_{rm}) - \log(t_p))} + \log(t_p) \qquad \textit{Eq. 21}$$

where t_{rR} is the corrected (RPC) time to rupture, t_{rm} the uncorrected model prediction (for WSF the BM master curve) and t_p a pivot point in time and R a curvature constant. The RPC correction is zero at the pivot point and reduces the predicted life elsewhere (see Fig. 28).

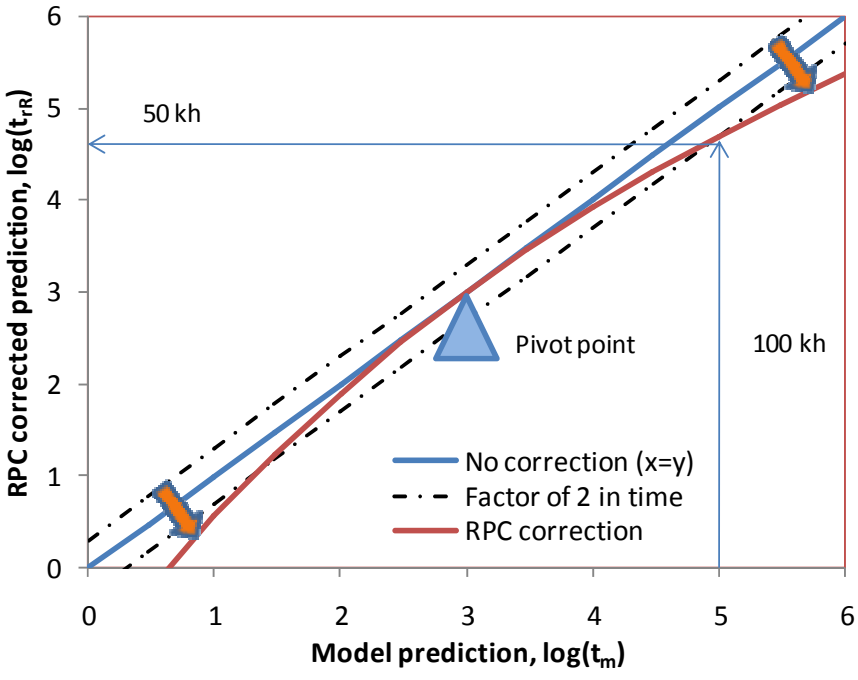

Fig. 28. The RPC principle of bending the basic master curve prediction around the pivot point t_p, here $\log(t_p) = 3$ and R = 0.089. The correction predicts half life at 100 000 h.

For long-term weld predictions the term $\log(t_p)$ can be fitted as a temperature dependent function or used (as here) as a constant. Any parent material master curve can be modified with the RPC instead to describe cross-weld data behaviour (see Fig. 29). The fitting is simply performed by minimising the root mean square error (RMS) and optimising the values of the rigidity factor *R* and $\log(t_p)$.

The main advantages of the RPC engineering tool are:

- the RPC can be applied to any creep model
- the RPC shows susceptibility to pivoting effect
- it can also be used as an additional "PAT" for balancing data and for finding best rupture model
- the WSF correlation is easy to use (only 2 additional parameters)
- the WSF is always lower at long times (conservative in nature).

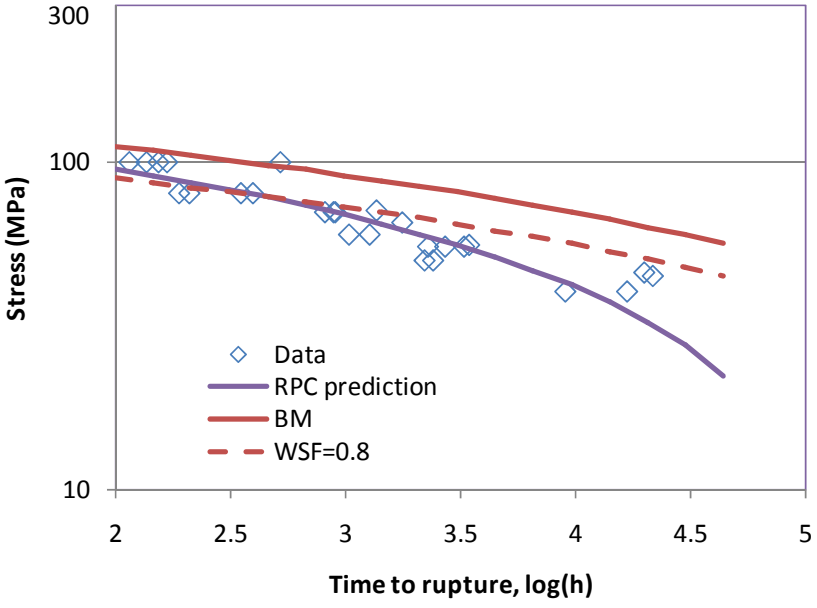

Fig. 29. Example of RPC modeling for cross-welded P91 data at 650°C, BM = base material.

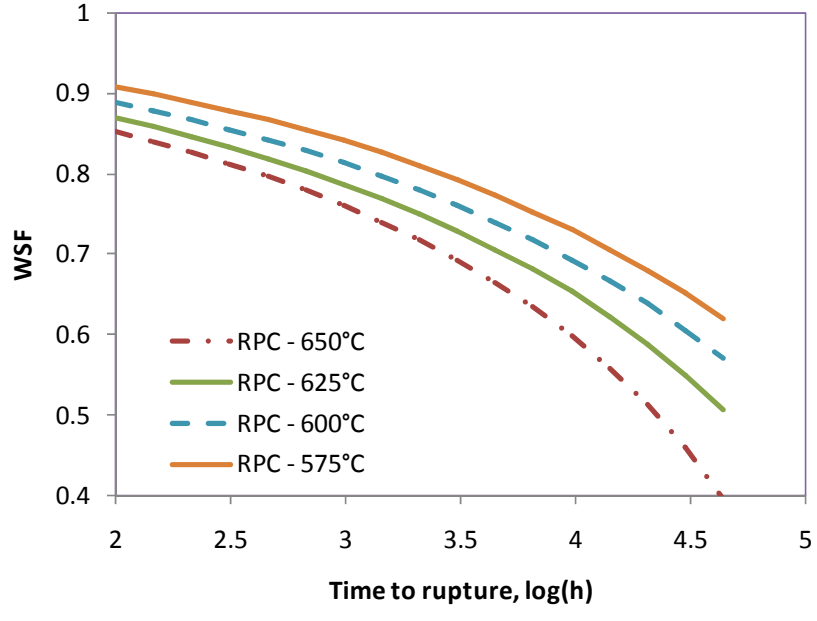

Fig. 30. WSF for P91 steel using the RPC approach [Paper II].

3.5.2 Sensitivity analysis of P91 steel weld strength factor

To be able to check the sensitivity of the WSF, a set of cross-welded P91 steel data (ECCC data) was assessed by using the Wilshire equation (see section "Creep rupture models for ferritic steels") using the RPC. The sensitivity of the WSF to changes in time to rupture was analyzed by random additions (or subtraction) of continuously distributed time constants leading to additional data scatter. The maximum time change was limited to a factor of two for each (base material) rupture point of the NIMS data set used. The changes affected the master curve directly influencing the corresponding weld strength values (through the RPC). The calculated WSF effects on the simulated strengths are presented in Table 13.

The predicted time to rupture values for the cross welds using this concept are presented in Fig. 31.

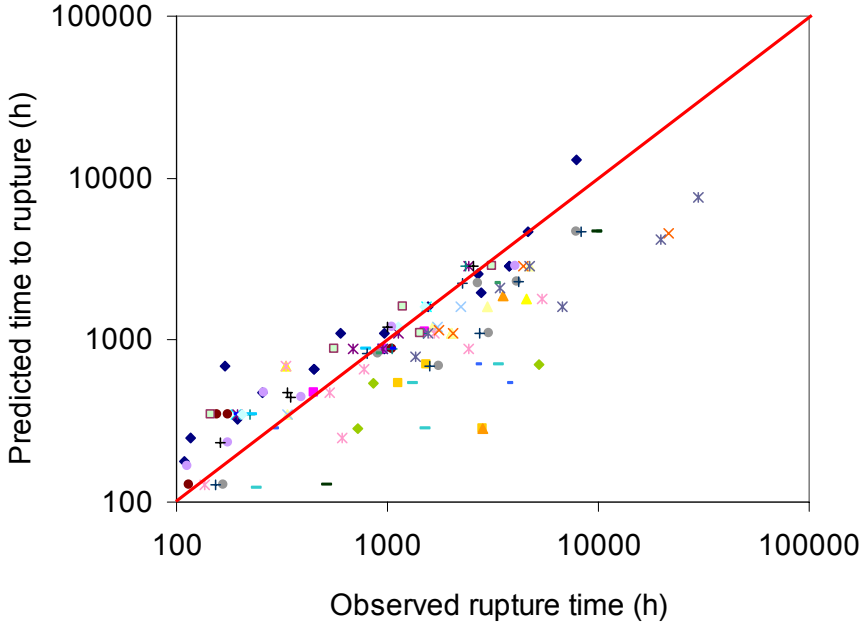

Fig. 31. Observed versus predicted time to rupture for P91 steel welds (XW) by using Wilshire equation for parent material (see Figs. 3–6) and RPC fitting for describing the XW ruptures. The data scatter factor for the weld data is 4.4.

Table 13. Monte-Carlo simulated (1000 simulations) WSF for rupture in 100 000 h for P91 steel with random changes in base material time to rupture.

Statistic	***575ºC***	**600ºC**
Max.	0.646	0.546
Min.	0.612	0.509
Mean	**0.629**	**0.528**
Std. Dev.	0.055	0.058

The WSF values calculated here are somewhat larger than those predicted for 100 000 h / 600ºC in the thesis Paper II, namely 0.48. The discrepancy is related to chosen base material master curve and the base material data used. In Paper II, the base material master curve was fitted to the standard 10, 100 and 250 kh rupture tables in the full temperature range described by the standard. To check for sensitivity to changes in the parameters *R* and $log(t_p)$ 10 000 random simulations were performed with ±10% variation to the parameters (triangular distributions). The results are presented in Table 14.

Table 14. Monte-Carlo simulated (1000 simulations) WSF for random changes in the R (10%) and $\log(t_p)$ (10%) parameter at 600°C / 100 000 h for P91 steel.

Statistic	$\Delta R = \pm 10\%$	$\Delta \log(t_p) \pm 10\%$
Max.	0.573	0.565
Min.	0.483	0.505
Mean	**0.527**	**0.531**
Std. Dev.	0.026	0.018

The results indicate that the standard deviations for the predicted WSF are smaller than for the case with induced time scatter. It could be claimed that the model indeed produces robust WSF predictions.

4. Creep strain modeling

Creep strain sets design limits for many components in power engineering, such as for blading, bolts and casings of steam and gas turbines. In addition, creep strain is also an important quantity to be followed for the fit-for-service inspections and follow ups of critical power plant components. The typical recommended limits range up to 1–2% of strain. However, measuring local strain and predicting it, in critical locations is not a simple task. The on-line monitoring equipments have today evolved to perform well, for instance, in the measurement of thick-walled high temperature components, but they are expensive and are of course not standard equipment in new installations. Also, the challenge would be to know where the most critical locations are.

From the FEA point of view the main contributor that creep modeling is not done very frequently is the short supply of relevant creep data and/or parameters for existing (implemented) creep routines. In comparison to creep rupture data, there is much less creep strain data available (especially in the public domain). Even for the commonly well established engineering steels such as P22 (10CrMo9-10) there is very few sources of creep strain data to be found.

Even today creep strain based remaining life assessments are based on minimum creep rate by Norton and the Monkman-Grant relationship. In work by Evans [77], the degree of uncertainty of the Monkman-Grant relationship has shown to be significantly underestimated. The simple minimum strain rate based models do not take the primary and tertiary creep regimes into account and therefore predict considerably lower strains.

The more advanced models usually need large creep-strain data sets to optimize a large number of material parameters. Some models have up to a total of 26 fitting constants [78] for defining the strain response in the defined stress and temperature range! Some strain models are quite established, such as the Ω-method [79] and the 4θ-method [80]. In the ECCC project “Advanced creep” a

round robin was performed analyzing model equations in common use for creep deformation together with new approaches presented by the participating organizations (see Table 16). The assessors involved were from several international research and industrial organizations. In this context VTT presented a parametric strain model based on the Manson-Haferd and Grounes (Paper III of this thesis). The model was by far the simplest and also the one giving the best results in the whole range of strain predictions. The materials assessed by VTT were the P22 and P91 steels. The data sets represented single (P22) and multi cast data (P91), with continuous and interrupted creep strain measurements. The models were evaluated and reviewed for their effectiveness for various materials and practical applications.

The round robin recognized 3 approaches that defined all the models assessed:

1) Modeling individual creep curves and establishing curve model parameters
   $\Rightarrow$ determination of stress and temperature dependence of these model parameters (examples: Mod. theta, Mod. Omega, BJF and Li-Akulov)

2) Producing synthetic data from the raw data in certain coordinates $\varepsilon(T,\sigma, t)$
   $\Rightarrow$ parametric model fitting to synthetic data (examples: MHG and the modified Sandström model)

3) Producing synthetic data $\sigma(T, \varepsilon, t)$ from $\varepsilon(T,\sigma, t)$ raw data
   $\Rightarrow$ model fitting to synthetic data (examples: Mod. Graham-Walles and Bolton)

In addition to this the new strain model presented in this thesis (see thesis Paper II), the logistic creep strain prediction (LCSP) adds a new approach to this list.

4) Fitting shape functions to strain curves or tabled stress to specific strain/time values with the true time to rupture value as end point
   $\Rightarrow$ model complete when combing shape functions and time to rupture model.

From these the approaches the 2 and 3 were producing the best fit for both P22 single heat data and the P91 multi cast strain data sets (see Table 16 and

Table 17). Note that the LCSP was not available at the time so it has been added to the end of the tables for comparison. The outcome of the round robin was used as platform for the ECCC recommendations and guidance for the assessment of creep strain and creep strength data (ECCC recommendations, Vol. 5 Part Ib). The recommendations include a review and references of the strain models listed in Table 15.

Table 15. Review of the ECCC round robin strain models [9].

Model reference	Creep equation
Norton, (Norton, 1929)	$\dot{\varepsilon}_{f,min} = d_1 \exp(-Q/RT)\sigma^n$
Modified Norton	$\dot{\varepsilon}_{f,min} = b_1 \exp(-Q_B/RT)\sigma^n + c_1 \exp(Q_C/RT)\sigma^n$
Norton–Bailey	$\varepsilon_f = d_1\sigma^n t^p$
Bartsch	$\varepsilon_f = e_1 \exp(-Q_1/RT)\sigma \exp(-b_1\sigma)t^p$
(Bartsch, 1995)	$+ e_2 \exp(-Q_2/RT)\sigma \exp(b_2\sigma)t$
Garofalo, (Garofalo, 1965)	$\varepsilon_f = \varepsilon_t[1 - \exp(-b_1 t)] + \dot{\varepsilon}_{f,min} t$
Modified Garofalo	$\varepsilon_f = \varepsilon_{f1}[1 - \exp(-g_1(t/t_{12})^u)$
(Granacher, *et al.*, 2001)	$+ \dot{\varepsilon}_{f,min} t + c_{23}(t/t_{23})f]$
BJF	$\varepsilon_f = n_1[1 - \exp(-t)]^\beta + n_2 t$
(Jones and Bagley, 1996)	where $t = (\sigma/A_1)^n \exp(-Q/RT)$
Li–Akulov model	$\varepsilon_f = \frac{\dot{\varepsilon}_{f,min}}{k} \ln\left(1 + \frac{\dot{\varepsilon}_i - \dot{\varepsilon}_{f,min}}{\dot{\varepsilon}_{f,min}}(1 - \exp(-kt))\right) + \dot{\varepsilon}_s t$
(Li, 1963; Akulov, 1964)	$+ \varepsilon_T(\exp(t/t_t) - 1)$
Theta	$\varepsilon_f = \theta_1[1 - \exp(-\theta_2 t)] + \theta_3[\exp(\theta_4 t) - 1]$
(Evans and Wilshire, 1985)	where $\log(\theta_i) = a_i + b_i T + c_i\sigma + d_i\sigma T$
Modified Theta	$\varepsilon_f = \theta_1[1 - \exp(-\theta_2 t)] + \theta_m t + \theta_3[\exp(\theta_4 t) - 1]$
	where $\theta_m = A\sigma^n \exp(-Q/RT)$
Graham–Walles	$\varepsilon_f = at^{1/3} + dt + ft^3$
(Graham and Walles 1955)	
Modified Graham–Walles	$\dot{\varepsilon}_f = e^{(Q_1/T)} 10^{A_1} \left(\frac{\sigma(1+\varepsilon)}{1+\omega}\right)^{n_1} \varepsilon^{m_1}$
	$+ e^{(Q_2/T)} 10^{A_2} \left(\frac{\sigma(1+\varepsilon)}{1+\omega}\right)^{n_2}$
	where $\dot{\omega} = e^{(-QD/T)} 10^{AD}(\sigma(1+\varepsilon))^{nD}\varepsilon^{mD}$
Rabotnov–Kachanov	$\dot{\varepsilon} = \frac{h_1\sigma^n}{(1-\omega)}\dot{\omega} = \frac{k_1\sigma^v}{(1-\omega)^\zeta}$
(Kachanov, 1986)	
Dyson and McClean,	$\dot{\varepsilon}_f = \varepsilon_0^{\cdot}(1 + D_d)\exp(-Q/RT)\sinh\left(\frac{\sigma(1-H)}{\sigma_0(1-D_p)(1-\omega)}\right)$
(Dyson and McClean, 1998)	
Baker–Cane model	$\varepsilon_f = At^m + \varepsilon_p + \phi\varepsilon_s + \varepsilon_s(\lambda - \phi)\left[1 - \frac{t/t_u - \phi}{1-\phi}\right]^{\frac{1-\phi}{\lambda-\phi}}$
(Baker and O'Donnell, 2003)	where $I = \varepsilon_u/\varepsilon_s$, $\varepsilon_s = \dot{\varepsilon}_m t_u$ and $\phi = t_p/t_u$
Mech. E (CSWP, 1983)	$R_{u/t/T} = (a_1 + b_1/\varepsilon - c_1\varepsilon^2)R_{\varepsilon/t/T} + d_1 + e_1/\varepsilon + f_1/\varepsilon^2 - g_1\varepsilon^2$
Characteristic strain	$\varepsilon_f(\sigma) = \varepsilon(R_{u/t/T}/R_{\varepsilon/t/T} - 1)/(R_{u/t/T}/\sigma - 1)$
model (Bolton, 2005a)	
MHG model, (Grounes, 1969)	$t_\varepsilon = \exp(TF(\varepsilon, \sigma) + C)$ where the $F(\varepsilon,\sigma)$ function is
(Holmström and	freely selected from multilinear combinations of σ
Auerkari, 2004)	and ε with an optimised value of C
Omega, (Prager, 1995)	$\dot{\varepsilon}_f = \dot{\varepsilon}_{f,min}/(1 - \dot{\varepsilon}_{f,min}\Omega t)$
Modified Omega	$\varepsilon_f = \left(\frac{1}{\Omega} - \frac{1}{2C_{tr}}\right)(-\ln(t_u - t) + \ln(t_u))$
(Merckling, 2002)	$+ C_{tr}(1 - \exp(m_{tr}t))$

Table 16. Scatter factors Z for the ECCC round robin strain models for steel P22 (single heat data). P/S/T = primary / secondary / tertiary. In brackets the number of free parameters in the model.

Model equation	***Creep regimes***	***Z for time to specified strain (all temperatures)***				
		0.2%	**0.5%**	**1%**	**2%**	**5%**
Omega model	S/T (8)	468	39	10	-	-
BJF model	P/S	15	6	4	-	-
Theta model	P/S/T	17	3	2	-	-
Modified Theta model	P/S/T	10	-	4	-	-
Creep strength ratio model	P/S/T	4	8	7	-	-
NPL model	P/S/T	12	7	3	-	-
Baker-Cane model	P/S/T	5		2	-	-
Bartsch model	P/S	3	2	4	-	-
Modified Garofalo	P/S/T (28)	2	2	2	-	-
Mod. Graham-Walles	P/S/T	3	3	2	2	2
Mod. Nadai	P/S/T (11)	3	2	2	2	2
MHG-4	**P/S/T (4)**	**3**	**3**	**3**	**3**	**3**
LCSP	**P/S/T(8[1])**	**3**	**2**	**2**	**2**	**2**

[1)] The $t_r(T,\sigma)$ parameters are not accounted for. Note that this model was not available at the time of the round robin.

Table 17. Calculated scatter factors Z for the assessed strain models for P91 steel (multi heat data set); P/S/T = primary / secondary / tertiary.

Model equation	Creep regimes	Z for time to specified strain (all temperatures)				
		0.2%	**0.5%**	**1 %**	**2%**	**5%**
BJF model	P/S	113	104	50	32	11
Modified Theta model	P/S/T	74	19	17	8	12
Li & Akulov	P/S/T	143	42	18	6	4
Modified Omega	S/T	138	19	11	8	5
Creep strength ratio model	P/S	38	7	7	6	5
Modified Sandström	P/S/T	11	7	6	6	6
Mod. Graham-Walles	P/S/T	7	7	6	7	5
MHG	**P/S/T**	**6**	**7**	**6**	**6**	**5**

4.1 Manson-Haferd-Grounes (MHG) strain model – engineering tool for creep strain prediction

The Manson-Haferd-Grounes model (MHG) is defined in depth in [81]. The main features are the simple method of predicting time to specific creep strain by assuming a parametric relationship (here Manson-Haferd) and that the creep mechanism remains the same following an Arrhenius type of temperature behavior. In addition it is assumed that the microstructural change (creep damage) can be related to the accumulated strain.

The MHG parameter is defined as:

$$MHG = [\ln(t_\varepsilon)-C]/T = F(T,\sigma,\varepsilon), \qquad \textit{Eq. 22}$$

where C is a constant, t_ε is the time to strain and $F(T,\sigma,\varepsilon)$ is a multi-linear combination of temperature T, stress σ and strain ε.

The MHG has mainly been tested for linear combinations of the following form:

$$[\ln(t_\varepsilon)-C]/T = a0+a1\cdot\ln(\sigma)^x+a2\cdot\ln(\varepsilon)^y \,, \qquad \textit{Eq. 23}$$

where *a0, a1, a2, x* and *y* are fitting constants. The *x* and *y* are low non-negative integers. The MHG parameters for P91 and P22 steels are given in Table 18. The MHG strain model for P22 steel is shown in Fig. 32.

Table 18. MHG strain functions for P22 and P91 steel.

Material	***Fitting constants***
P22	$[\ln(t_\varepsilon)-55.62]/T = -33.2-0.95\cdot\ln(\sigma)^2-0.2\cdot\ln(\varepsilon)^2$
P91	$[\ln(t_\varepsilon)-77.25]/T = -54.064-1.048\cdot\ln(\sigma)^2-0.0294\cdot\ln(\varepsilon)^3$

The results suggest that the MHG model performs well and is robust with minimal number of fitting constants. The approach is theoretically applicable with both constant stress and constant load creep tests. Although the MHG model performed better than many of the other complex models (Table 16 and 17), some room for further improvement is possible, as is seen from the apparent systematic S-shaped trend in the PAT2 type prediction effectiveness plot for the multicast P91 data set (see Fig. 33).

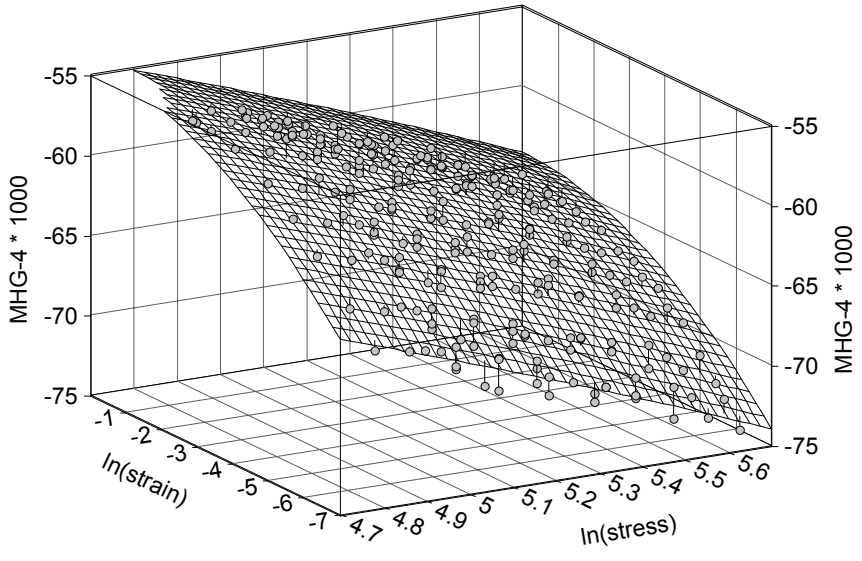

Fig. 32. Fitted MHG-4 master curve surface for P22 steel (single heat data).

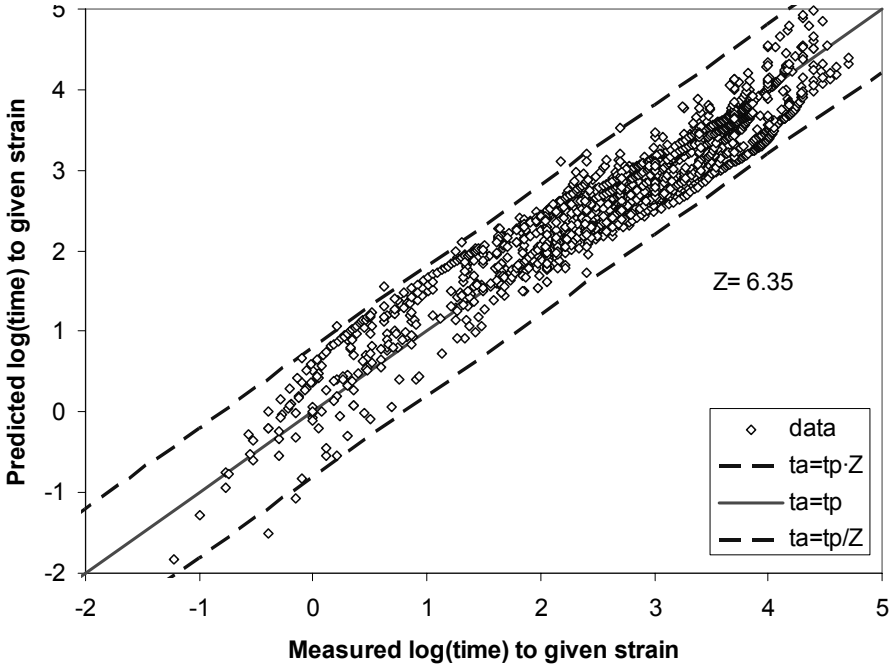

Fig. 33. PAT2 presentation for time to strain (MHG fitted) for multi heat P91 steel data.

The main observation from working with the parametric creep strain model MHG was that the parametric approach works surprisingly well but it could be further improved by a relationship to the curve end point (time to rupture). This observation was in fact the starting point of the development for the rupture based creep strain model LCSP described below.

4.2 Logistic Creep Strain Prediction (LCSP) – engineering tool for robust creep strain prediction

The logistic creep strain prediction (LCSP) model is a creep strain prediction tool able to predict representative creep strain curves and strain rates in a large stress and temperature range. The limits of the stress/temperature are set by the available creep rupture data for the material in question. This is made possible with the help of actual (fitted to existing strain data) or assumed "shape" functions together with the time to rupture prediction. The best result in time to strain or strain at specified time is of course attained using the actual (true) rupture

time of the individual creep curve. In extrapolation, or when data is missing the true rupture time is replaced by the master curve prediction for rupture.

The LCSP can be regarded as a further development of the MHG parametric models. The TTP based strain models were giving good fits and the incorporation of the "end points", namely the rupture time gives an advantage in comparison to many other equations. The method introduces a transition in a temperature compensated time parameter (P_{LM}) as a function of creep strain at specified temperature and stress. The P_{LM} parameter calculated with time to strain instead of time to rupture changes as the strain accumulates from a parametric value of zero (small strain, short time) to a maximum value restricted by the rupture life and the LCSP parameter C (related to the Larson-Miller parameter C).

The LCSP function chosen for time to specified strain was the non-linear asymmetric transition function with a steepness regulated by two variables (p and x0, see Eq. 24). The reason for choosing this specific transition equation was due to its simple inverted form giving an algebraic solution for strain as a function of time (Eq. 25). This inverted form was again easy to differentiate to give strain rate at a specified time. Further differentiation and finding the root of the expression gave the minimum creep rate.
The LCSP equations for time to strain t_ε, strain at time ε_t and strain rate at specified time $\dot{\varepsilon}(t_\varepsilon)$ are:

$$\log(t_\varepsilon) = \frac{\log(t_r) + C}{1 + (\frac{\log(\varepsilon)}{x_0})^p} - C, \qquad \textit{Eq. 24}$$

$$\log(\varepsilon_t) = \left(\frac{\log(t_r) + C}{\log(t_\varepsilon) + C} - 1 \right)^{1/p} \cdot x_0, \qquad \textit{Eq. 25}$$

$$\dot{\varepsilon} = -\varepsilon \cdot k_1 \cdot k_2 \cdot x_0, \qquad \textit{Eq. 26}$$

where t_r is the time to rupture and x_0, p and C are fitting factors. In its simplest form the last three are constants. The factors k_1 and k_2 are functions of time to strain. For the material models presented in this thesis the factors x_0 and p are in all cases temperature and stress dependent multi-linear functions of the form:

$$x_0 = x_1 + x_2 \cdot \log(\sigma) + x_3/(T+273) \text{ and} \qquad \textit{Eq. 27}$$

$$p = p_1 + p_2 \cdot \log(\sigma) + p_3/(T+273), \qquad \textit{Eq. 28}$$

where x_i and p_i are constants.

By knowing the time to rupture and the material specific shape parameters p, x_0 and C, the whole creep curve at any temperature and stress (within the limits of allowable extrapolation) can be determined.

Inversely it would be possible to predict time to rupture by knowing only one time to strain point on the strain curve (and again the material specific parameters p and x_0). This feature was used for estimating rupture times for unfailed OFP copper creep tests in the thesis Paper V. It was found that for this material the straight usage of the inverse LCSP gave very different values than straight forward rupture modeling, and that the strain rate at the specified time was a better descriptor. The reason to this is in the very inexact determination of the initial strain and the amount of actual creep strain accumulated at the specified test time, since the OFP copper is tested at stresses within or just at the border of power law break-down, causing significant plastic straining.

The values of the shape function constants for the steels assessed are presented in Table 19 and the calculated values at 560ºC / 100 MPa are given in Table 20. In Table 21 the shape functions for the OFP copper are in normalized stress form as is needed for the Wilshire rupture equation. An example of minimum strain rate comparison is shown in Fig. 34 for X20 steel.

Table 19. Shape parameters (see *Eq. 27* and *Eq. 28*) for selected ferritic steels.

Material	x_1	x_2	x_3	p_1	p_2	p_2	C
P22	-0.391	0.696	-3392.5	4.363	-2.271	3874.9	3.5
P23	4.21	0.696	-7860	14.3	-2.271	-4829	3.5
P91	-2.24	1.37	-3170	4.21	-7.27	14200	3.5
0.5CMV	-6.09	3.02	-3150	-25.2	4.89	18400	4.64
X20	3.04	3.64	-11900	12.6	4.85	-13600	20

Table 20. Calculated shape parameters at 560ºC / 100 MPa.

Material	$x_0(560,100)$	$p(560,100)$	*C*
P22	-3.072	4.473	3.5
P23	-3.834	3.961	3.5
P91	-3.306	6.717	3.5
0.5CMV	-3.832	6.669	4.64
X20	-3.966	5.973	20

Table 21. Shape functions x_0 and p for OFP copper (σ in MPa, T in °C), C=3.5.

Shape function factors for OFP copper
$x_0(\sigma/\sigma_{TS}, T) = -2.179 + 4.397\cdot\ln(\sigma/\sigma_{TS}) - 0.008\cdot T$
$p(\sigma/\sigma_{TS}, T) = 7.235 + 0.460\cdot(\sigma/\sigma_{TS})/\ln(\sigma/\sigma_{TS}) - 0.012\cdot T$

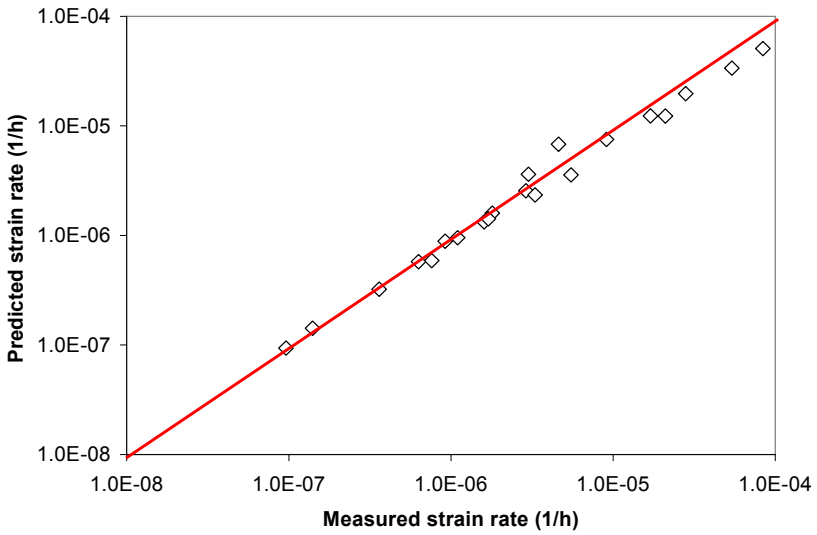

Fig. 34. LCSP predicted minimum creep rates for X20 (12CrMoV 11-1) steel against measured creep rates.

5. Multi-axial creep strain and damage

Structures operating in the creep regime will consume their creep life at a greater rate in locations where triaxiality constraint is unfavorable. Many structures develop different multi-axial stress states during creep related to their shape and dimensions. In addition discontinuities such as welds introduce multiple material zones with differing microstructures and material properties. These are also the locations where creep damage is found in service.

The solution of complex creep problems requires a method for handling multi-axial stresses and strains. The classical approach for describing the multi-axial stress state has been the von Mises yield criterion and its associated flow rule. It was, however, shown in the 60s [82] that the von Mises criterion underestimated creep for some cases in comparison to available data. This was corrected by introducing the general model of correlating damage under uniaxial tension with damage under more complex conditions by adopting an equivalent stress. Therefore, most early works on multi-axial long-term strength assessments are based on the equivalent stress. The equivalent stress concept is governed either by the maximum principal stress or by the von Mises effective stress. Generally it has been assumed that (macroscopically) the Von Mises effective stress controls creep deformation while maximum principal stress governs creep void formation (creep damage). Several other (mixed) components of stress have been proposed to describe the multiaxial rupture criterion [83], [84].

For structural integrity assessments, the calibration of the multi-axial material models has to be in place. This means that the multi-axial creep stress rupture criterion and/or the multi-axial creep ductility should be determined. For this purpose the notched-bar test programs [85] or maximum constraint testing (using compact tension specimens) is valuable. The best tests to gain confidence in the established models are naturally large scale component tests successfully modeled without any model calibration.

The influence of creep life and ductility exhaustion under multi-axial conditions are implemented in some design codes [86], [87] but the implementation for life management and remaining life predictions of service exposed components is not yet satisfactorily solved. The work done with the FEA strain model implementation together with the multi-axial strain exhaustion filter described below is a sincere attempt to change this.

5.1 Engineering tool – multi-axial LCSP for FEA

The creep strain rate formulation is based on the logistic creep strain prediction (LCSP) model implemented to ABAQUS, including primary, secondary and tertiary creep.

5.1.1 The FEA COMSOL implementation

For the COMSOL FE implementation the multi-axial LCSP creep strain rate expression has been attained from *Eq. 26* by using a von Mises type flow rule and by deriving the expression for multi-axial creep strain rate (strain rate tensor) as follows:

$$\dot{\varepsilon}_{ij} = f(\varepsilon_u) \cdot (\delta\alpha_1 + \delta\alpha_2\beta(T) + \frac{3}{2}\alpha_3 \cdot s_{ij}), \qquad \textit{Eq. 29}$$

where the first $f(\varepsilon_u)$ is a function of the uniaxial LCSP model, δ, α_i are constants, β(T) a function of temperature and s_{ij} is the deviatoric stress tensor.

The FE implementation itself is formulated using a mixed FE approach for the strain rate and solution of the balance equations using the weighted Galerkin method. The FE equations are interpolated adaptively varying the order of polynomic interpolation basis from 2 to 5. Time integration of the rate equations is carried out using an implicit back differentiation routine, with variable step-size and order.

The first versions of the LCSP implementation were used for determining creep damage in a simple girth welded pipe in the thesis Paper VI. Today the model implementation has been upgraded considerably and can now be used in more demanding case studies such as creep damage accumulation at defects and creep crack initiation predictions for compact tension (CT) specimen. In Fig. 35 a friction stir weld (FSW) test specimen (∅ 8 mm) with a weld root defect has

been simulated. The creep lives of the specimens taken from actual FSW welds are heavily reduced [18] in comparison to welds taken as cross-weld samples.

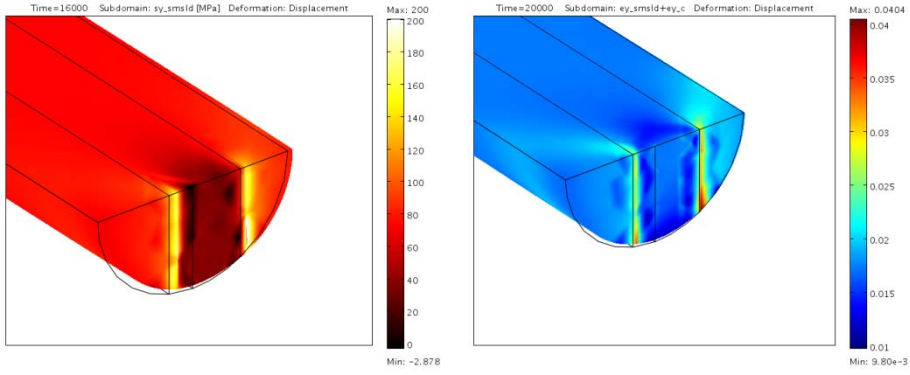

Fig. 35. Stress and strain state after 16 000 h of simulated creep testing (LCSP model) at nominal stress 80 MPa and 175ºC for a friction stir welded OFP copper creep specimen with a centrally located root defect.

5.1.2 The FEA ABAQUS implementation

For the ABAQUS implementation the LCSP model was implemented in its strain rate form, utilizing the CREEP user subroutine [88] and the Euler backward algorithm. The implementation is defined closer in the thesis Paper VII.

5.2 Engineering tool – multi-axial exhaustion parameter

It is commonly known that for long-term creep of pressure vessels the maximum equivalent stresses and strains develop on the inner vessel surface whereas the maximum principal stress will redistribute towards the outer surface due to creep. The multi-axial creep ductility (due to the triaxiality constraint) will reduce towards the outer surface as creep proceeds under long-term service. To be able to visualize this, a technique for filtering the acquired FE strains and stresses has been developed. The expression for rigid plastic deformation was used as a basis for the Λ-filtering technique (see *Eq. 30* and *Eq. 31*). The equations and their background are defined in the thesis Paper VII.

The Λ-filter is defined as:

$$\Lambda = \frac{\varepsilon}{1.65 \cdot \exp(-1.5 \cdot h)} = \frac{\varepsilon_{fu}}{\varepsilon_{fm}} \cdot \varepsilon \qquad \textit{Eq. 30}$$

$$h = \left[\frac{\sigma_{kk}}{3 \cdot q} \right], \qquad \textit{Eq. 31}$$

where σ_{kk} is the trace of a stress tensor σ_{ij}, ε the accumulated strain (maximum principal or von Mises), ε_{fu} and ε_{fm} the multiaxial and uniaxial creep ductility, respectively.

The main benefit of the filtering technique is that it does not require local creep ductility values. The Λ parameter is expressed as a ratio dependent on stress and momentary strain only, thus, making the strain exhaustion a ductility dependent quantity. The same basic concept is going to be used for further planned development of the strain exhaustion parameter. An example of a Λ-filtered FEA result (3D) for a repair welded P22 steam mixer is shown in Fig. 36.

The weld repair was performed after 100 000 h in service to lengthen the life of the creep damaged component. The full assessment is presented in [20].

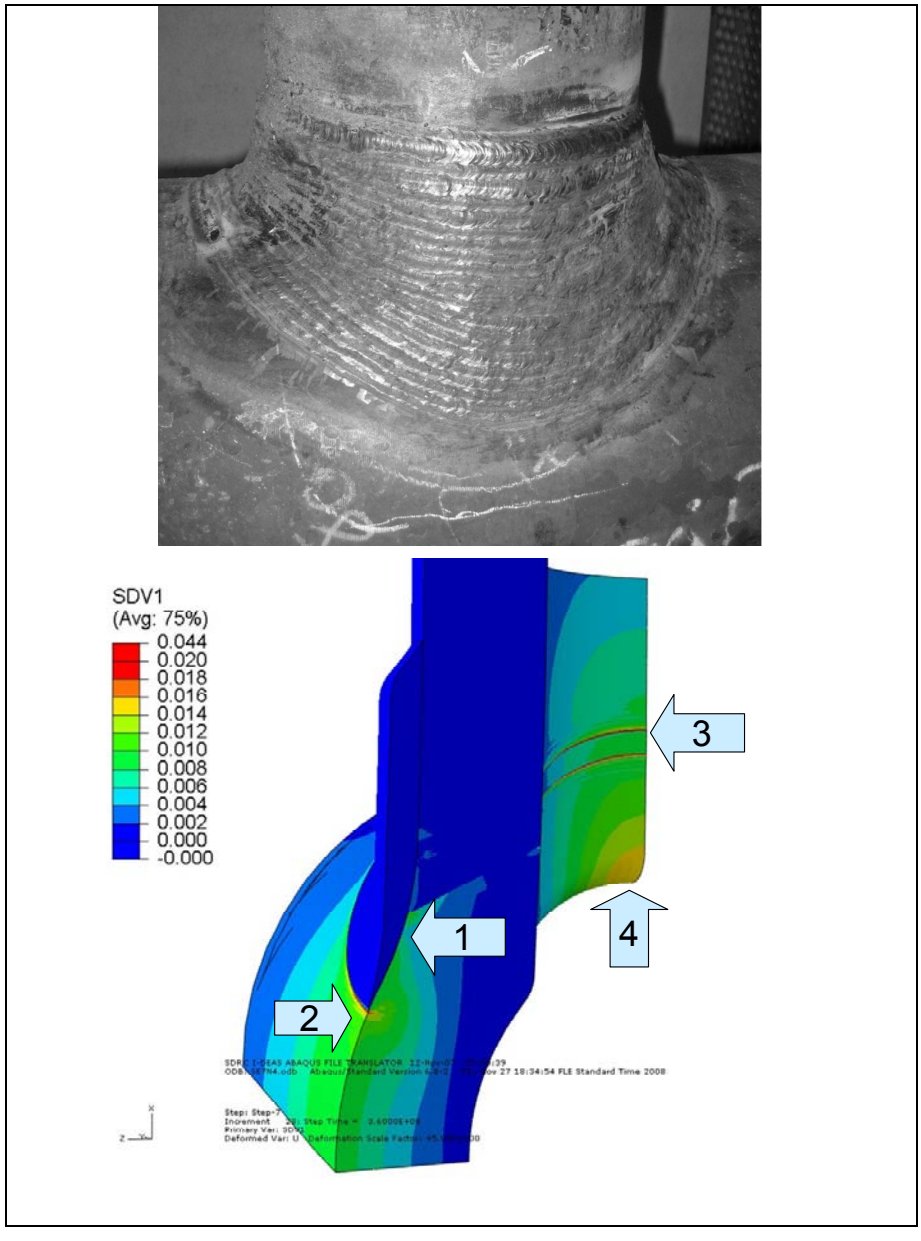

Fig. 36. Overlay weld repair and simulated continued service for additional 100 000 h service for a creep damaged P22 steam mixer nozzle. The marked arrows point to (1) location of creep cracking, (2) predicted new location of damage, (3) secondary potential damage location at inner HAZ and (4) location of maximum creep strain. SDV1 = Λ-filter.

6. Discussion

The models and methodologies presented give a rather complete set of tools for assessing the creep rupture and/or creep strain data sets. The tools have been verified for a number of ferritic steels and the OFP copper for nuclear waste disposal canisters.

The MHG strain formulation was the first successful attempt of describing the strain response by a TTP parameter. The excellent fitting accuracy acquired from simple TTP strain relation was unexpected. The further refinement of the TTP based strain models finally lead to the current form of the LCSP model. The "rupture based" strain model has the benefit of utilizing the "robustness" acquired in the rupture model to be transferred into the strain model. The fitting accuracy to the strain data has not been compromised in the cases where both MHG and LCSP have been tested.

The LCSP is well suited also for producing parameters for other models as well. For instance the Norton law parameters are easily extracted from the full predicted creep curves by localizing the time of minimum strain rate at varying stresses and temperatures (Fig. 36). It is to be seen that the stress parameter n is both stress and temperature dependent and the classically temperature dependent parameter A(T), here presented in logarithmic form logA(T), is in fact also clearly stress dependent. The activation energy Q_c, calculated both from minimum strain rate and rupture time, shows a very similar stress and temperature dependence as the Norton stress parameter (see Fig. 37).

The Omega method parameters widely used in the U.S [79], [89] are also easily extractable by linearization of the tertiary creep regime modeled with the LCSP.

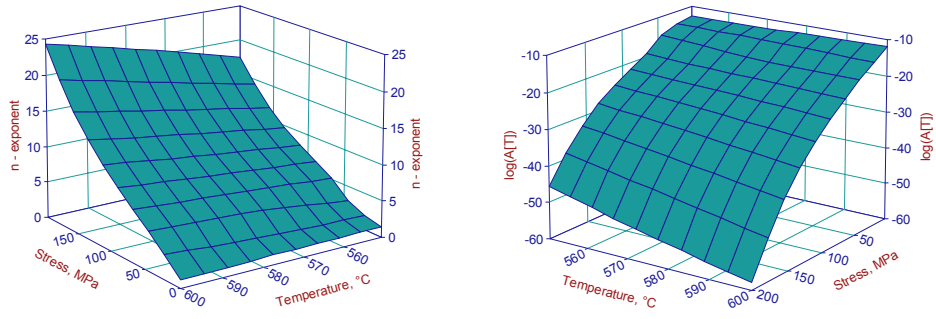

Fig. 37. Norton stress exponent *n* and the "temperature" dependent parameter *log(A[T])* calculated from LCSP minimum creep rates for P91 steel (550–600ºC).

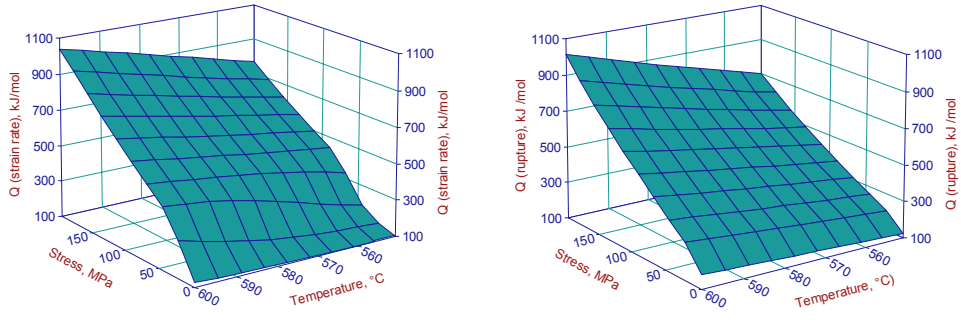

Fig. 38. Activation energies calculated from a) minimum creep rates and b) rupture times for P91 steel (550–600ºC).

The "robustness" of the LCSP as well as any rupture model attempted in this thesis is the result of extensive testing of the model, mainly comparing predicted versus true obtained values. The ECCC post assessment tests (PATs) together with the RPC engineering tool substantially lower the risk of ending up with an nonconservative model for rupture. Using the rupture time of a larger more equally distributed data set as basis (as the BM data usually is) instead of modeling separate master curve for weldments improves the robustness of WSF calculations. These tools optimally fitted and properly verified decrease the uncer-

tainty of the extrapolated values. This will in turn lead to less premature damage in high temperature applications.

The models and tools presented are by no means complete and, for instance, the further development of the physical relationships to the shape curves of the LCSP should be attempted. Also, additional flexibility of the strain response fitting curves could be accomplished by temperature and perhaps even stress dependence for the C parameter. Maybe the p or x_0 parameters could be turned into constants instead.

The LCSP applicability on the creep response of austenitic stainless steels should be investigated. A first step could be the SS 316 steel creep strain data assessed by ECCC.

The further assessment of OFP copper is also of great importance for the Finnish nuclear waste disposal scheme. The life predictions have been lowered at almost every step of data set updating or model refinement. The present life predictions should be further refined when knowledge of creep ductility from long-term tests is available. Today the longest test duration for the OFP copper data at VTT has reached 70 000 h with over 20% of accumulated creep strain. The intergranular cracking detected on the specimen surface is somewhat alarming, since the phosphorus doping has been believed to remove the ductility and creep cracking problems of pure oxygen-free copper.

As already mentioned earlier, the multi-axial damage parameter needs further tuning to become more physically correct. The relationship of creep damage with maximum principal stress, hydrostatic stress and von Mises stress should be investigated further. However, the concept of using normalized strain exhaustion as a filter can be applied with improved versions of the Λ-filter.

The Wilshire model is a very promising rupture (and perhaps minimum creep rate) model. The best feature of this model is the low amount of modeling parameters. Actually the only parameter that has to be determined is the apparent activation energy. Pre-determining the Q_c* gives scatter factors higher than optimal. The minimization of the scatter factor induces an offset to the linear function describing the parameters u and k (Fig. 39). The activation energy used has though a significant impact on the long-term (thousands of years) predictions of the copper canister.

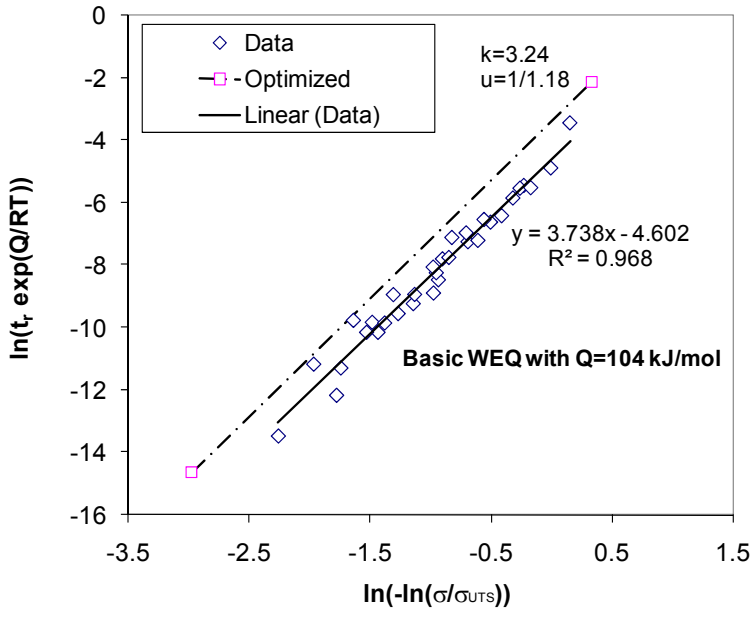

Fig. 39. Wilshire parameter u and k determination for OFP copper using basic equation format and optimized values minimizing the scatter factor Z.

7. Conclusions

Creep damage is unavoidably inflicted to materials stressed at high temperature, resulting in gradual strain accumulation and limited life. Suitable engineering tools are essential for satisfactory prediction of the creep performance in material development, design of components and structures, and life assessment of high temperature facilities.

In this thesis new tools have been described, tested and verified for accurate prediction of creep strain, damage and rupture for parent materials and welds of selected high temperature steels and OFP copper. The tools have been particularly designed aiming for reliability even when the background creep data sets are limited in size and scope.

The developed RPC and the LCSP methods can be used with the ECCC PATs to obtain robust creep strain and rupture models for parent materials and welds in the range of the test data up to the acceptable level of extrapolation. Comparison within the ECCC suggests that the MHG and LCSP models for creep strain response are superior in performance to most if not all previous and more complex models, while only requiring a minimal number of fitting constants. Using a similar rule for predicted time to creep strain as for time to rupture, the allowable extrapolation could be for example extended by introducing lower bound LCSP simulated synthetic data into a PD 6605 assessment that can utilize unfailed data. This could be applied together with the current time in the running tests to obtain the maximum likelihood prediction of time to rupture. This approach needs to be further verified with data from long-term creep (strain) testing.

The fact that the LCSP model makes use of the background rupture models has clear advantages. This improves the experimental support for the model, as there are generally much more rupture data than creep strain data for any given material. The strain model is also simple and allows for straightforward expressions for strain, strain rate and life fractions. The model can define the strain

response with only three parameters (two stress and temperature dependent) in addition to those in the rupture models.

The new rupture and strain models have been implemented to finite element analysis (FEA) codes. The performance of the multi-axial version of the LCSP model appears superior to conventional Norton law based simulations. Case studies on steels and OFP copper have demonstrated the stability and usability of the implemented models. Simulations of girth welds in 10CrMo9-10 (P22) and X10CrMoVNb9-1 (P91) steels have shown that the LCSP model is working smoothly in COMSOL and ABAQUS FEA with acceptable calculation times. The introduced multi-axial creep exhaustion parameter (Λ) was shown to pin-point the realistic damage locations in welded high temperature components, although the concept may also benefit from further physical modeling of creep damage.

In conclusion, using the new tools with appropriate materials modeling and implementation of numerical analysis, the creep response can be evaluated for both uniaxial and multi-axial loading with benefits in both accuracy of the results and efficiency in the analysis. Supporting creep data may be obtained from creep testing, materials standards and public domain sources. Ideally, relatively extensive data sets can be applied for this purpose, such as those from ECCC in Europe or NIMS in Japan. One of the main remaining sources of uncertainty is creep ductility, which is not well defined in most creep testing results.

8. Summary

The work done in this thesis has provided new simple yet well performing tools to predict creep strain and life for material evaluation, component design and life assessment purposes. The uncertainty related to selecting the type of material model or determining weld strength factors has been reduced by the selection procedures and by linking the weld behavior to the base material master equation. Much of the resulting improvements and benefits are related to the reduced requirements for supporting creep data. The simplicity and robustness of the new tools also makes them easy to implement for both analytical and numerical solutions.

The thesis includes creep rupture and strain models for several ferritic steels for high temperature applications. The steels assessed are P22, P23, P24, 0.5CMV, X20, P91 and E911. Also, OFP copper with required extrapolation to very long service life has been assessed for the foreseen repository conditions of nuclear waste canisters. Furthermore, multi-axial creep damage behavior modeled with the new tools has been verified and visualized for a welded ex-service component.

References

[1] Holmström, S. & Auerkari, P. Effect of short-term data on predicted creep rupture life – pivoting effect and optimised censoring. Materials at High Temperatures, Vol. 25 (2008), pp. 103–109.

[2] Holmström, S. & Auerkari, P. Predicting weld creep strength reduction for 9% Cr steels. International Journal of Pressure Vessels Piping, Vol. 83 (2006), pp. 803–808.

[3] Holdsworth, S. R., Askins, M., Baker, A., Gariboldi, E., Holmström, S., Klenk, A., Ringel, M., Merckling, G., Sandstrom, R., Schwienheer, M. & Spigarelli, S. Factors influencing creep model equation selection. International Journal of Pressure Vessels and Piping, Vol. 85 (2008) 1–2, pp. 80–88.

[4] Holmström, S. & Auerkari, P. Robust prediction of full creep curves from minimal data and time to rupture model. Energy Materials, Materials Science & Engineering for Energy Systems, Vol. 1 (2006), pp. 249–255.

[5] Holmström, S. & Auerkari, P. Predicting creep rupture from early strain data. Materials Science and Engineering: A, Vol. 510–511 (2009), pp. 25–28.

[6] Holmström, S., Laukkanen A. & Calonius, K. Finding critical damage locations by Λ-filtering in FE modelling of a girth weld. Materials Science and Engineering: A. Vol. 510–511 (2009), pp. 224–228.

[7] Holmström, S., Laukkanen, A., Rantala, J., Kolari, K., Keinänen, H. & Lehtinen, O. Modeling and verification of creep strain and exhaustion in a welded steam mixer. Journal of Pressure Vessel Technology, Vol. 131 (2009), 061405 (5 pages).

[8] EN 10216-2:2002+A2, 2007. Seamless steel tubes for pressure purposes - Technical delivery conditions - Part 2: Non-alloy and alloy steel tubes with specified elevated temperature properties.

[9] Abe, F., Kern, T.-U. & Viswanathan, R. (Eds). Creep-resistant steels. Abington Hall, Cambridge, England: Woodhead Publishing Ltd., March 2008. 700 p. ISBN 1 84569 178 4, ISBN-13: 978 1 84569 178 3.

[10] Kloos, K. H., Granacher, J. & Monsees, M. Creep equation for heat resistant steels. Steel Research, Vol 69 (1998), pp. 446–453.

[11] Kloos, K. H., Granacher, J. & Monsees, M. Optimization and verification of creep equations for heat resistant steels. Steel Research, Vol. 69 (1998), pp. 454–462.

[12] Holmström, S. & Auerkari P. Prediction of creep strain and creep strength of ferritic steels for power plant applications. International Conference on Life Management and Maintenance for Power Plants. Helsinki–Stockholm–Helsinki, 8–10 June 2004. Espoo: Technical Research Centre of Finland. VTT Symposium 234, Vol. 2, pp. 513–521.

[13] Holmström, S., Laukkanen A. & Calonius, K. Visualising creep exhaustion in a P22 girth weld. International Conference on Life Management and Maintenance for Power Plants. Helsinki–Stockholm–Helsinki, 12–14 June 2007. Espoo: Technical Research Centre of Finland. VTT Symposium 247, Vol. 2, pp. 208–221.

[14] Holmström, S., Auerkari, P. & Holdsworth S. Predicting creep strain response from rupture data and robust creep curve model. International Conference on Life Management and Maintenance for Power Plants. Helsinki–Stockholm–Helsinki, 12–14 June 2007. Espoo: Technical Research Centre of Finland. VTT Symposium 246, Vol. 1, pp. 185–195.

[15] von Hartrott, P., Holmström, S., Caminada, S. & Pillot, S. Life time prediction for advanced low alloy steel P23. Materials Science and Engineering: A, Vol. 510–511 (2009), pp. 175–179.

[16] Rantala, J., Auerkari, P., Holmström S., Salonen J. & Laukkanen, A. Creep strain, damage and life prediction for welded 0.5CMV steel. 2nd International ECCC Conference. Creep & Fracture in High Temperature Components – Design & Life Assessment. EMPA, Dübendorf, Switzerland, 21–23 April 2009, pp. 669–680.

[17] Auerkari, P., Holmström, S., Veivo. J. & Salonen J. Creep damage and expected creep life for welded 9–11% Cr steels. International Journal of Pressure Vessels and Piping, Vol. 84 (2007), pp. 69–74.

[18] Holmström, S., Auerkari, P. & Rantala, J. Engineering approach to creep strain modeling for multicast 9Cr steel. 11th Conference on Pressure Vessel Technology, ASME PVP 2006/ICPVT-11. Vancouver, BC, Canada 25–27 July 2006. American Society of Mechanical Engineers, ASME. 10 p.

[19] Auerkari, P., Holmström, S., Rantala, J. & Salonen, J. Creep damage, ductility and expected life for materials with defects. Proceedings of 2008 ASME Pressure Vessels and Piping Conference (PVP 2008). Chicago, Illinois, USA, 27–31 July 2008. PVP2008-61428.

[20] Holmström, S., Rantala, J., Kolari, K., Keinänen, H., Laukkanen, A., Veivo, J. & Lehtinen, O. Life prediction for a weld repaired steam mixer. 2nd International ECCC Conference. Creep & Fracture in High Temperature Components – Design & Life Assessment. EMPA, Dübendorf, Switzerland, 21–23 April 2009, pp. 309–319.

[21] Frost, H. J. & Ashby, M. F. Deformation Mechanism Maps. Oxford: Pergamon, 1982.

[22] Sandström, R., Andersson, H.C.M., Creep in phosphorus alloyed copper during power-law breakdown. Journal of Nuclear Materials, Vol. 372 (2008), pp. 76–88.

[23] Wilshire, B. & Bache, M. B. Cost effective prediction of creep design data for power plant steels. Proceedings of the ECCC Creep Conference. Creep & Fracture in High Temperature Components - Design and Life Assessment Issues. Zürich, Switzerland, 21–23 April 2009. Lancaster, Pa: DEStech Publications, Inc, 2009. ISBN 978-1-60595-005-1.

[24] NIMS Atlas of creep deformation property No. D-1, Creep deformation properties of 9Cr-1Mo-V-Nb steel tubes for boiler and heat exchangers, 2007.

[25] Evans, M. Critical review and appraisal of traditional and new procedures for the qualification of creep fracture behaviour using 1Cr-1Mo-0.25V steel. Journal of Engineering Materials and Technology, Vol. 131 (2009), 021011 (14 pages).

[26] EN 10291:2000. Metallic materials – Uniaxial creep testing in tension – Method of test.

[27] EN ISO 7500-2: 2000. Metallic materials. Verification of static uniaxial testing machines. Part 2: Tension creep testing machines. Verification and calibration of the force-measuring system.

[28] Granacher, J., Oehl, M. & Preussler, T. Comparison of interrupted and uninterrupted creep rupture tests. Steel Research, issue No. 1/92 (1992), pp. 39–45.

[29] EN 10216-2:2002+A2. Seamless steel tubes for pressure purposes – Technical delivery conditions – Part 2: Non-alloy and alloy steel tubes with specified elevated temperature properties.

[30] Standard Data tables Vol. 2, Ferritic steels, SPRINT Specific project SPI-249, Implementation of Power Plant Component Life Assessment Technology Using a Knowledge-based system, 1995.

[31] Holdsworth, S. The European Creep Collaborative Committee (ECCC) approach to creep data assessment. Journal of Pressure Vessel Technology, Vol. 130 (2008), 024001 (6 pages).

[32] von Hartrott, P. & Holmström, S. Lebensdauermodelle für den fortschrittlichen Stahl P23. 31. Vortragsveranstaltung der Arbeitsgemeinschaft für warmfäste Stähle und der Arbeitsgemeinschaft für Hochtemperaturwerkstoffe. 28 Nov. 2008. Düsseldorf, Germany: Stahlinstitut VDEh, 2008, pp. 27–36.

[33] EN-SFS 10319-1:2003. Metallic materials. Tensile stress relaxation testing. Part 1: Procedure for testing machines.

[34] EN-SFS 10319-2:2006. Metallic materials. Tensile stress relaxation testing. Part 2: Procedure for bolted joint models.

[35] De Bruycker, E., Kaustermans, J-P. & Huysmans, S. Stress relaxation testing as an alternative to Conventional Creep Rupture testing. 2nd International ECCC Conference. Creep & Fracture in High Temperature Components – Design & Life Assessment. EMPA, Dübendorf, Switzerland, 21–23 April 2009.

[36] Steen M., Creep life assessment by low strain rate tensile testing. International Journal of Pressure Vessels and Piping Vol.14 (1983), Issue 4, pp. 201–225.

[37] Penttilä, S., Toivonen, A., Heikinheimo, L. & Novotny, R. SCC properties and oxidation behaviour of austenitic alloys at supercritical water conditions. 4th International Symposium on Supercritical Water-Cooled Reactors. Heidelberg, Germany, 8–11 March 2009. 16 p.

[38] Sun, E., Hyde, T. H. & Brett, S. J. Application of impression creep data in life assessment of power plant materials at high temperatures. Proceedings of the Institution of Mechanical Engineers, Part L: Journal of Materials: Design and Applications, Vol. 222 (2008) 3, pp. 175–182.

[39] Hyde, T. H., Sun, W. & Becker, A. A. Analysis of the impression creep test method using a rectangular indenter for determining the creep properties in welds. International Journal of Mechanical Sciences, Vol. 38 (1996) 10, pp. 1089–1102.

[40] Tu, S.-T., Segle, P. & Gong, J. M. Creep damage and fracture of weldments at high temperature. International Journal of Pressure Vessels and Piping, Vol. 81 (2004) 2, pp. 199–209.

[41] Hyde, T. H., Yehia, K. A. & Becker, A. A. Interpretation of impression creep data using a reference stress approach. International Journal of Mechanical Sciences, Vol. 35 (1993) 6, pp. 451–462.

[42] Blagoeva, D. T. & Hurst, R. C. Application of the CEN (European Committee for Standardization) small punch creep testing code of practice to a representative repair welded P91 pipe. Materials Science and Engineering: A, Vol. 510–511 (2009) June, pp. 219–223.

[43] CEN Workshop Agreement, CWA 15627:2006 E, “Small Punch Test Method for Metallic Materials”. CEN, Brussels, Belgium, December 2006.

[44] Webster G. A., Holdsworth, S. R., Loveday, M. S., Nikbin, K., Perrin, I. J., Purper, H., Skelton, R. P. & Spindler, M. W. A Code of Practice for conducting notched bar creep tests and for interpreting the data. Fatigue & Fracture of Engineering Materials & Structures, Vol. 27 (2004) 4, pp. 319–342.

[45] Besson, J., Leclercq, S., Gaffard, V. & Gourgues-Lorenzon, A.-F. Analysis of creep lifetime of a ASME Grade 91 welded pipe. Engineering Fracture Mechanics (2009), Vol. 76, pp. 1460–1473.

[46] Holdsworth, S. R. & Merckling, G. ECCC developments in the assessment of creep-rupture data. In: Proceedings of Sixth International Charles Parsons Conference on Engineering Issues in Turbine Machinery, Power Plant and Renewables. Trinity College, Dublin, 16–18 September 2003.

[47] ECCC Recommendations. Creep data validation and assessment procedures. In: Holdsworth, S. R. et al. (Eds.) ECCC Publication (a) Vol. 1: Overview, (b) Vol. 2: Terms and terminology, (c) Vol. 3: Data acceptability criteria, data generation, (d) Vol. 4: Data exchange and collation, (e) Vol. 5: Data assessment, (f) Vol. 6: characterisation of microstructure and physical damage for remaining

life assessment, (g) Vol. 7: Data assessment - creep crack initiation, (h) Vol. 8: Data assessment – multi-axial, (i) Vol. 9: Component assessment.

[48] BS PD 6605. Guidance on methodology for assessment of stress-rupture data. London, UK: British Standard Institution, 1998.

[49] Fehér, A., Linn, S., Schwienheer, M., Scholz, A. & Berger, C. An interactive approach to creep behavior modeling. Materials Science and Engineering: A, Vol. 510–511 (2009), June, pp. 29–34.

[50] Goldhoff, R.M. Journal of Testing and Evaluation. Vol. 2 (1974), pp. 387–424.

[51] Manson, S. S. & Ensign C. R.. Interpolation and extrapolation of creep rupture data by the minimum commitment method. Part I, Focal point convergence. Pressure Vessel & Piping Conference, Montreal (1978), pp. 299–398.

[52] Trunin, I.I., Golubova, N.G. & Loginov, E.A. New method of the extrapolation of creep-test and long-time strength results. Proc 4th Int Symp on Heat-Resistant Metallic Materials, Mala Fatra, CSSR (1971), pp. 168–176.

[53] Norton, F. N. The Creep of Steel at High Temperature. New York: McGraw-Hill, 1929.

[54] ECCC Data sheets, issue 2005. Creep rupture data sheet for E911 (X11CrMoWVNb9-1-1), assessed 2005. European Technology Development Publishers, 2005.

[55] ECCC Data sheets 2005. Creep rupture data sheet for P91 (X10CrMoVNb9-1), assessed 1995. European Technology Development Publishers, 2005

[56] ECCC Data sheets 2009. Creep rupture data sheet for P91 (X10CrMoVNb9-1) Released in the near future.

[57] Maruyama, K. & Yoshimi, K. Influence of data analysis method and allowable stress criterion on allowable stress of Gr.122 heat resistant steel. Trans ASME, Journal of pressure vessel technology, Vol. 129 (2007), pp. 449–453.

[58] Kimura, K., Sawada, K. & Kushima, H. Influence of stress on creep deformation properties of 9–12Cr ferritic creep resistant steels. 34th MPA-Seminar and VGB-Symposium “Materials and Components Behaviour in Energy & Plant Technology”, Stuttgart, 9–10 October 2008.

[59] Maruyama, K., Ghassemi Armaki, H., Chen, R.P., Yoshimi, K., Yoshizawa, M. & Igarashi, M. Cr-concentration dependence of overestimation of long-term creep life in strength enhanced high Cr ferritic steels. Proceedings of the ECCC Creep Conference. Creep & Fracture in High Temperature Components - Design and Life Assessment Issues. Zürich, Switzerland, 21–23 April 2009. Lancaster, Pa: DEStech Publications, Inc, 2009. ISBN 978-1-60595-005-1.

[60] Spindler, S.L & Baker, A.J. Creep deformation and rupture of ½Cr½Mo¼V parent material. British Energy, AGR Power Stations report E/TSK/AGR/5516. May 2008.

[61] Bendick, W. Entwicklung von Zeitstandschäden in den Stählen X10CrMoVNb9-1 (P91) und X20CrMoV12-1, Bericht zum Forschungsvorhaben VGB-Nr 160. Untersuchungsbericht 35/1999.

[62] Bendick, B., Gabrel, J., Hahn, B. & Vandenberghe, B. New alloy heat resistant ferritic steels T/P23 and T/P24 for power plant application. International Journal of Pressure Vessels and Piping, Vol. 84 (2007) 1–2, pp. 13–20.

[63] Seitisleam, F., Andersson H. & Lindblom, J. Creep of copper for nuclear waste containment – results of creep and tensile tests on Cu-OF and Cu-OFP, cathode copper and welded joints. Swedish Institute for Metals Research, IM-3327, Feb. 1996.

[64] Lindblom, J., Henderson, P. & Seitisleam F. Creep testing of oxygen-free phosphorus copper and extrapolation of the results. Swedish Institute for Metals Research, IM-3197, Feb. 1995.

[65] Sandström, R. & Andersson, H. The effect of phosphorus on creep in copper. Journal of Nuclear Materials, Vol. 372 (2008), pp. 66–75.

[66] Yao, X. & Sandström, R. Study of creep behavior in P-doped copper with slow strain rate tensile tests. SKB Technical Report, TR-00-09, 2000.

[67] Andersson, H., Seitisleam, F. & Sandström R. Creep testing of thick-walled copper electron beam and friction stir welds at 75, 125 and 175°C. SKB Technical report TR-05-08, Jan 2005

[68] Auerkari, P., Holmström, S., Veivo, J., Salonen, J., Nenonen, P. & Laukkanen, A. Uniaxial and multi-axial creep testing of copper. Swedish Nuclear Power Inspectorate. SKI Report 2003:06.

[69] Auerkari, P., Holmström, S. & Salonen, J. Creep and creep damage in copper under uniaxial/multi-axial loading. Swedish Nuclear Power Inspectorate. SKI Report 2003:29.

[70] Auerkari, P., et al., Effects of defects on low temperature creep of OFP copper. 2nd International ECCC Conference. Creep & Fracture in High Temperature Components – Design & Life Assessment. EMPA, Dübendorf, Switzerland, 21–23 April 2009.

[71] Sandström, R. & Andersson, H.C.M. The effect of phosphorus on creep in copper. Journal of Nuclear Materials, Vol. 372 (2008) 1, pp. 66–75.

[72] Raiko, H. Disposal canister for spent nuclear fuel – design report. Posiva 2005-2, ISBN 951-652-134-7.

[73] Francis, J. A., Mazur, W. & Bhadeshia, H.K D.H. Type IV cracking in ferritic power plant steels. Materials Science and Technology, Vol. 22 (2006) 12, pp. 1387–1395.

[74] Wilshire, B. & Scharning, P. J. Creep ductilities of 9–12% chromium steels. Scripta Materialia, Vol. 56 (2007), pp. 1023–1026.

[75] Kimura, K., Kushima, H. & Sawada, K. Long-term creep deformation property of modified 9Cr–1Mo steel. Materials Science and Engingeering: A, Vol. 510-511 (2009), June, pp. 58–63. doi:10.1016/j.msea.2008.04. 095.

[76] Spindler, M. W. & Spindler, S. L. Creep deformation, rupture and ductility of Esshete 1250. International Journal of Pressure Vessels and Piping, Vol. 85 (2007) 1–2, pp. 89–98. doi:10.1016/j.ijpvp.2007.06.004.

[77] Evans, M. Some interpolative properties of the Monkman-Grant empirical relation in steel tubes. International Journal of Pressure Vessels and Piping, Vol. 72 (1997) 3, August, pp. 177–191.

[78] Granacher, J., Möhlig, H., Schwienheer, M. & Berger, C. Creep equations for high temperature materials. Proceedings of Seventh International Conference on Creep and Fatigue at Elevated Temperatures (CREEP 7). NRIM, Tsukuba, 3-8 June 2001. Tokyo: The Japan Society of Mechanical Engineers, pp. 609–616.

[79] Prager, M. Development of the MPC Omega method for life assessment in the creep range. ASME Journal of Pressure Vessel Technology, Vol. 117 (1995) May, pp. 95–103.

[80] Evans, M. Combining predictions in a simplified 4Θ methodology for creep life assessment: an application to 2Cr-1Mo steel. Materials Science and Technology, Vol. 22 (2006) 2, pp. 173–185.

[81] Holmström, S., Auerkari, P. & Holdsworth, S. An effective parametric strain model for creep. Materials for Advanced Power Engineering 2006. Proceedings of the 8th Liège Conference, part III. Forschungszentrum Jülich GmbH, pp. 1309–1318.

[82] Manson, S. S. Design considerations for long life at elevated temperatures (James Clayton Lecture). Proc. Institution of Mechanical Engineers, 1963–1964.

[83] Yao, H-T., Xuan, F-Z., Wang, Z., Tu, S-T. A review of creep analysis and design under multi-axial stress states. Nuclear Engineering and Design, Vol. 237 (2007) pp. 1969–1986.

[84] Gorash, Y. Development of a creep-damage model for non-isothermal long-term strength analysis of high-temperature components operating in a wide stress range. Ph.D. Thesis. Zentrum für Ingenieurwissenschaften der Martin-Luther-Universität, Halle-Wittenberg, Germany, 21 July 2008. 106 p.

[85] Yatomi, M., Bettison, A. D., O'Dowd N. P. & Nikbin, K. M. Modelling of damage development and failure in notched-bar multi-axial creep tests. Fatigue & Fracture of Engineering Materials & Structures, Vol. 27 (2004) 4, pp. 283–295.

[86] R5 (2001) Assessment procedure for the high temperature response of structures. British Energy, Glouchester, UK.

[87] RCC-MR (1987), Design and construction rules for mechanical components of FBR nuclear islands, Paris, France.

[88] ABAQUS. ABAQUS Online Documentation: Version 6.7-1. Theory Manual [CD-ROM]. ABAQUS Inc., 2007.

[89] Prager, M., The Omega method: an engineering approach to life assessment. ASME Trans., Journal of Pressure Vessel Technology, Vol. 122 (2000), pp. 273–280.

Appendices II, III, V and VI of this publication are not included in the PDF version.
Please order the printed version to get the complete publication (http://www.vtt.fi/publications/index.jsp).

Paper I

Effect of short-term data on predicted creep rupture life – pivoting effect and optimized censoring

In: Materials at High Temperatures.
Vol. 25 (2008) 3, September, pp. 103–109.
Northampton, UK: Science Reviews 2000 Ltd.

Effect of short-term data on predicted creep rupture life – pivoting effect and optimized censoring

S. Holmström and P. Auerkari
VTT, Espoo, Finland

ABSTRACT

Fitting data to classical creep rupture models can result in unrealistically high extrapolated long-term strength. As a consequence, the standard strength values for new steel grades have frequently needed downward correction after obtaining more long-term test data. The reasons for non-conservative extrapolation include the influence of short-term data, which are easiest to produce but tend to pivot upwards the extrapolated values of creep rupture strength. Improvement in extrapolation could be expected by reducing this effect through model rigidity correction and censoring of very short-term data, but it may not be immediately clear how to justify the correction of particular models or censoring.

Analogously to the instability parameter in the minimum commitment model for creep rupture, a rigidity parameter correction (RPC) is introduced to assess the pivoting effect of creep rupture models for the purpose of reducing potential to non-conservativeness in extrapolation. The RPC approach can be used with any creep rupture model for comparing the model rigidity and the potential benefit from censoring short-term data. The correction itself will never introduce non-conservatism, regardless of the model. The RPC approach is demonstrated by analyzing an ECCC data set for cross-welded 9%Cr steel (E911).

Keywords: short-term data, creep rupture life, pivoting effect, optimized censoring

1. INTRODUCTION

The creep rupture data used for evaluating the representative creep strength typically spans over several orders of magnitude in time. As relatively short-term tests are obviously fastest and cheapest to perform, they are better represented than long-term tests in the data sets. In addition, the damage and failure mechanisms in the short-term tests tend to differ from those in the long-term tests, which may better represent the foreseen service conditions. Although the fitted creep rupture models can accommodate much of the resulting curvature in the creep rupture strength vs. time curves, some residual curvature is not included. This has often resulted in overestimated values of new material strength, so that standard values had to be later reduced when additional long-term data have become available. The reasons for the overestimates can include long-term degradation and bias in material sampling, for example. However, the common reasons can also include the pivoting effect by ''over-represented'' short-term tests, which may unduly increase the extrapolated creep rupture strength (and life) unless at least partially censored for fitting. This effect also depends on the rigidity or the creep rupture model, or its inherent ability to describe both the short and the long duration data. The main interest in most cases is in extrapolation towards long-term service conditions, and therefore the effect of pivoting and data censoring are of interest for extrapolation accuracy.

The rigidity parameter correction (RPC) method presented here is a tool for quantifying the rigidity of creep rupture models and the likely extrapolation error due to pivoting, and for optimized data censoring. As an example, an ECCC data set with cross-welded 9%Cr material (E911) data is analyzed using RPC. First a series of models are compared for rigidity and likely extrapolation error due to pivoting. For this data set it is known that the fracture location is changing from base material fractures to fractures in the heat affected zone (HAZ), leading to a change in the curvature. Most creep rupture models are expected to show pivoting problems with such data sets. Finally, some data-censoring options are tested for this data set.

2. METHODS, APPLIED MODELS AND TEST DATA

The RPC approach applies a similar non-linearity formulation as the master curve equation of the Manson's [1] minimum commitment method (MCM):

$$\log(tr^*) = \frac{G(\sigma) - P(T)}{1 + A \cdot P(T)} \tag{1}$$

0960-3409/3/2008

doi: 10.3184/096034008X354747

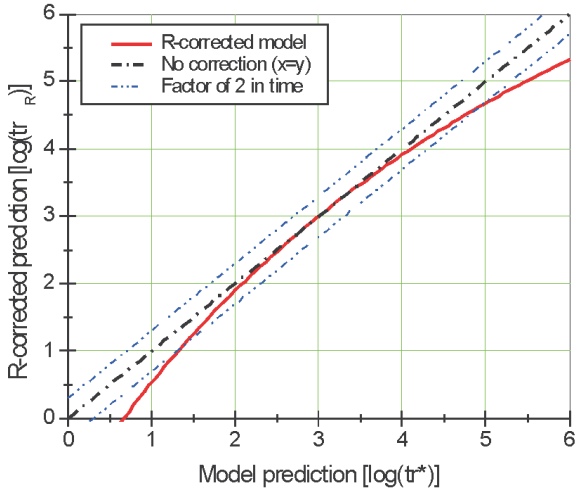

Figure 1 *R*-parameter corrected vs. uncorrected predicted rupture life (in h). $R = 0.089$ halves the predicted rupture time from 100 000 h when the pivot point is set at 1000 h.

where tr^* is the predicted time to rupture, $P(T)$ and $G(\sigma)$ are respectively the temperature and stress functions of the expression, and A is a constant called the instability parameter. Increasing negative values of the instability parameter A will reduce the predicted life (and creep strength) in extrapolation. MCM is not included in standard PD6605 [2] models for creep rupture data fitting (except as a simplified linear MC model with $A = 0$), but is used below as one of the creep rupture models for rigidity testing.

Analogously to Eqn (1), a rigidity parameter R can be defined to correct the predicted rupture time by bending any creep model prediction to the conservative side over a pivot point in time (Figure 1). The corresponding corrected time to rupture is defined as

$$\log(tr_R) = \frac{\log(tr_m) - \log(t_p)}{1 + R \cdot (\log(tr_m) - \log(t_p))} + \log(t_p) \quad (2)$$

where tr_R is the rigidity corrected time to rupture, tr_m the uncorrected (model predicted) time to rupture and t_p the pivot point in time. The correction is zero at the pivot point and reduces the predicted life elsewhere. Any creep model can be *R*-parameter corrected by minimising the root mean square error (RMS, Eqn (3)) or the standard error of estimate (see Eqn (4) [3]) by optimizing the value of R.

RMS is defined as

$$RMS = \sqrt{\frac{\Sigma(\log(tr) - \log(tr^*))^2}{n - 1}} \quad (3)$$

where tr is the observed rupture time, tr^* the corresponding rupture time predicted by the model, and n the number of data points.

SEE is defined as

$$SEE = \sqrt{\frac{\Sigma(\log(tr) - \log(tr^*))^2}{n - k - 1 - m}} \quad (4)$$

where k the degree of regression and m the number of constants in the model. The ECCC recommendations [4,5] further define a convenient fitting efficiency parameter or scatter factor as

$$Z_{PARAM} = 10^{2.5 \cdot PARAM} \quad (5)$$

where the PARAM = RMS or SEE.

The pivot point could be similarly selected as a part of the fitting procedure. As most creep rupture data points are concentrated in the mid-region in logarithmic time, where any model could be expected to give similar prediction, the pivot point could be also defined as the logarithmic mean of the testing times. However, since most of the pivoting effect can be expected from the extreme values in time, the pivot point can be taken as the average of the shortest and longest test duration.

For example, a pivot point of 1000 h and $R = 0.089$ will shorten the uncorrected 100 000 h prediction by a factor of 2, independently of the applied creep rupture model, as seen in Figure 1. To estimate the likely error in extrapolated time, optimization is below however only done for data with rupture times longer than the pivot point.

Table 1 Creep rupture models of PD6605

Soviet model 1 (SM1)

$$\log(t_r) = \beta_0 + \beta_1 \cdot \log[T] + \beta_2 \cdot \log[\sigma_0] + \beta_3/T + \beta_4 \cdot \sigma_0/T$$

Soviet model 2 (SM2)

$$\ln(t_r) = \beta_0 + \beta_1 \cdot \log[T] + \beta_2 \cdot \log[\sigma_0]/T + \beta_3/T + \beta_4 \cdot \sigma_0/T$$

Simplified minimum commitment method (MC)

$$\ln(t_r) = \beta_0 + \beta_1 \cdot \log[\sigma_0] + \beta_2 \cdot \sigma_0 + \beta_3 \cdot \sigma_0^2 + \beta_4 \cdot T + \beta_5/T$$

Simplified Mendelson–Roberts-Manson (MRn)[a]

$$\ln(t_r) = \left\{ \sum_{k=0}^{n} \beta_k \cdot (\log[\sigma_0])^k \right\} / (T - T_0)^r + \beta_5$$

Larson-Miller (LMn)[1)] (MRn with $T_0 = 0$, $r = 1$)

$$\ln(t_r) = \left\{ \sum_{k=0}^{n} \beta_k \cdot (\log[\sigma_0])^k \right\} / T + \beta_5$$

Manson-Haferd (MHn)[a]

$$\ln(t_r) = \left\{ \sum_{k=0}^{n} \beta_k \cdot (\log[\sigma_0])^k \right\} \cdot (T - T_0) + \beta_5$$

Manson-Haferd with $T_0 = 0$ (MH0n)[a]

$$\ln(t_r) = \left\{ \sum_{k=0}^{n} \beta_k \cdot (\log[\sigma_0])^k \right\} \cdot T + \beta_5$$

Orr-Sherby-Dorn (OSDn)[a]

$$\ln(t_r) = \left\{ \sum_{k=0}^{n} \beta_k \cdot (\log[\sigma_0])^k \right\} + \beta_5/T$$

[a] For $n = 2$, 3 or 4.

Table 2 Calculated values of R and Z for selected creep rupture models, optimized on all data. The model scatter factors (both RMS and SEE Z-values) are presented before and after RPC. The pivot point is set to 1000 h

Model	Z_{RMS} (uncorrected/R-corrected)	Z_{SEE} (uncorrected/R-corrected)	R-parameter
MC	4.95/4.68	5.11/4.87	0.095
OSD3	4.90/4.27	5.03/4.42	0.165
MH03	4.85/4.23	4.97/4.37	0.159
MR03	5.16/4.47	5.30/4.62	0.181
SM1	5.76/5.07	5.92/5.26	0.179
SM2	5.75/5.04	5.91/5.23	0.182
MR02	7.99/7.15	8.21/7.43	0.197
MH02	9.23/8.26	9.49/8.61	0.185
OSD2	9.07/7.96	9.34/8.29	0.219
MCM (A = −0.155)	3.82/3.69	3.95/3.85	0.052

In this work the non-linear MCM model was tested together with a selection of PD6605 [2] creep rupture models. The PD6605 supported models (18 model variants in total, see Table 1) apply maximum likelihood linear fitting to the rupture test data. An advantage of this approach is the possibility of using unfailed data (ongoing or interrupted tests) in the assessment.

Applying RPC for models selected by ECCC post assessment testing (PAT) will further characterise their suitability for extrapolation. A rigid model or a ''difficult'' data set might require left censoring (in time) or stress censoring (isothermal) for improved reliability. Optimizing R on data with longer rupture times than the pivot point again quantifies the likely error in the extrapolated life. A large positive value of R would suggest a model (and/or data) susceptible to pivoting errors, and non-conservative (uncorrected) predicted life.

To show the potential of RPC, an ECCC data set of cross-welded 9%Cr material (E911) is fitted to the selected creep ruptured models. A series of models are compared for their fitting efficiency with and without RPC, and then their likely extrapolation error due to pivoting is quantified. Finally, data censoring options are tested for potential improvement in extrapolation. For this data set it is known that the fracture location is changing from the base material to the heat affected zone (HAZ). Such a data set can be expected to show pivoting problems with most creep rupture models. The full data set consists of 159 ruptured and 36 unfailed data points including specimens ruptured in the parent material, weld metal and in the heat affected zone (HAZ). The data covers a temperature range of 550–690°C and stress range of 26–230 MPa, with the longest ruptured test about 32 000 h and the longest unfailed test about 65 000 h in duration. In addition to the full data set, subsets of data are analyzed on HAZ failures without censoring and with left censoring up to 1000 h. A source for error in the PD6605 models is possible when assessing HAZ data only; caused by the fact that there are unfailed data in isotherms (550 and 575°C) where there are no failed data. The impact of this situation on the models should be clarified in future work.

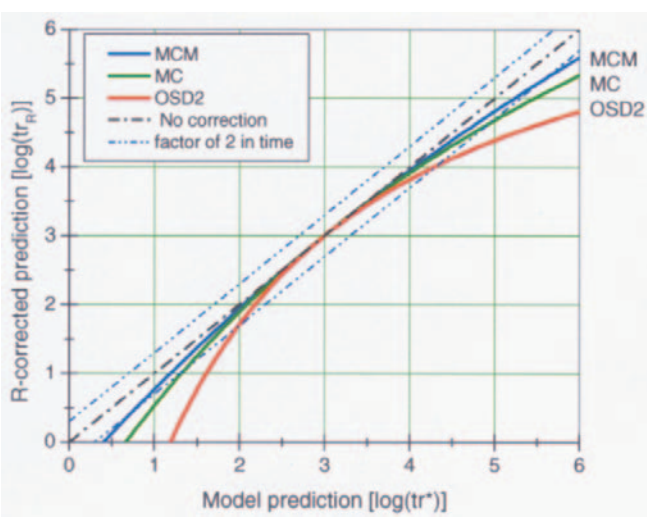

Figure 2 RPC fits of the two best performing models (MCM, MC) and the worst performing OSD model, with a pivot point at 1000 h.

3. COMPARISON OF CREEP MODELS WITH RPC FOR CROSS-WELDED 9Cr STEEL

Nine best-fitting PD6605 models and the MCM model were selected for RPC applied to the ECCC data set on cross-welded 9Cr steel. The RPC optimization results on all data are shown in Table 2, when the pivot point is set at 1000 h. For all models it can be noted that the RPC reduces the scatter factor Z_{SEE} by 5–13%.

Rating the models according to the result of the RPC (the smaller the R-parameter the better), the best (MCM and MC) and worst (OSD2) performing models are compared with uncorrected models in Figure 2.

For comparison, the same data set was RPC optimized on data longer than the pivot point. The resulting values of R and Z for the models before and after RPC are presented in Table 3, and a comparison of uncorrected and corrected best and worst performing models is shown in Figure 3. The time ratio tr_R/tr_m at longest observed rupture time (about 30 000 h) and at 100 000 h are also listed to characterise the effect of optimized RPC. Again, Z_{SEE} is systematically reduced by RPC but the reduction is now between 0.4 and 4.1%. The predicted life at 30 000 h (uncorrected) is reduced by about 15–30% depending on model. Of the PD6605 models, the MC model showed smallest value of Z and R (and largest time ratio), while OSD2 showed the largest Z and R. The non-linear MCM gave no more obvious improvement in this case in comparison with the simplified minimum commitment model (MC).

Table 3 Calculated values of R and Z for the same creep rupture models as in Table 2, optimized on all rupture data above the pivot point (1000 h). The scatter factors (Z) are shown with and without RPC. The models shown in bold are further applied to the data points of HAZ failures

Model	Z_{RMS} (uncorrected/R-corrected)	Z_{SEE} (uncorrected/R-corrected)	R	Time ratio tr_R/tr_m at 30 000 h/100 000 h
MC	**2.40/2.37**	**2.45/2.44**	**0.032**	**0.858/0.758**
OSD3	2.59/2.48	2.64/2.55	0.055	0.774/0.634
MH03	2.60/2.49	2.65/2.56	0.057	0.768/0.624
MR03	2.62/2.50	2.68/2.57	0.058	0.765/0.620
SM1	2.93/2.83	3.0/2.91	0.057	0.768/0.624
SM2	2.95/2.83	3.01/2.92	0.058	0.765/0.620
MR02	3.46/3.34	3.54/3.45	0.061	0.755/0.606
MH02	3.78/3.62	3.86/3.74	0.071	0.724/0.564
OSD2	**3.89/3.72**	**3.98/3.84**	**0.074**	**0.715/0.552**
MCM (A = −0.155)	**2.48/2.42**	**2.56/2.51**	**0.045**	**0.809/0.684**

Note that here the usually well behaving SM1 model appears to behave rigidly, giving inferior results in comparison with MC and MCM.

Table 4 Calculated values of R and Z for MC, OSD2 and the MCM models, fitted and RPC optimized on uncensored data of HAZ failures (pivot point at 3000 h)

Model	Z_{RMS} (uncorrected/R-corrected)	Z_{SEE} (uncorrected/R-corrected)	R
MC	2.20/2.09	2.26/2.16	0.166
OSD2	2.21/2.11	2.25/2.17	0.145
MCM (A = −0.13)	2.09/2.09	2.17/2.18	0.028

Table 5 Calculated values of R and Z for best and worst performing PD6605 models and MCM model on the full data set, optimized on HAZ data with longer durations than 3000 h (pivot point)

Model	Z_{RMS} (uncorrected/R-corrected)	Z_{SEE} (uncorrected/R-corrected)	R	Time ratio at time of 30 000 h/100 000 h
MC	2.22/2.12	2.31/2.23	0.134	0.762/0.552
OSD2	2.26/2.16	2.32/2.24	0.133	0.763/0.554
MCM (A = −0.13)	2.15/2.14	2.26/2.29	0.019	0.958/0.906

4. OPTIMAL CENSORING OF 9Cr CROSS-WELD DATA USING RPC

Three cross-weld data subsets of the 9Cr material were tested for optimal performance by left censoring. The first subset included HAZ failures only, the second the same data set censored up to 300 hours and the third subset the same data set censored up to 1000 hours. In all cases the pivot point is set at 3000 h (mid-range of data with HAZ failures).

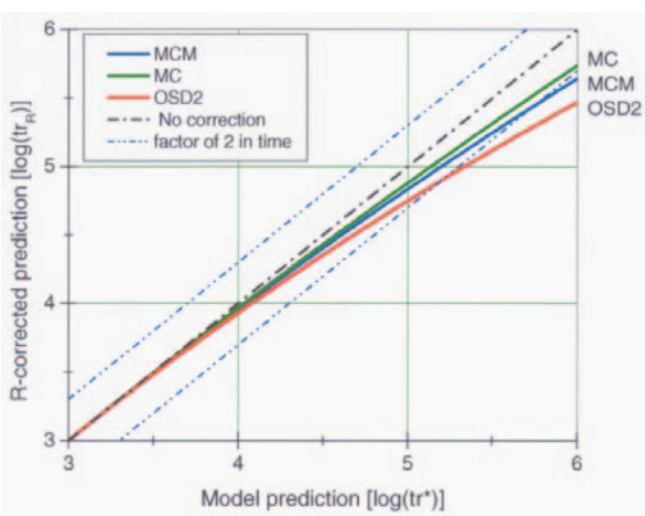

Figure 3 RPC fits of the best performing models (MC and MCM) and the worst performing (OSD2) model. The models are optimized on data above the pivot point (1000 h).

4.1 HAZ failures, no censoring

With RPC, the predicted life is shortened by a factor of two in time from 100 000 h with $R = 0.1618$, when the pivot point is set at 3000 h. The RPC optimization results with all data are shown for the MC, MCM and the ODS2 models in Table 4, and the corresponding results for data above pivot point in Table 5.

The removal of data not failing in the HAZ changes the order of the MC and OSD2 models indicating that the MC behaves more rigidly for these data. However, the MCM model hardly changes at all by RPC, in fact the Z_{SEE} is getting worse which indicate that the RPC does not represent a true improvement for this model.

From the extrapolation point of view the two PD6605 models perform very similarly, and both MC and OSD2 models seem to suffer from the pivoting effect in extrapolation. The MCM model again shows decline in the Z_{SEE} scatter factor by RPC. The MCM is thereby nearly optimal without further correction, and would be selected as preferred model for the HAZ failure data assuming it also passes all PAT tests. However, again one has to remember

Table 6 Calculated values of R and Z for best and worst performing PD6605 models on all HAZ failure data, left censored at 300 h

Model	ZRMS (uncorrected/R-corrected)	ZSEE (uncorrected/R-corrected)	R
MC	2.19/2.09	2.25/2.17	0.152
OSD2	2.20/2.12	2.24/2.18	0.135

Table 8 Calculated values of R and Z for best and worst performing PD6605 models on the full HAZ data set, optimized on data left censored at 1000 h

Model	Z_{RMS} (uncorrected/R-corrected)	Z_{SEE} (uncorrected/R-corrected)	R
MC	2.18/2.08	2.22/2.16	0.131
OSD2	2.18/2.14	2.23/2.20	0.108

that the MCM model has not utilised the unfailed data and might therefore show better fits.

4.2 HAZ failures, left censoring at 300 h

It is to be noted that the difference from the uncensored data set is only one failed data point at 262 hours ($\log(t_r) = 2.4$); the next shortest test has a logarithmic rupture time of 2.8 (630 h). The RPC optimization results are shown here for the MC and OSD2 models in Table 6 for the whole data range and in Table 7 for the data above the pivot point. The pivoting point is still kept at 3000 h.

The OSD2 model seems to behave more flexibly than the MC model. From the extrapolation point of view the MC model shows no change in the R-parameter as an effect of the left censoring (in comparison to the uncensored HAZ data set), indicating that the culling does not affect this model. The OSD2 model shows some decrease in the value of R, suggesting an improvement.

4.3 HAZ failures only, left censoring at 1000 h

The pivot point is still kept at 3000 hours for comparison reasons and to avoid a too short bending range for the long-term data. The RPC optimization is performed on the left censored HAZ data using the same MC and OSD2 models as before. The RPC results are presented in Table 8 for optimized R-parameter on the whole range and in Table 9 on the data above the pivoting point.

From the rigidity point of view both the MC and the OSD2 show only slight improvement in the R-parameter (in comparison to the less culled and un-culled data sets). The location of the pivoting point closer to the short duration end (due to culling) emphasizes the long duration end, which can be seen comparing Table 8 and Table 9 (which are nearly identical). This indicates that any pivoting due to the shorter test data (1000 to 3000 h) can be ruled out.

The OSD2 performs better the more left-censoring is applied whereas the MC show no clear improvement in the R-parameter. This suggests that the uncensored HAZ data is already the optimal data set for MC to perform the assessment, and that further censoring only favours relatively simple models such as the OSD2.

5. DISCUSSION AND CONCLUSIVE REMARKS

The RPC approach is available to supplement any classical creep rupture model, including those supported by PD6605. RPC will typically reduce the common inherent non-conservatism in predicted life, because it can justify additional downward curvature to the (*e.g.* isothermal) extrapolated creep rupture curves. As the correction is zero at the selected pivot point and reduces life elsewhere, RPC itself is not likely to be non-conservative. In the example case of cross-welded 9Cr steel, the data fits were improved by RPC (improvement in scatter factor) for all tested PD6605 creep models, and in each case by additional curvature towards the non-conservative side. This suggests good potential in reducing the commonly observed non-conservatism in extrapolated creep rupture life. In the example data set for cross-welded 9Cr steel, the resulting reduction in predicted life was 15–25% at 30 000 h and 24–45% at 100 000 h for the tested models, which corresponds to the maximum observed failure time and maximum target extrapolation time.

For the full data set the MC and MCM models were least affected by pivoting (see Figure 4). The relatively inflexible SM1 and SM2 models require more correction, and should be RPC tested when post assessment tests (PAT) suggest these as preferred models.

Table 7 Calculated values of R and Z for best and worst performing PD6605 models on HAZ failure data, left censored at 300 h and above the pivot point

Model	Z_{RMS} (uncorrected/R-corrected)	Z_{SEE} (uncorrected/R-corrected)	R	Time ratio at max rupture time (30 000 h/100 000 h)
MC	2.22/2.11	2.31/2.22	0.134	0.762/0.552
OSD2	2.24/2.15	2.30/2.24	0.125	0.774/0.571

Table 9 Values of R and Z as in Table 8 but for failures above the pivot point

Model	Z_{RMS} (uncorrected/R-corrected)	Z_{SEE} (uncorrected/R-corrected)	R	Time ratio at max rupture time (30 000 h/100 000 h)
MC	2.18/2.09	2.27/2.19	0.130	0.767/0.560
OSD2	2.19/2.13	2.25/2.21	0.107	0.800/0.612

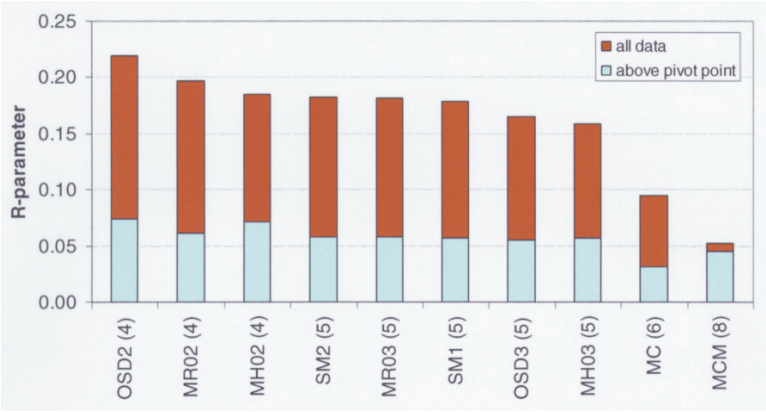

Figure 4 The optimized value of R for 10 rupture models (in the order of least to most flexible model, *i.e.* order of R) using either all data or data above the pivoting point. The numbers in brackets refer to the numbers of free fitting variables in each model.

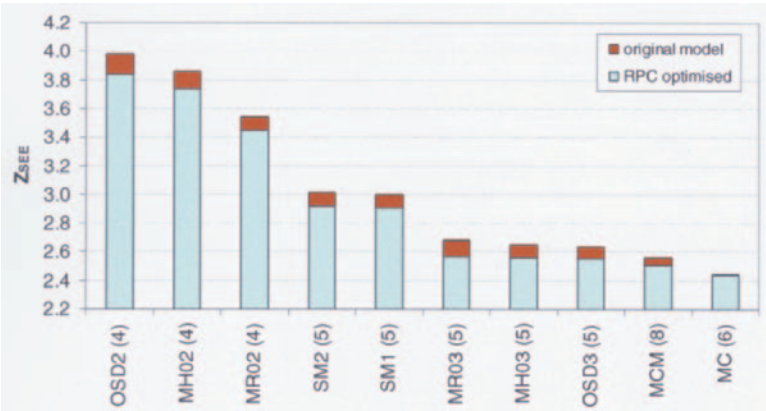

Figure 5 The RPC optimization impact on Z_{SEE} (in the order of worst to best fitting models above pivoting point). The improvement in Z appears to be unrelated to the initial model performance, *i.e.* initially poorly fitting models do not improve more than good ones.

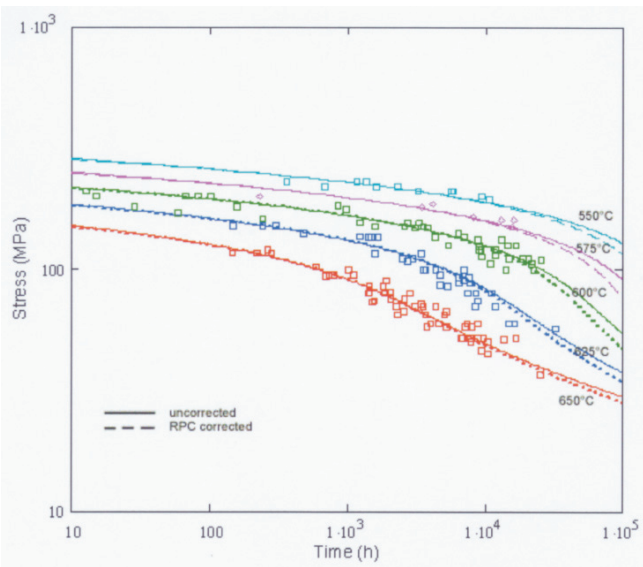

Figure 6 RPC fit of the full data set using the MC model (pivot point = 1000 h, $R = 0.032$). The main improvement appears to be in the 625°C isotherm. The stress ratio (uncorrected/corrected) at 600°C and 100 000 h is 0.86.

Looking at the improvement of fit above the pivoting point (see Figure 5), it appears that the RPC does not improve badly fitting models (in expected time scatter) more than the initially better ones.

Plotting the corrected and uncorrected models (all data case, see Figure 6) it can be seen that for this data set the 625°C isotherm is improved the most from the RPC.

For the subsets on HAZ failures it was shown that left censoring does not improve the MC model performance from the flexibility point of view, whereas the OSD2 benefits from more left censoring (Figure 7). The Z_{SEE} for the MCM model became worse by RPC for the uncensored HAZ data set, suggesting that it is already close to the optimum fit.

The HAZ failures data set without censoring was hence the best data set in this assessment for both the MCM and the MC model. Left censoring the HAZ data only improves the flexibility performance of simple models such as the OSD2 model. All the PD6605 models, however, show some improved fitting by RPC suggesting that none of the uncorrected models are optimal. The nonlinear MCM and the MC models show considerably less change by RPC than the others, not perhaps surprisingly for the MCM since it already includes a similar non-linearity formulation comparable to RPC. However, MCM fitting does not take unfailed data into account.

Model rigidity, however, is a double-edged sword. A model with numerous fitting parameters can be more flexible than one with only few, but a good fit to the existing data (in interpolation) does not guarantee good performance in extrapolation. The number of fitting constants to be optimized in the models considered above varies from 4 (LM2) to 8 (full MCM). This variation involves a part of the inherent rigidity, and conventional fitting efficiency is therefore better described by the Z_{SEE} than the Z_{RMS}. However, provided that the fitted data set is reasonably large in comparison with the number of fitting parameters, the inherent rigidity of the models is bound by their phenomenological description of the underlying creep (rupture) process. In this respect the models rather similarly apply a temperature dependence

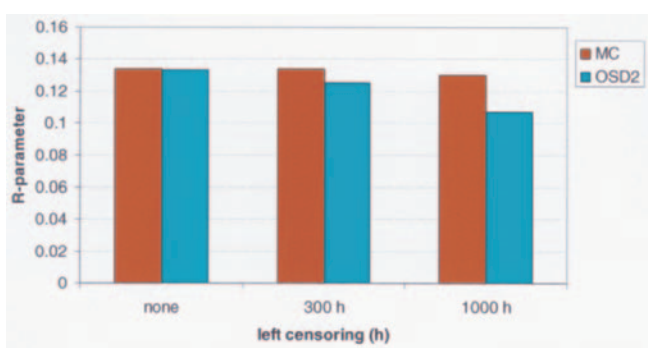

Figure 7 Influence of left censoring on the optimized value of R (above pivoting point) for the MC and OSD2 models.

related to the Arrhenius rate expression. In contrast, the stress dependence is given by a polynomial without real theoretical background, except for the SM models which assume a stress activation term for creep [6]. Not surprisingly, the SM1 and SM2 models may then appear relatively rigid, as was found above in RPC testing of the example data set. None of the PD6605 models explicitly include terms for thermal degradation or creep damage, and the expected additional downward curvature in isothermal creep rupture curves is only accommodated to the extent allowed by the (mostly polynomial) stress expressions. MCM, however, includes the instability parameter to model for additional ''damage'', and a similar approach has been adopted for RPC. The observed improvement in the fitting capability of MCM and all rigidity corrected PD6605 models suggests that some of the non-conservatism in extrapolation is due to models rather than the data not yet reflecting long term degradation. The potential benefit of the RPC approach should be investigated with a wider range of data sets.

6. REFERENCES

[1] Manson, S.S. and Ensign, C.R. (1978) Interpolation and extrapolation of creep rupture data by the minimum commitment method. Part I, Focal point convergence. *Pressure Vessel and Piping Conference*, Montreal, pp. 299–398.

[2] PD 6605 (1998) *Guidance on methodology for assessment of stress rupture data*, Part 1 and 2, BSI, London 51+27p.

[3] NIMS Creep Data Sheet No. 36B (2003) *Data sheet on elevated temperature properties of quenched and tempered 2.25Cr-1Mo steel plates for pressure vessels* (ASTM A542/A542M).

[4] ECCC recommendations (2003) Volume 5 Part 1a [Issue 5], *Generic recommendations and guidance for the assessment of full size creep rupture data sets*.

[5] ECCC recommendations (2003) Volume 5 Part 1b [Issue 2]. *Recommendations and guidance for the assessment of creep strain and creep strength data*.

[6] Holmström, S. and Auerkari, P. (2000) *Strength of structural materials for new generation power plants*, VTT Manufacturing Technology, VALB-418, 53p.

Paper IV

Robust prediction of full creep curves from minimal data and time to rupture model

In: Energy Materials, Materials Science
& Engineering for Energy Systems.
Vol. 1 (2006) 4, pp. 249–255, Maney Publishing.
Reprinted with permission from the publisher.

Robust prediction of full creep curves from minimal data and time to rupture model

S. Holmström* and P. Auerkari

A description of creep strain evolution is frequently needed in design or life assessment of components subjected to service at high temperatures. Unfortunately, long term creep strain data are not as easily available as rupture data or rupture models. One of the most demanding tasks in this context is to predict the creep behaviour reasonably accurately beyond the range of available data. Much effort has been invested into developing reliable methods to extrapolate creep rupture data, for example in the recommended procedures of the European Creep Collaborative Committee (ECCC) and PD6605 of BSI. However, for strain no such tools are currently available. Here a new and robust creep strain model is suggested to provide the whole creep curves based on the corresponding creep rupture model. This logistic creep strain prediction (LCSP) model defines the creep curve only with three additional parameters to those of the corresponding rupture model. In its basic form the LCSP model optimises a non-linear asymmetric logistic transition function fitted in logarithmic strain against a time temperature parameter (TTP), giving time to specified strain. Unique features of the model include its simple inverted expression for strain and strain rate. The fitting effectiveness of the new method is shown to match all the contesting creep strain models of the ECCC intercomparison activity on a single heat data set of the steel P22 (10CrMo9-10). The model is also shown to produce accurate predictions of the stress to 1% strain up to 100 000 h, when compared to the values given in DIN 17243.

Keywords: Creep, Strain, Model, Ferritic steel, ECCC

Introduction

Creep strain sets design limits for many components in power engineering, for example in the case of blading, bolts and casings of steam and gas turbines. In addition, creep strain is considered to be an important quantity to be monitored in the in-service inspections and life assessment of turbines, boilers and steam pipes, with typical recommended limits up to 1 or 2% of strain. However, predicting creep strain is frequently less than straightforward. This is partly because there is much less creep strain data available even on common well established engineering steels than creep rupture data, and partly because most publicly available good models to describe creep behaviour only apply to creep rupture.

Intercomparison activities[1,2] of different strain modelling alternatives have shown that effective prediction of time to specified strain can be achieved from time–temperature parameter formulations.[3,4] The most challenging task, however, is to predict realistic strain response outside the range of available strain data. Creep strain data are often hard to come by, and in the most interesting long term range scarce or lacking. In contrast, rupture data and models for time to rupture are much easier to access. The rupture models are well established and considered to be relatively reliable at least for common engineering alloys with sufficient long term test data. Therefore, it could be an advantage if creep strain models can utilise such data and models as a baseline.

Another problem area in any materials modelling is related to model robustness, i.e. how resilient it is against error or instability due to scatter or when extrapolating outside the range of data. A model is unlikely to be robust if it includes a large number of free fitting constants, although some are inevitably needed to achieve good fit. Robustness is particularly needed for small data sets, but robustness is also inherently related to the mathematical formulation of the model. In this respect, differences also exist between rupture models, but by using strain modelling with rupture models as a baseline, the main contribution to robustness is likely to be limited to the additional fitting constants of the strain model.

Finally, realistic creep strain models should be physically plausible. For example, it is mathematically possible but not really physically plausible to model for creep strength (for strain or rupture) that continuously increases in time, shows discontinuity in its evolution rates, or turns back in time when extrapolated outside

VTT Technical Research Centre of Finland, Kemistintie 3, 02044 VTT, Finland

*Corresponding author, email stefan.holmstrom@vtt.fi

Received 30 December 2006; accepted 2 February 2007
DOI 10.1179/174892406X173594

the range of data. Such behaviour can be also prevented or limited if strain evolution can be suitably related to rupture models that are known not to suffer from these drawbacks at least within the range of interest in terms of time, stress and temperature.

To avoid complex creep strain models with too many fitting constants, and to achieve robust extrapolation with minimal data, a new creep strain model, the logistic creep strain prediction (LCSP) model, has been developed and will be described below. The method relies on the time to rupture (true data or master curve predicted) to provide the end point of each creep curve. The shape of the creep curve is modelled with three additional parameters as output from data fitting for each curve or curve family. The LCSP model is a logistic non-linear asymmetric transition function fitted in logarithmic strain versus time–temperature parameter (TTP) at specified stress and temperature. The model offers an improved sensitivity and robustness to the strain prediction closely related to the work performed on rupture assessments[5] such as the post-assessment tests of the European Creep Collaborative Committee (ECCC),[6] and of PD6605.[7] With confidence to the shape parameters, the LCSP can be used for rupture predictions similarly to the Monkman–Grant[8] expression, except that the LCSP approach is not limited to predictions using the minimum strain rate. Consequently, the LCSP model could be used in assessing tests still running or discontinued. Even for rupture models, this is so far only possible with the PD6605 rupture assessment tool. An estimate of the long term creep ductility[5,9,10] can also be extracted from the model.

The model is unique in the sense that the function of time to specific strain, strain at specified time and strain rate at specified time is all algebraic and can therefore readily be for instance incorporated into finite element (FE) codes. It also makes the extraction of the constants of the Norton creep expression easy for using them in common FE codes.

The fitting effectiveness and extrapolation robustness of the method is shown by comparing LCSP results to both more complicated[11] and simpler creep strain models[1,5] with the same single heat data set in the ECCC intercomparison on steel P22 (10CrMo9-10, with a maximum rupture time of only 3000 h) and incorporating time to 1% strain at stress levels of the DIN 17243 standard[12] up to 100 000 h.

LCSP model and its validation for steel P22 (10CrMo9-10)

The modelling aims to produce representative creep strain curves at specified stress and temperature with the help of available creep strain and rupture data. In this paper, the time to rupture in fitting is represented by the actual rupture time, but in extrapolation exercises it is replaced by a master curve prediction for rupture.

If the availability of creep strain data is very poor, the curve shape modelling can be extended with a standard strength value for rupture together with corresponding strengths for a specified strain such as 1%.

The LCSP method introduces a transition in a temperature compensated time parameter (such as the Larson–Miller or Manson–Haferd parameter) as a function of creep strain at specified temperature and stress. In this work, the predicted time to specified strain is based on the Larson–Miller parameter, i.e. the TTP has a transition over strain between a parametric value of zero for very small strain (and very short time) to a maximum value restricted by the rupture life and the parameter β as described in equation (1). The function is a non-linear asymmetric transition function with a steepness regulated by the variables p and x_0. It is to be noted that the LCSP approach can be used with any growth function that is shown to accommodate the data, but the possibility of having an algebraic solution for predicting the strain as a function of time (equation (2)) might then be compromised. The LCSP model states that knowing the time to rupture (maximum TTP level) and the material specific parameters p and x_0 is sufficient to describe the whole creep curve at specified temperature and stress. Inversely it is possible to predict time to rupture by knowing only one point on the strain curve (and again the material specific parameters p and x_0). This feature however must be investigated further for limits of applicability.

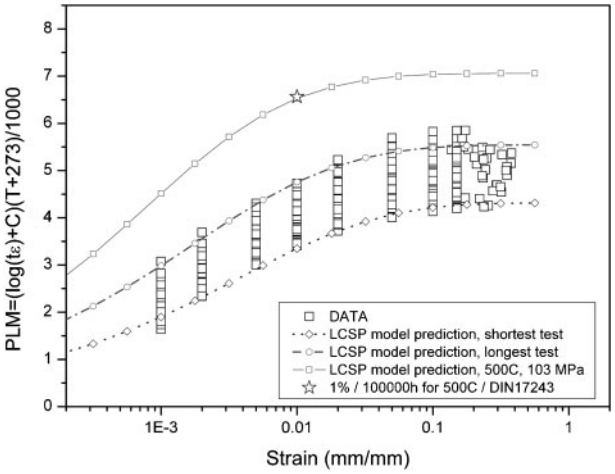

1 P22 data at 0·1, 0·2, 0·5, 1, 2, 5, 10, 15% and ε_t, presented in TTP form as defined by LCSP (30 curves): predicted strain curve at 500°C and 103 MPa is also presented together with 1%/100 000 h standard value at same temperature and stress

The LCSP method defines time to strain ε at engineering stress σ and temperature T as

$$\log(t_\varepsilon) = \frac{\log(\alpha t_r) + \beta}{1 + \left(\frac{\log \varepsilon}{x_0}\right)^p} - \beta \qquad (1)$$

where t_ε is the time to given strain, t_r is the time to rupture and x_0, p, β and α are fitting factors. In its simplest form, the latter four are all constants. The TTP presentation of equation (1) is shown in Fig. 1 with the assessed P22 strain data from.[1]

In the case of P22, the factors x_0 and p were temperature and stress dependent, and β and α were found to be constants. The model was fitted as time to specific strain at specified temperature and stress (equation (1)). Fitting the function in time makes it possible to use the post-assessment tests for checking fitting accuracies and extrapolation robustness as recommended for creep rupture assessments by ECCC. The inverted equation (1) describing strain as a function

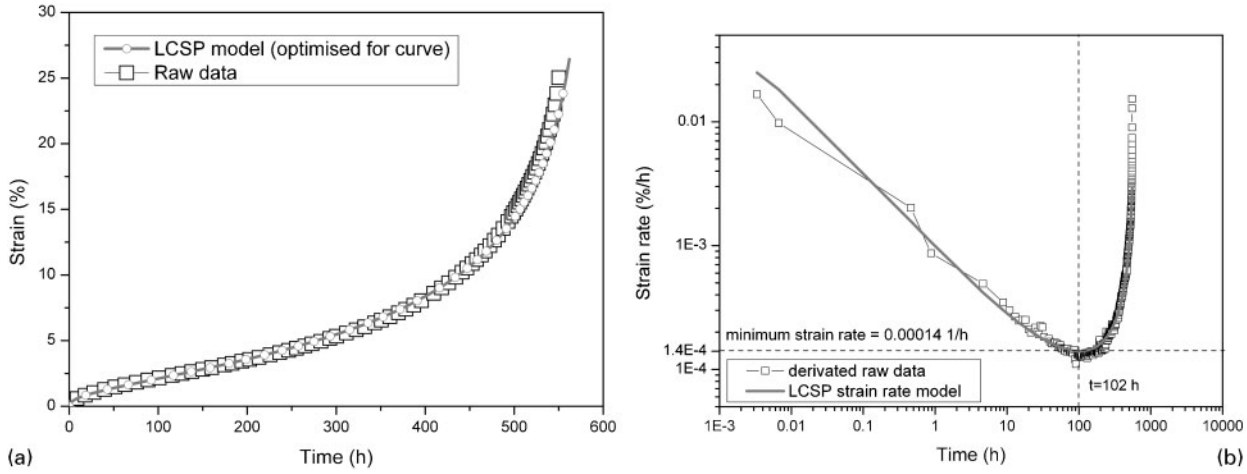

2 Example of *a* LCSP predicted versus measured creep and *b* predicted creep strain rate for P22 at 600°C: model parameters are optimised for curve in question

of time (still algebraic), can be written as

$$\log(\varepsilon_t) = (\mathrm{LTF}-1)^{1/p} x_0 \tag{2}$$

with

$$\mathrm{LTF} = \frac{\log(\alpha t_r)+\beta}{\log(t_\varepsilon)+\beta} \tag{3}$$

The equations (1)–(3) imply that at strain $\varepsilon=1$ the time to rupture is attained ($\alpha \times t_r$). The constant α can correct the strain at time to rupture to correspond to the actual creep ductility but for the case of P22 and other creep ductile materials this is unlikely to be necessary. For the data set available $\alpha=1$ also gave the best overall fit for the master equation incorporating all creep curves.

An example of the LCSP predicted versus measured creep strain for P22 steel is presented in Fig. 2*a*.

By differentiating equation (3) with respect to time, the resulting strain rate as a function of stress and temperature can be written as

$$\dot{\varepsilon} = -\varepsilon \cdot k1 \cdot k2 \cdot x_0 \tag{4}$$

where ε is given by equation (2), and

$$k1 = \frac{(\mathrm{LTF}-1)^{1/p}}{p} \tag{5}$$

and

$$k2 = \frac{\log(\alpha \cdot t_r)+\beta}{[\log(t_\varepsilon)+\beta]^2 \cdot t_\varepsilon \cdot (\mathrm{LTF}-1)} \tag{6}$$

Again, this provides an algebraic expression for creep strain rates, and an example of this with comparison to P22 data is shown in Fig. 2*b*.

A second differentiation of the LCSP model equation in time produces a function (still algebraic) of which the root gives the time to minimum creep rate, and thereby the minimum strain rate by using equation (4) (*see* Fig. 3).

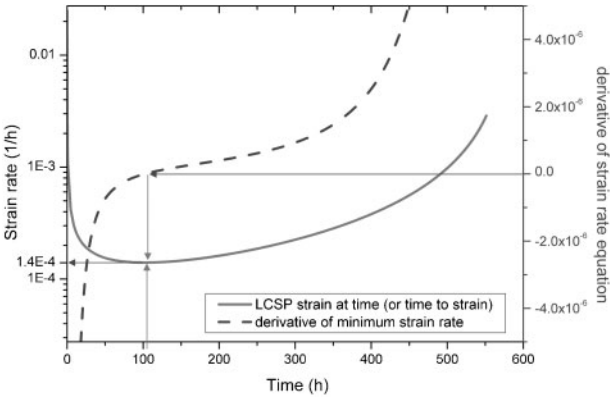

3 Strain rate (continuous line) and its derivative (broken line) for creep curve of Fig. 2, showing time to minimum strain rate and minimum creep rate

The LCSP model factors for P22 steel are presented in Table 1, and the shape factors p and x_0 as a function of temperature and stress in Fig. 4.

The accuracy of a creep rupture model can be described by the root mean square (RMS) error calculated from the predicted time to rupture.[5] Similarly, the model accuracy of the predicted time to specified strain can be described as

$$\mathrm{RMS} = \left\{ \frac{\sum \left[\log(t_{\varepsilon-\mathrm{actual}}) - \log(t_{\varepsilon-\mathrm{predicted}})\right]^2}{n} \right\}^{1/2} \tag{7}$$

where n is the number of data points. The better the fitting efficiency, the smaller the scatter factor Z, defined as

$$Z = 10^{2.5\mathrm{RMS}} \tag{8}$$

In a creep rupture assessment, a scatter factor close to 2 is considered to be good. This value can be approached in creep strain assessments for homogenous well behaving creep strain data, but for multicast mixed continuous and interrupted data it can be expected that $Z>6$.

Table 1 Logistic creep strain prediction fitting factors for steel P22 (10CrMo9-10)

$x_0(\sigma,T)$	$p(\sigma,T)$	C	α
−0·391+0·696log (σ)−3392·5/(T+273)	4·363−2·271log (σ)+3874·9/(T+273)	3·49	1

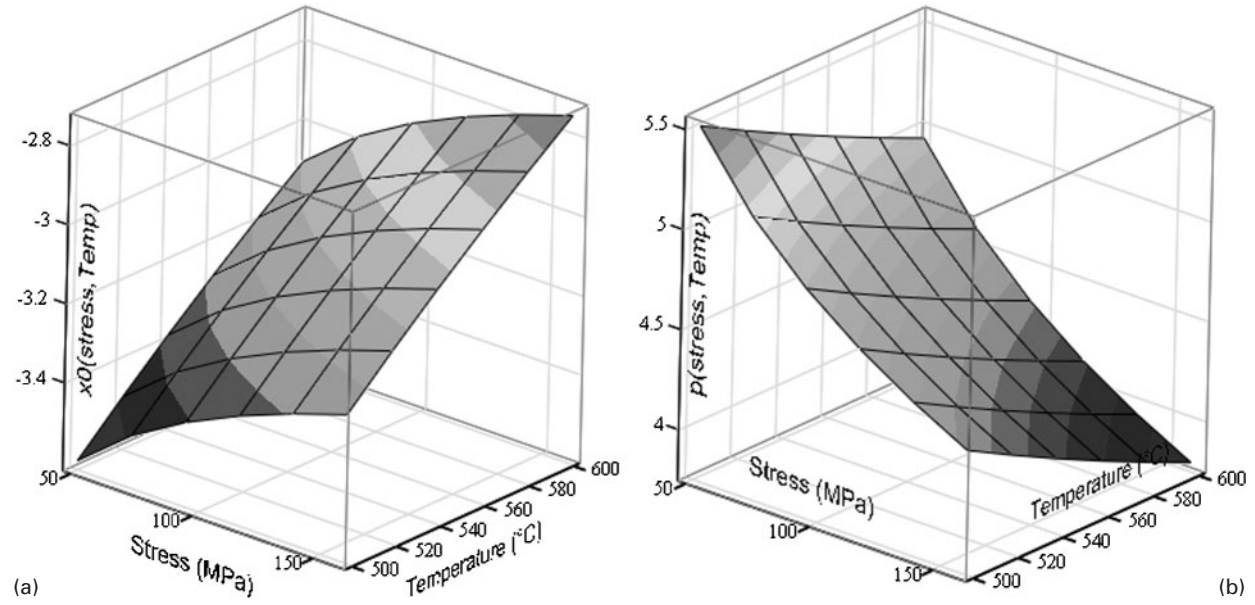

4 Temperature and stress dependence of shape factors *a* x_0 and *b* *p* for P22

To validate the LCSP model the same P22 creep strain data have been used as for the ECCC intercomparison exercise. The single heat data set contained 30 creep curves, with a temperature range of 510–600°C and a stress range of 180–280 MPa. The maximum testing time was ~3000 h. To support longer term prediction, the data were simultaneously fitted with the 10 000 and 100 000 h/1% creep strength values of the DIN 17243 standard.

A comparison of Z values of the LCSP model and those predicted by other models in an ECCC intercomparison of the same data set (Table 2) shows that the LCSP model performs at least as well as the best one from the previous intercomparison. The LCSP value $Z=2{\cdot}38$ calculated on all data can be considered to be excellent. It is to be noted that the long term predictions of time to 1% strain for stress levels of the standard are also well defined by the LCSP, namely the predicted times give a Z value below 2, as shown in Fig. 5.

Discussion

A particular strength of the LCSP model is its linkage to the rupture time and the robustness of the rupture model. The small number of fitting parameters when compared to the other models with similar Z values in Table 2 is also favourable. The LCSP model is robust and simple mainly because of relatively low number of degrees of freedom (constants to be fitted), and because no complex numerical operations such as numerical integration are needed for fitting. In this case, the LCSP model performs as well as the best model in the intercomparison (MHG-10, modified Garofalo model, Modified Graham–Walles) but with only eight fitting constants. The model is also predicting well the time to 1% strain at specified stress levels up to 100 000 h with $Z<2$ (Fig. 5). According to the Norton law (equation (9)) parameters A and n, and the minimum creep rate can be easily extracted from the LCSP model, as a function of stress and temperature (Figs. 6 and 7). Also the parameters of Nadai's (equation (10)) strain hardening model, the continuum damage mechanic model (equation (11)),[14] the Omega[15] and modified Omega model[16] can readily be calculated utilising the LCSP model.

The uniaxial steady state or minimum rate of creep strain ε under stress σ and at temperature T can be

Table 2 Scatter factor *Z* for strain models[1–3] on steel P22 (single heat data)*

		Z for time to specified strain (all temperatures)				
Model equation	**Creep regimes (param)**	**0·2%**	**0·5%**	**1%**	**2%**	**5%**
Omega model	S/T (8)	468	39	10		
BJF model	P/S	15	6	4		
Theta model	P/S/T	17	3	2		
Modified theta model	P/S/T	10		4		
Creep strength ratio model	P/S/T	4	8	7		
NPL model	P/S/T	12	7	3		
Baker–Cane model	P/S/T	5		2		
Bartsch model	P/S	3	2	4		
Modified Garofalo model[11]	P/S/T (27)	2	2	2		
Modified Graham–Walles	P/S/T	3	3	2	2	2
Modified Nadai	P/S/T (11)	3	2	2	2	2
MHG-4	P/S/T (4)	3	3	3	3	3
MHG-10	P/S/T (10)	3	2	2	2	2
LCSP	P/S/T (8†)	3	2	2	2	2

*In creep regime column, P/S/T=primary/secondary/tertiary (number of free parameters in the model).
†The parameters needed for $t_r(T,\sigma)$ are not accounted for.

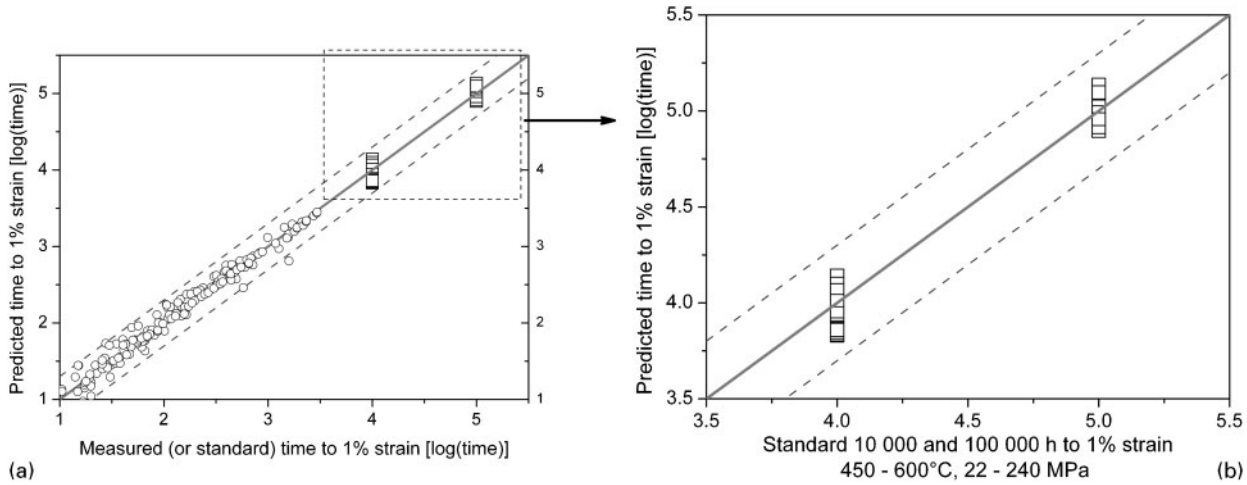

5 Predicting time to 1% creep strain for ECCC data and 10 000 and 100 000 h DIN 17243 standard values using data set specific material rupture models and the shape parameters presented in Table 1: for DIN 17243 time to 1% strain predictions LCSP model utilised rupture model based on EN 10216[13] standard values for rupture; acquired scatter factor for standard values is Z=1·8

described by the Norton law

$$\dot{\varepsilon} = B\exp\left(-\frac{Q}{kT}\right)\sigma^{n} = A\cdot\sigma^{n} \tag{9}$$

where $\dot{\varepsilon}$ is the minimum strain rate, B is a rate coefficient, Q is the apparent activation energy for creep, k is the Boltzmann constant and n is the Norton creep exponent. Here $B\exp(-Q/kT)$ is treated as a constant for given temperature

To predict primary to secondary creep deformation the Nadai form can be used. In this work, the formulation is fitted as used in the ABAQUS software (Abaqus Inc.)

$$\dot{\varepsilon} = \{A\sigma^{n}[(m+1)\varepsilon]^{m}\}^{1/m} \tag{10}$$

where $\dot{\varepsilon}$ is the strain rate at specified creep strain and A, n and m are fitting factors. The Norton model (equation (9)) is obtained from equation (10) by setting m=0.

The LCSP model predictions can also be compared to a classical simple strain model based on continuum damage mechanics (CDM). The time to specified strain of the CDM model is defined as

$$t_{\varepsilon}(\sigma,T) = \left[1-\left(1-\frac{\varepsilon}{\alpha_0}\right)^{1/\alpha_1}\right]t_{r} \tag{11}$$

$$\varepsilon_{t}(\sigma,T) = \left[1-\left(1-\frac{t}{t_{r}}\right)^{\alpha_1}\right]\alpha_0 \tag{12}$$

where t_{ε} is the time to specific strain, ε_{t} is the strain at specific time, t_{r} is the time to rupture, α_0 and α_1 are fitting factors, T is the temperature (K), σ is the engineering stress (MPa) and ε is the creep strain.

A comparison of the predicted strain at specified times for the LCSP, Norton minim strain rate, Nadai and the CDM model is presented in Fig. 8. In the primary creep regime the CDM and the Norton minim strain rate

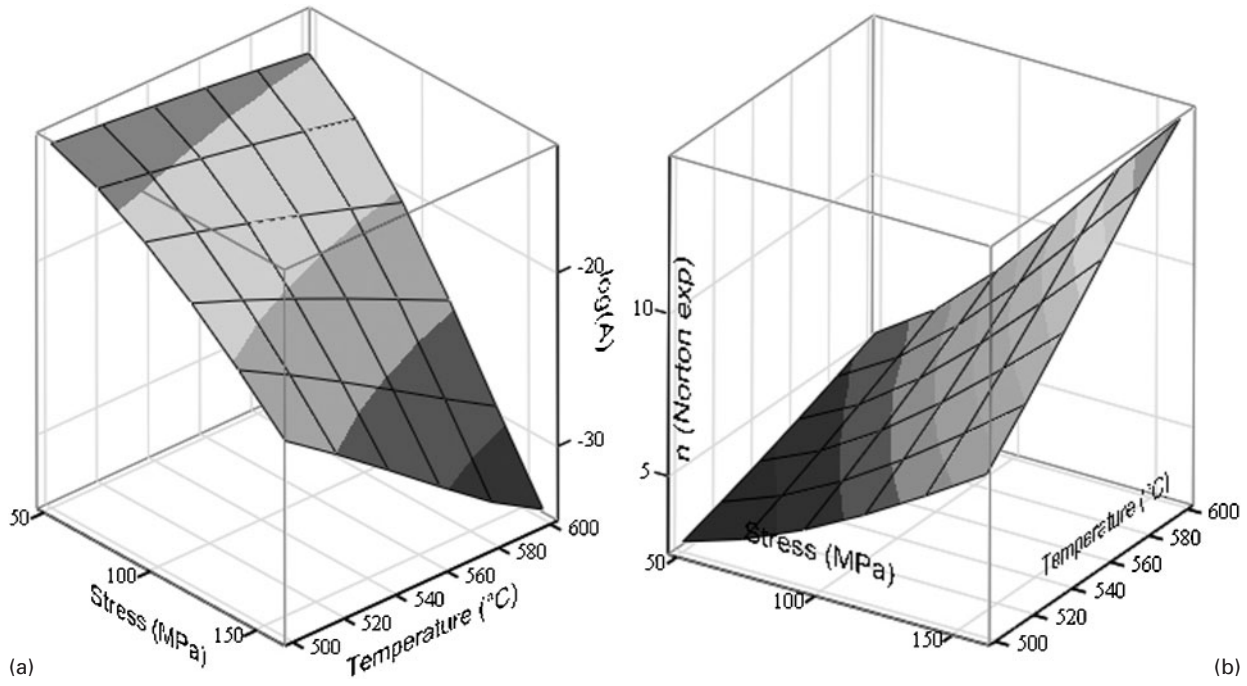

6 Norton law parameters *a A* and *b n* for steel P22, as predicted by LCSP model

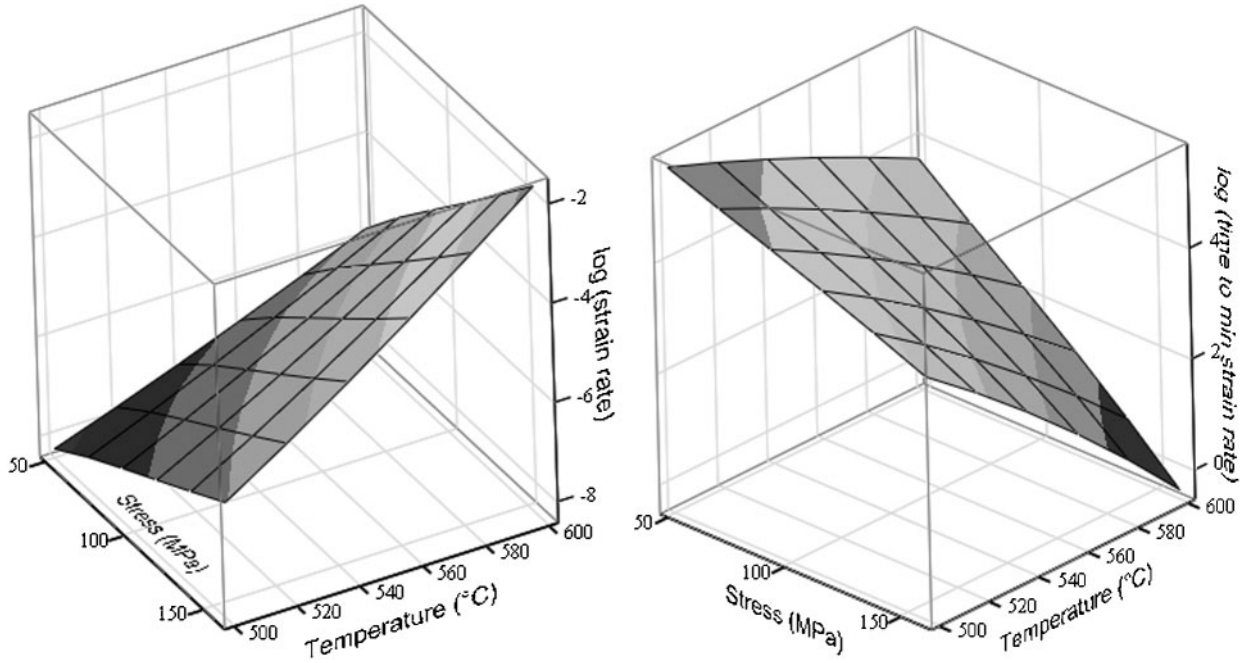

7 Minimum creep rate and time to minimum creep rate for P22 steel, as predicted by LCSP model

models behave similarly (*see* Fig. 8*b*), but the predicted strain is underestimated. The Nadai model improves the primary creep strain prediction, but the model is not flexible enough to accommodate data accurately, at least when fitting to raw data up to time to minimum strain rate. Some configuration of synthetic data or data point weighting in the fitting routine might improve this shortcoming. In the secondary to tertiary creep regimes, the CMD model produces improved strain predictions closing in on the raw data and the LCSP results. The Nadai and the Norton model do naturally not produce good predictions beyond this point since they do not accommodate tertiary creep. It is to be noted that the LCSP creep strain model was able to represents all three regimes accurately. The presented LCSP case is calculated on the true rupture time of the test and using optimal shape parameters, the CDM, Nadai and the basic Norton are also all optimal fits.

One of the main features of the LCSP is the temperature and stress dependence on the curve shape. As the rupture life becomes longer (low temperature or low stress) the shape of the creep curve changes. The differences in the shape of the predicted short and longer term creep curves for steel P22 are demonstrated in Fig. 9.

Many common creep related design and assessment problems can be solved by using FE software packages that typically include some creep models to describe strain evolution in time. However, the corresponding generic materials data in e.g. EN standards are usually expressed in terms of time to rupture rather than time to given strain. Even though generic strain related data exist, it tends to be limited to few fixed points such as time to 1% strain, without information of important preceding strain evolution. For example for many design problems the strains $<1\%$ are the most important, as this can be the limit to the end of the design life.

Here a new simple and robust creep strain model (LCSP) has been described to include all essential features of typical uniaxial constant load or constant

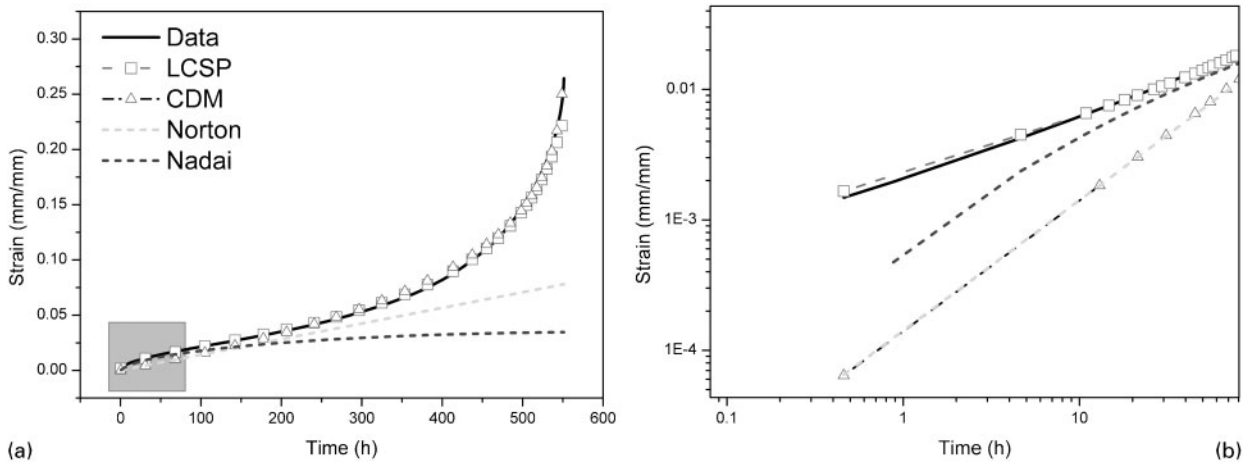

a linear presentation of creep curve and model predictions; *b* blow up of squared section presented in logarithmic scales for emphasis on primary creep representation

8 Comparison between basic Norton (equation (9), Nadai (equation (10), CDM (equation (12) and LCSP (equation (2) predictions of strain at specified time for creep curve presented in Fig. 2

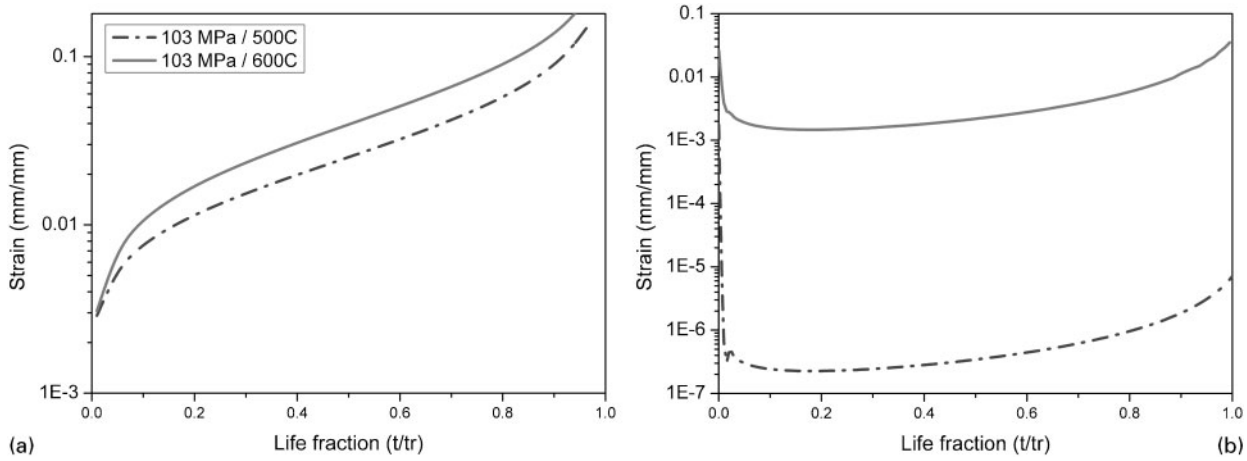

9 Comparison of *a* normalised short term (rupture at 600°C for 40 h, continuous line) and longer term (rupture at 500°C for 100 000 h, dotted line) creep curves for steel P22 and *b* corresponding strain rates

stress creep curves, with capabilities to predict realistic strain for design and life assessment. When needed, the same model can also predict through simple algebraic formulation time to given, strain rates and minimum strain rates. The LCSP model can be implemented to FE codes directly, or if preferred, by providing the required description of simplified models (such as Norton and Nadai) that are commonly included in the commercial FE packages.

The LCSP model is robust, because it requires minimal numerical transformations and relatively few free fitting constants. The model is also accurate and shows generally very competitive fitting to the creep testing data, as was shown when comparing to the results of the ECCC intercomparison exercise.

A particular advantage of the LCSP approach is its ability to utilise the existing creep rupture models (or data) that are much more widely available than information on creep strain. In principle, a correlation between time to given creep strain and time to rupture can be expected from the often observed correlation among the primary, secondary and tertiary stages of creep.

Conclusions

A robust strain model based on the time to rupture curves has been developed to cover the whole creep curve. This LCSP model makes use of the creep rupture model of the same material, to fully utilise the robustness and usually much more extensive data base of creep rupture information. The strain model itself is simple and defines a creep curve only with three parameters (stress and temperature dependent) in addition to those of the corresponding rupture model. In its basic form the LCSP model optimises a non-linear asymmetric logistic transition function fitted in logarithmic strain against a TTP, giving the time to a specified strain. Unique features of the LCSP model include simple inverse expressions for strain and strain rates. The new model has been shown to be very competitive when compared with any other creep strain models of the ECCC intercomparison activity on a single heat data set of the steel P22 (10CrMo9-10). By comparing with the stress values to 1% creep strain as given in DIN 17243 for the same material type, the model was shown to provide accurate predictions at 10 000 and 100 000 h.

Acknowledgements

The authors wish to acknowledge the support from Academy of Finland (decision 117700), the RFCS project *Aloas* and the *Extreme* project of VTT. Also the discussion and data support of the ECCC (WG1) are greatly acknowledged.

References

1. S. Holmström, P. Auerkari and S. Holdsworth: Proc. 8th Liege Conf. on 'Materials for advanced power engineering', Liege, Belgium, September 2006, Forschungszentrum Jülich GmbH, 1309–1318.
2. S. R. Holdsworth, M. Askins, A. Baker, E. Gariboldi, S. Holmström, A. Klenk, G. Merckling, R. Sandström, M. Schwienheer and S. Spigarelli: Proc. ECCC Conf. on 'Creep and fracture in high temperature components – design and life assessment issues', London, UK, September 2005, DeStech Publications, Inc., 441–451.
3. S. Holmström, P. Auerkari and J. Rantala: Proc. 11th Conf. on 'Pressure vessel technology', Vancouver, BC, Canada, July 2006, American Society of Mechanical Engineers, 10.
4. S. Holmström and P. Auerkari: Proc. Baltica Conf. on 'Life management and maintenance for power plants', VTT Symposium 234, Espoo, Finland, June 2004, VTT, 513–521.
5. S. R. Holdsworth and G. Merckling: Proc. 6th Int. Charles Parsons Conf. on 'Engineering issues in turbine machinery, power plant and renewables', Trinity College, Dublin, Ireland, September 2003, 411–426, IOM.
6. 'Creep data validation and assessment procedures', (ed. S. R. Holdsworth *et al.*), ECCC recommendations; 2001, Leatherhead, UK, ERA Technolgy publ.
7. 'Guidance on methodology for the assessment of stress-rupture data', BS PD6605, British Standard Institution, London, UK, 1998.
8. M. Evans: *Mater. Sci. Technol.*, January 1999, **15**, 91–100.
9. S. R. Holdsworth: *Mater. High Temp.*, 2004, **21**, (1), 125–132.
10. F. V. Ellis and S. Tordonato: *J. Pres. Ves. Technol.*, February 2000, **122**, 66–71.
11. K. H. Kloos, J. Granacher and M. Monsees: *Steel Res.*, 1998, **10–11**, 446–453.
12. 'Weldable heat resisting steel forgings and rolled or forged steel bars; technical delivery conditions', DIN 17243, Deutche Institut für Normung E.V., Germany, 1987.
13. 'Seamless steel tubes for pressure purposes – technical delivery conditions – part 2: non-alloy and alloy steel tubes with specified elevated temperature properties', CEN EN 10216–2, 2002.
14. W. Bendick: *Int. J. Pres. Ves. Pip.*, 1991, **47**, 57–78.
15. M. Prager: *J. Pres. Ves. Technol.*, August 2000, **122**, 273–280.
16. J.-P. Clech: Proc. Conf. on 'Electronic components and technology', Orlando, FL, USA, May–June 2005, 1261–1271.

Paper VII

Modeling and verification of creep strain and exhaustion in a welded steam mixer

In: Journal of Pressure Vessel Technology.
Vol. 131 (2009), 061405 (5 pages).

PVT -08-1091

MODELING AND VERIFICATION OF CREEP STRAIN AND EXHAUSTION IN A WELDED STEAM MIXER

Stefan Holmström (stefan.holmstrom@vtt.fi), Juhani Rantala, Anssi Laukkanen, Kari Kolari, Heikki Keinänen
VTT Technical Research Centre of Finland, P.O. Box 1000, FI-02044 VTT

Olli Lehtinen, Fortum Power & Heat, Finland

ABSTRACT

Structures operating in the creep regime will consume their creep life at a greater rate in locations where the stress state is aggravated by triaxiality constraints. Many structures, such as the welded steam mixer studied here, also have multiple material zones differing in microstructure and material properties. The 3-dimensional structure as such in addition to interacting material zones is a great challenge for finite element analysis (FEA), even to accurately pinpoint the critical locations where damage will be found. The studied steam mixer, made of 10CrMo 9-10 steel (P22), has after 100 000 hours of service developed severe creep damage in the several saddle point positions adjacent to nozzle welds. FE-simulation of long term behaviour of this structure has been performed taking developing triaxiality constraints, material zones and primary to tertiary creep regimes into account. The creep strain rate formulation is based on the logistic creep strain prediction (LCSP) model implemented to ABAQUS, including primary, secondary and tertiary creep. The results are presented using a filtering technique utilising the formulation of rigid plastic deformation for describing and quantifying the developing "creep exhaustion".

INTRODUCTION

The structural integrity of high temperature welded structures has been widely studied and published, often however as rather simple girth weld cases [1]-[10]. In these the development of stress (von Mises or maximum principal stress) and strains (axial or hoop) are followed and conclusions regarding critical locations are usually drawn from the locations of maximum stresses or strains. Furthermore simulations are often based on steady state creep strain rates and the impact of triaxiality constraints and multiaxial creep ductility are seldom taken into account. As a consequence these studies often fail to pinpoint the locations where service exposed components actually would develop creep damage. In the design stage this could become a problem emerging later in the life of the component, as it did with the mixer studied here at about half the desired (design) life. The influence of creep ductility exhaustion under multiaxial conditions has

been studied [11]-[14] and also implemented in design codes [15]-[17] in recent years but the implementation for life management and remaining life predictions of service exposed components is not yet satisfactorily solved. Here the LCSP method [18][19] has been implemented to ABAQUS finite element analysis software and used for the long term creep deformation simulation of a mixer tank with a welded nozzle. The model is able to predict creep in primary to tertiary stage. In addition the evolving creep exhaustion related to multiaxial constraint is visualised through a new filtering technique [20] , based on a classical relation [21] for creep ductility ratio. The filtering technique is accurately pinpointing the critical locations (showing most creep damage) in the saddle point of the component. The mixing vessel operates at nominal pressure of 185 bar equalling a skeletal von Mises stress around 37 MPa in the main body when calculated as a simple pipe. The future challenge will be to predict the impact of weld repair for the life extension of the component. The creep models and rupture properties for the material 10CrMo 9-10 are based on the standard EN 10216 [22] and ECCC recommendations [23].

THE ASSESSED STEAM MIXER

The studied steam mixer (10CrMo 9-10) has after 100 000 h severe creep damage (see Fig. 1 and Fig. 2) in the saddle point position adjacent to the weld. The maximum crack lengths encountered were over 200 mm in length and even with 4 mm ground from the wall thickness oriented cavitation was still found.

The main dimensions of the steam mixer are:

main body: outer diam. 376 mm, wall 66 mm

nozzle pipe: outer diam. 300 mm, wall 61 mm

The operating pressure of 185 bars introduces skeletal stresses (calculated as pipes) of 31 MPa in the nozzle pipe and 37 MPa in the main body. The design pressure, selected for the simulation, is 206 bar equalling in 34 and 41 MPa skeletal stresses correspondingly.

At 600°C the design stress relates to uniaxial rupture times at about 60 000 h [22] , but at the operating temperature of 525°C the predicted rupture time exceeds one million hours for parent material which is far beyond recommended extrapolation range.

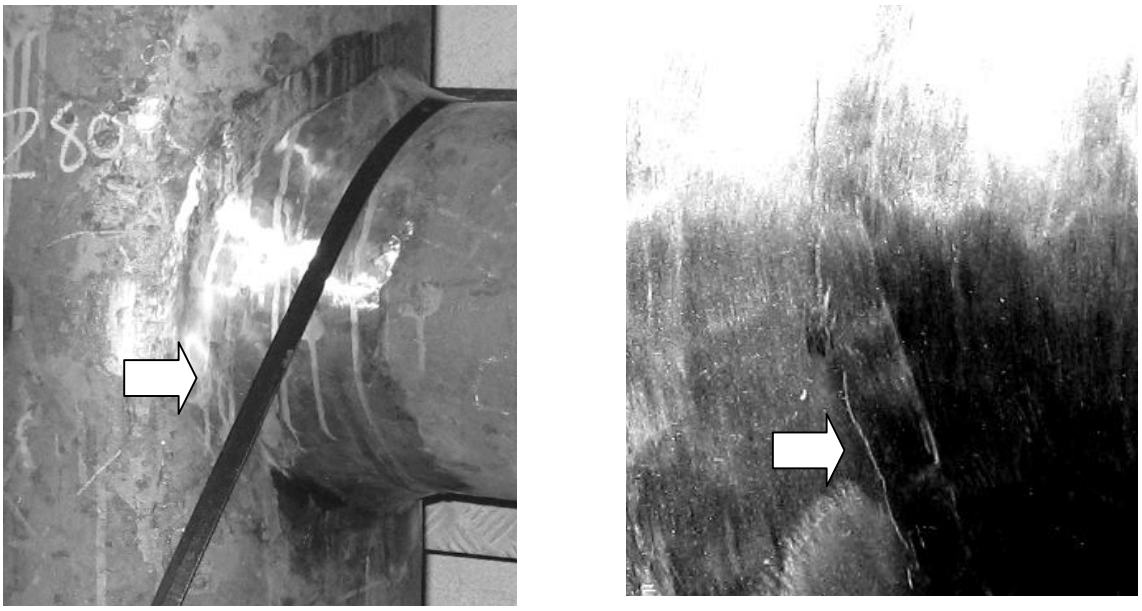

A B

Fig. 1. A) Upper nozzle of high pressure mixer. B) Detail of 200 mm crack at nozzle weld (HAZ).

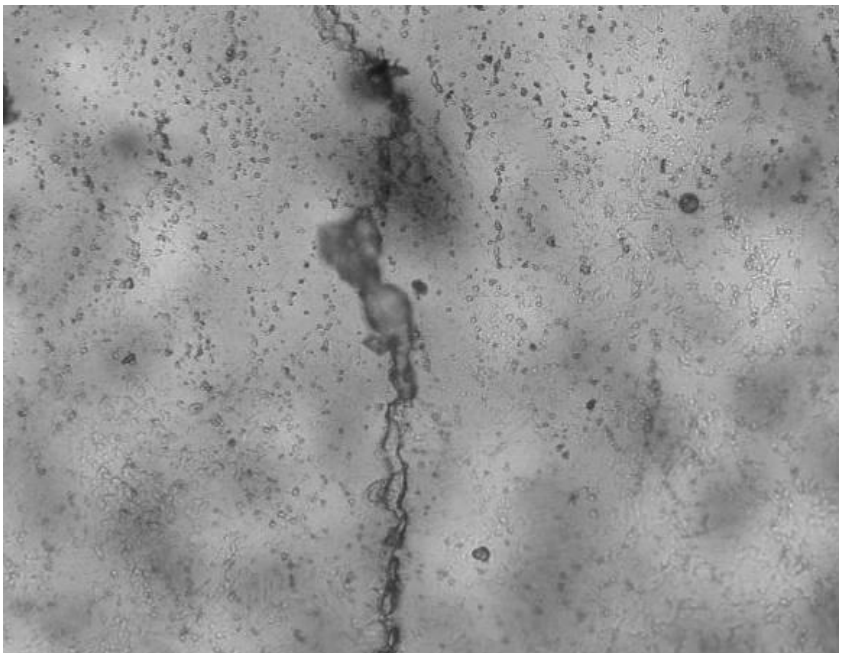

Fig. 2. A) Creep cavitation and crack formation in one of the upper nozzles.

THE STRAIN MODEL

The creep strain model, logistic creep strain prediction method or LCSP, is based on time to rupture and shape functions. This is also the models greatest strength since nearly the same interpolation and extrapolation robustness can be achieved for the strain model as for the rupture model. The LCSP model assumes that the full creep strain curves at

specified temperature and stress can be acquired from knowing only the time to rupture and two material specific shape functions p(σ,T) and x0(σ,T) (see Eq.1).

In LCSP time t_ε to creep strain ε^{cr} is defined as

$$\log(t_\varepsilon) = \frac{(\log(t_r) + C)}{1 + (\frac{\log(\varepsilon^{cr})}{x_0})^p} - C \qquad (1)$$

where t_r is the time to rupture from a creep rupture model, and x0, p and C are fitting factors defining the curve shape. The LCSP can easily be rewritten to give strain at specified time and then differentiated (analytically) to give strain rate as a function of time, stress and temperature.

As an example of the LCSP data fit some short term P22 creep curve data (0.1, 0.2, 0.5, 1, 2, 5, 10, 15% and fracture strain [18]) of an ECCC short term data set (10CrMo 9-10), is presented in Fig. 3 as accumulated strain against the temperature compensated time to strain (Larson-Miller parameter form).

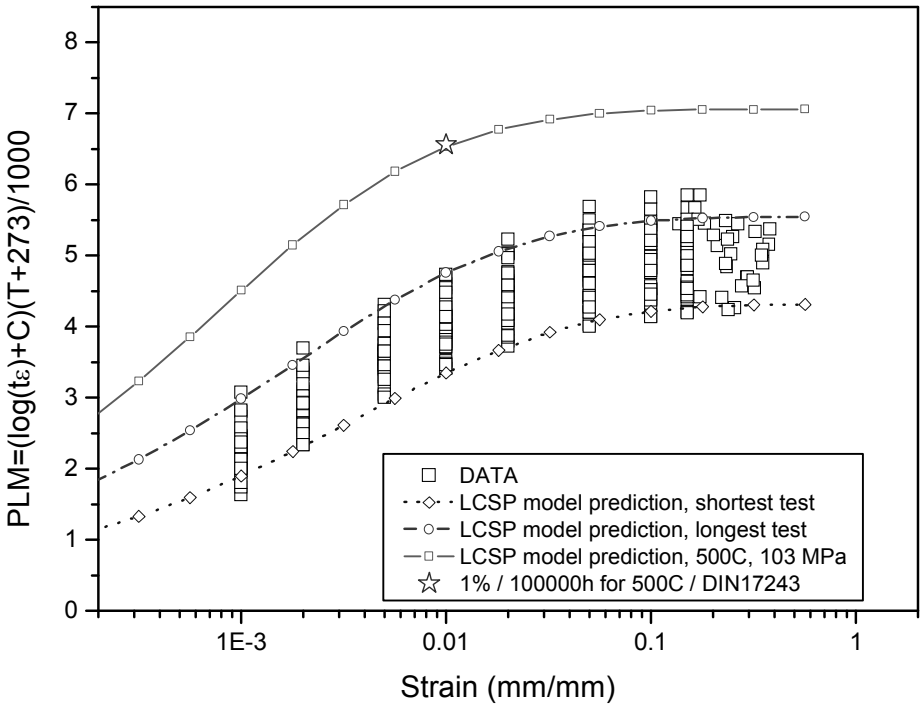

Fig. 3. ECCC short term 10CrMo 9-10 strain data (0.1 to fracture strain) presented in time temperature parameter form with modelled LCSP predictions of longest and shortest test and for the standard value stress 500°C /103 MPa giving 1% at 100 000 h (marked as a star, [25]).

The LCSP model has earlier been successfully implemented on strain measurement data from the same power plant on another steam mixer exceeding 200 000 h of service [26].

For the ABAQUS FEA software the LCSP model has been implemented as a CREEP user subroutine [27]. The subroutine is called at each integration point of the mesh. The steam mixer was modelled using 20-node brick elements (C3D20R). The number of elements in the model was 11 592 and the total number of variables (including Lagrange multiplier variables) was 158 523.

In the subroutine the equivalent creep strain increment $\Delta\varepsilon^{cr}$ must be defined for each time step. The equivalent creep strain ε^{cr} must be a conjugate to the von Mises stress q so that the strain energy rate density $\dot{W}^{cr}$ equals

$$\dot{W}^{cr} = \int_0^{\dot{\varepsilon}^{cr}} q \, \mathrm{d}\dot{\varepsilon}^{cr} = \int_0^{\dot{\varepsilon}} \sigma_{\mathrm{ij}} : \mathrm{d}\varepsilon_{\mathrm{ij}}{}^{cr} \tag{2}$$

where elastic strain rates are ignored. In the CREEP subroutine the equivalent creep strain increment $\Delta\varepsilon^{cr}$ is then integrated by the Euler backward algorithm:

$$\Delta\varepsilon^{cr} = \dot{\varepsilon}^{cr} \, \Delta t \tag{3}$$

where $\dot{\varepsilon}^{cr}$ is obtained from Eq. (1) after some manipulation.

In addition the following derivate

$$\Delta K = \frac{\partial \Delta\varepsilon^{cr}}{\partial q} \tag{4}$$

is required for implicit creep integration.

At very small stresses linearization and Taylor series development has been made both for the rupture master curves (danger of turn-back) and shape parameters (outside range of data), these modifications enable safe operation of the model, i.e. non-physical (such as infinite strain rate) constitutive response does not result from values typically outside the scope of the experimentally determined LCSP model parameters (such as very small field variables and solution time). Terms required by Abaqus, Eqs. 3. and 4., can be computed with relative ease since the LCSP model provides a closed form expression of the equivalent creep strain and creep strain rate. The internal routines of Abaqus translate the uniaxial response to a multiaxial one by using a conventional J_2 incremental plasticity flow rule.

THE CREEP PROPERTIES FOR BM, HAZ AND WM

The successful simulation of the welded structure needs rupture and shape models for base (BM), weld metal (WM) and heat affected zone (HAZ). In this work, for the heat affected zone (HAZ), it is assumed that the time to rupture is following a 20% reduction in strength (WSF=0.8) in relation to the base material. For the WM three different situations were simulated based on different time factors (or normalised rupture time of 1, 2 and 0.5) as defined in Eq 9. in relation to the base material as in *Table 1*. The base material creep response was defined using a creep rupture master curve (any model type is possible) for P22 material such as the minimum commitment or the Mendelson-Roberts-Manson (MRM) methods [24] fitted to available rupture data. The rupture master curve can then be applied for t_r in Eq 1. together with the creep curve shape functions (Eq. 5-6);

$$x_0(\sigma,T) = -0.391+0.696\cdot\log(\sigma)-3392.5/(T+273) \quad (5)$$

$$p(\sigma,T) = 4.363-2.271\cdot\log(\sigma)+3874.9/(T+273) \quad (6)$$

in the place of *x0* and *p* in Eq.1.

Material property ratios have been used by Perrin and Hayhurst [2][3] for characterising the creep properties of weld metal and the heat affected zone in relation to the base material. In this work the normalised parameters chosen for characterisation of the material zones are;

normalised primary creep strain $$\kappa = \left[\frac{\varepsilon_{prim}}{\varepsilon_f}\right] \quad (7)$$

ratio of minimum creep rates β $$\beta = \left[\frac{\dot{\varepsilon}_{\min}}{\dot{\varepsilon}^{b}_{\min}}\right] \quad (8)$$

normalised rupture time = time factor $$\xi = \left[\frac{t_R}{t^{b}_R}\right] \quad (9)$$

where ε_{prim} is the primary creep strain component, ε_f is the fracture strain (simulated at 95% of life), t_R is the time to rupture and $\dot{\varepsilon}_{\min}$ the minimum creep strain rate. The superscript *b* (in β and ξ) is indicating the base material property. The resulting normalised property ratios are listed in *Table 1* showing the material zone differences.

Table 1. Calculated and pre-determined material property ratios for BM, HAZ and WM at 525 °C. Note the assumed time factors for the simulated WM (in bold).

Zone	LCSP simulation		
	κ	β	ξ
BM	0.036	1.00	1.00
HAZ	0.035	2.58	0.46
WM1 (=BM)	0.036	1.00	**1.00**
WM2	0.036	0.536	**2.00**
WM3	0.034	2.05	**0.50**

An example of predicted creep strain response (uniaxial) in the different zones of a weld at 525°C / 37 MPa is shown in *Fig. 4.*

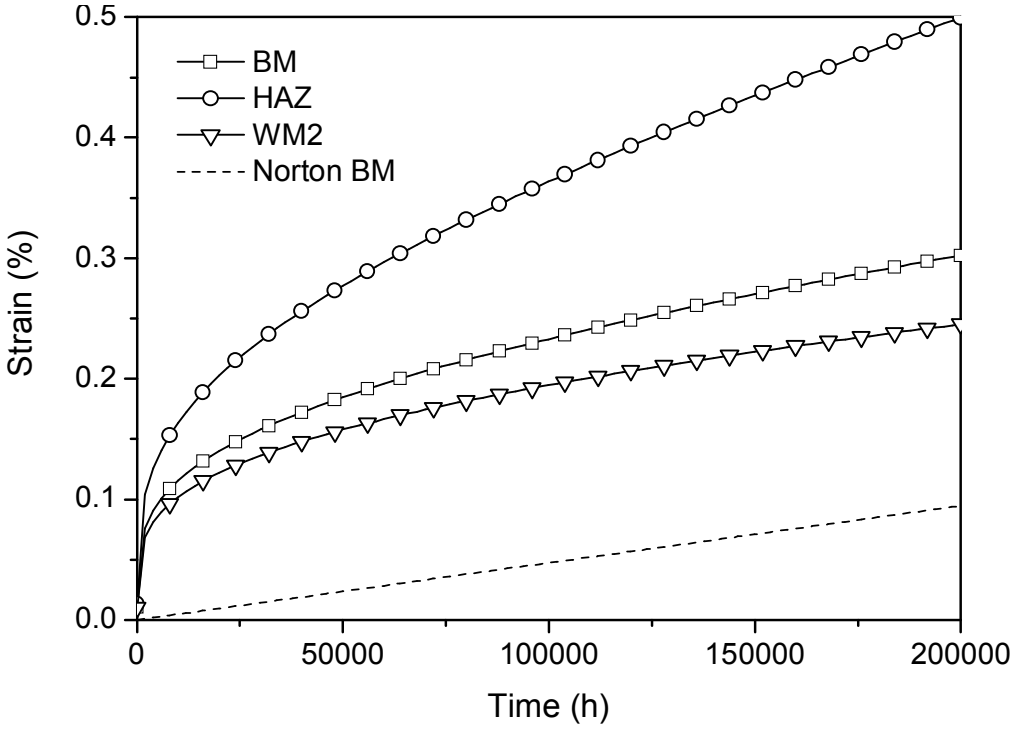

Fig. 4. Simulated creep curves at service pressure and temperature (first 200 000 h) for BM, HAZ (WSF=0.8) and WM2 as in Table 1. The dashed line represents the accumulated strain if using minimum creep rate only (BM).

MANAGING CONSTRAINT BY Λ-FILTERING

It is commonly known that for long term creep of pressure vessels the maximum equivalent stresses and strains develop on the inner surface vessel whereas the maximum principal stress will redistribute towards the outer surface due to creep. The multiaxial creep ductility again (due to the triaxiality constraint) will reduce towards the outer surface as creep proceeds under long term service. Therefore a technique for filtering the acquired FE results has been developed using the expression for rigid plastic deformation [11] as presented in Eq. 10-11;

$$\Lambda = \frac{\varepsilon^{cr}}{1.65 \cdot \exp(-1.5 \cdot h)} = \frac{\varepsilon_{fu}}{\varepsilon_{fm}} \cdot \varepsilon^{cr} \tag{10}$$

$$h = \left[\frac{\sigma_{kk}}{3 \cdot q} \right] \tag{11}$$

Where σ_{kk} is the trace of a stress tensor σ_{ij}, q the von Mises stress, ε_{fu} the uniaxial creep ductility, ε_{fm} the corresponding multiaxial creep ductility and ε_m the multiaxial creep strain at the time of observation (momentary strain). Eqs. 10. and 11. are founded on a classical Rice-Tracey type of damage model incorporating the effects of multiaxial stress state to failure strain [29]. The Rice-Tracey approach is the simplest model for inclusion of constraint effects to failure properties, and is founded on an analysis of growth of a spherical void under differing conditions of stress triaxiality. Different stress states yield different void growth rates, thus resulting in the dependency of failure strain on stress triaxiality. The Rice-Tracey approach is particularly feasible due to its simplicity. i.e. it does not couple to the time history of the problem and can be used a filtering technique on top of analysis results.

The filtering technique does not require local creep ductility values since it is expressed as a ratio dependent on stress and momentary strain only. Previous experience from Λ-filtering has been acquired from finding critical damage locations in simple girth welds [28].

FEA RESULTS FOR THE MIXER

The mixer case was evaluated under design pressure for the three combinations of weld metals with constant HAZ and BM properties at 600°C and for weld metal (WM2) at 525°C. The 600°C simulations were initial test runs with less extrapolation involved (in stress) though at too high a temperature for the material as such. The 525°C simulation case represents an actual life prediction at design pressure, however with an extrapolated uniaxial rupture prediction exceeding one million hours.

The results were studied at 1000 hours for the 600°C simulations and at 100 000 h for the 525°C simulation. The runtime of the steam mixer simulation to 100 000h was 8 hours of CPU time (8 h 20 minutes of wall clock time) with an 3.80GHz Intel Xeon PC.

The selected time of study for the 600°C cases was determined through a simple Larson-Miller time-temperature transformation. At the selected simulation time strains, stresses and "creep exhaustion" (Λ-values as defined by Eq. 10.) were determined (see *Table 2*).

Table 2. Creep exhaustion localisation (critical location), maximum calculated Λ-value, von Mises stress and maximum principal strain at the specified location.

Case	**Critical location**	**maximum Λ-value**	**σ_{VM} (MPa)**	**ε_1 (%)**
600°C WM1	saddle point surface (HAZ)	0.015	54	0.5
600°C WM2	saddle point surface (HAZ)	0.018	56	0.7
600°C WM3	overflow at 422 h shear in WM	-	-	>20
525°C WM2	saddle point surface (HAZ)	0.015	57	0.6

The 525°C simulation results (Λ-values, maximum principal strain and von Mises stress) are presented in Fig. 5-Fig. 7.

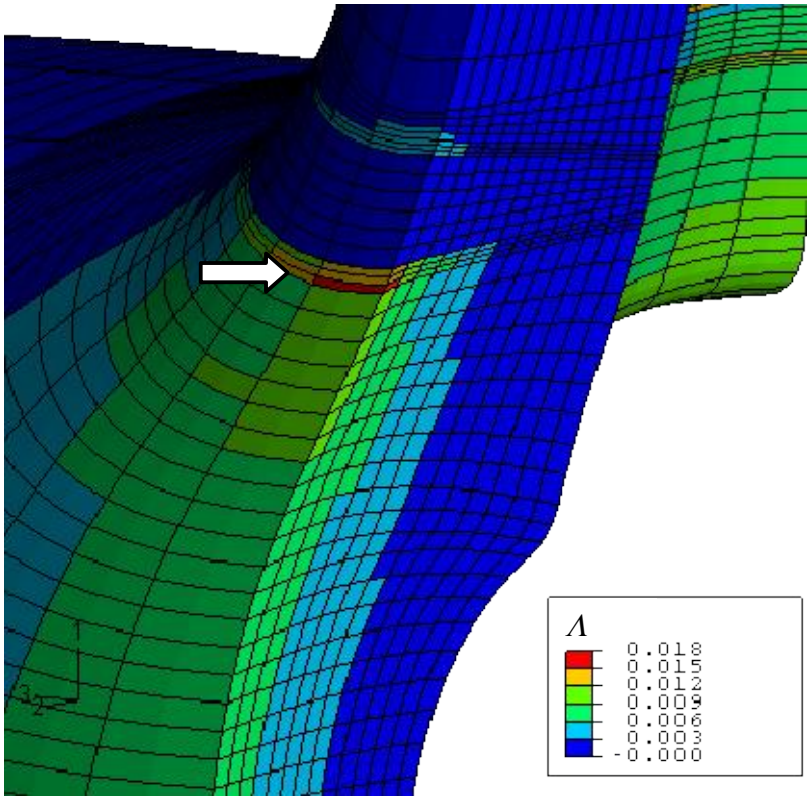

Fig. 5. Creep exhaustion (Λ-values) after 100 000 h / 525°C.

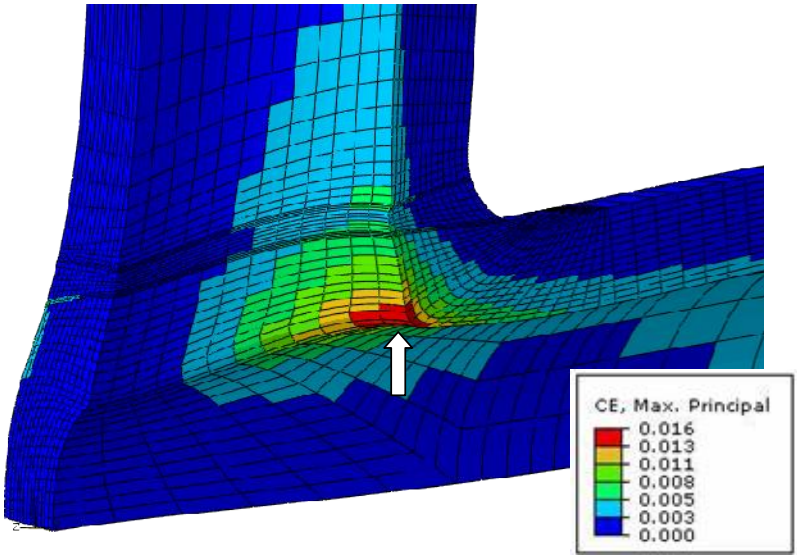

Fig. 6. Creep strain (maximum principal) after 100 000 h / 525°C, note location (inner surface BM)

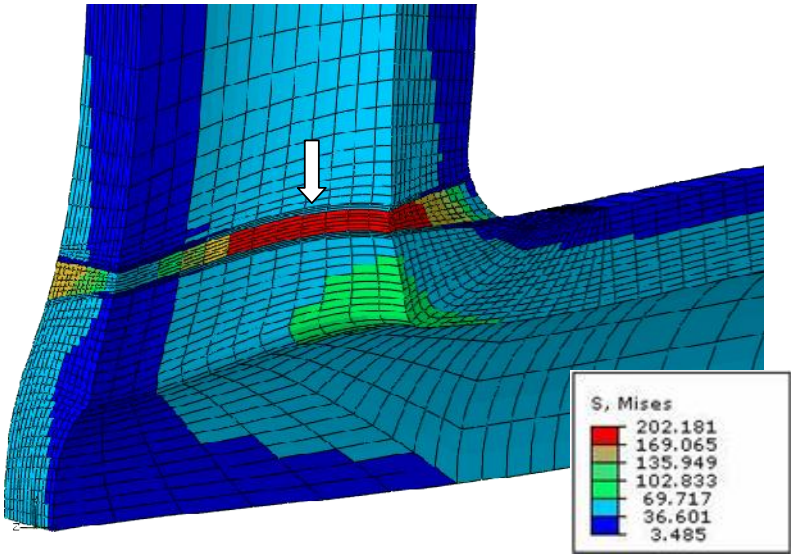

Fig. 7. Stress (von Mises) after 100 000 h / 525°C, note location (inner surface WM)

The maximum Λ-values acquired from the simulations with WM1 and WM2 seem low but when divided with values for uniaxial creep fracture strain as in Eq. 10, the consumed creep strain can be attained (see *Table 3*). At the point of observation (100 000 h) the results are very reasonable for expected low ductility in uniaxial long term tests of cross welds.

Table 3. Consumed creep strain (% of available) in the critical HAZ location of Fig. 5 after 100 000 h of service (design pressure) as a function of uniaxial creep ductility.

Uniaxial creep ductility	**Consumed creep strain**
10 %	15 %
8 %	19 %
6 %	25 %
4 %	37 %
2 %	75 %
1.5 %	100 %

As earlier stated the filtering technique as such does not require local creep ductility values since it is expressed as ratio dependent on stress and momentary multiaxial creep strain. The 600°C simulations with different WM show the difference in damaging mechanism. The weld with a over-matched weld metal (WM2) shows maximum Λ-values in the outer HAZ saddle point surface (see Fig. 8) and the weld with a very weak weld metal (WM3) fails prematurely due to extensive deformation in the WM (see Fig. 9).

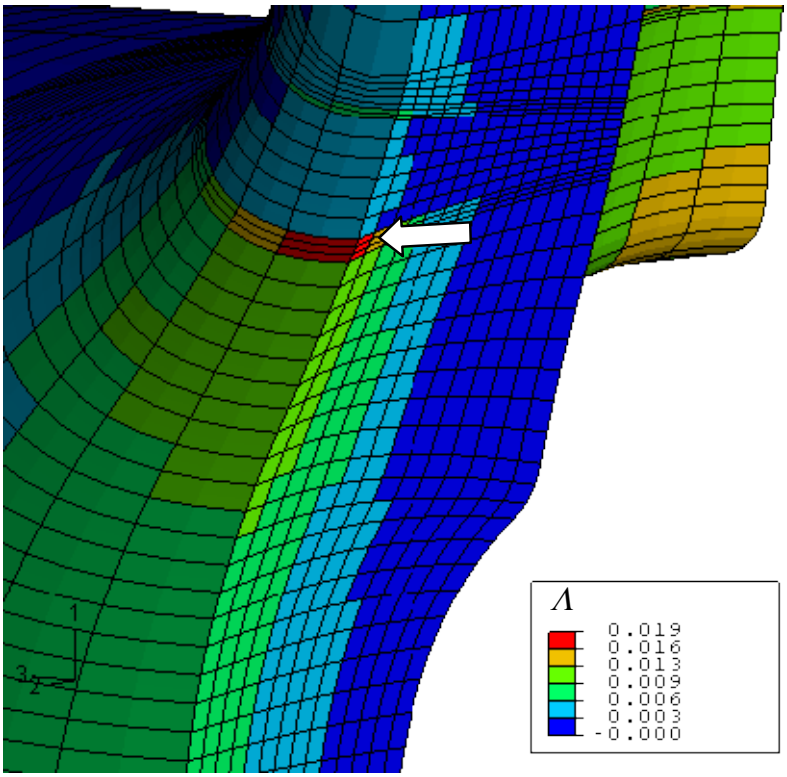

Fig. 8. Creep exhaustion after 1000 h at 600°C with over-matched weld metal (WM2). Compare with 525°C simulation in Fig. 5.

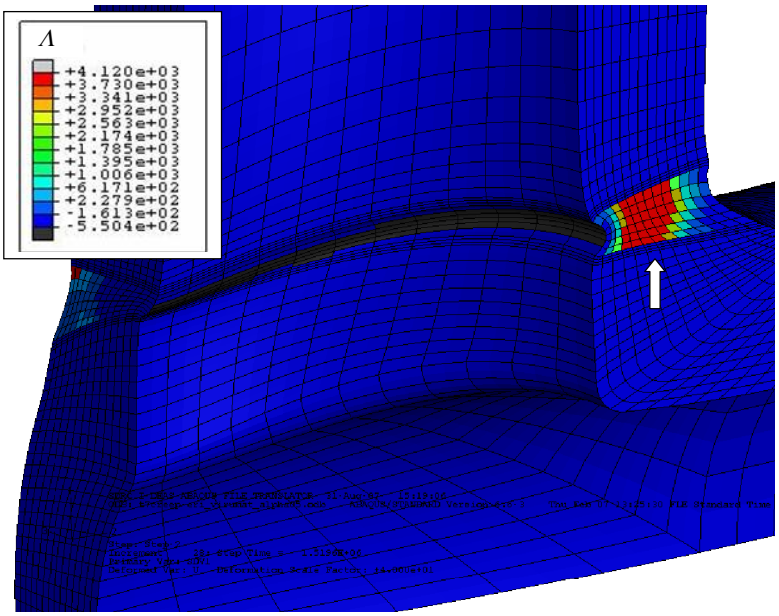

Fig. 9. Creep exhaustion after 422 h at 600°C with weak weld metal (WM3). Note the failing weld metal.

DISCUSSION AND CONCLUSIONS

The LCSP creep strain model has been used for the steam mixer simulations, including primary to tertiary creep. The ABAQUS implementation of the model is working smoothly with satisfactory processing time. The numerical analysis, especially utilising the Λ-filtering technique seems to accurately pinpoint the critical damage locations of the steam mixer. The 3-zone weld simulation (BM, WM and HAZ) produce differing amounts of damage and a change of critical location depending on selected WM properties. Earlier inspection data exists for the case mixer and also for another mixer in the same power plant. This data will eventually be used for further calibration of the filtering technique. The current of the Λ-filter seem to work well for estimating the consumed creep strain but other forms more suitable for creep such as the creep ductility functions proposed by Cocks and Ashby referenced in [18], Andreas [13] or Spindler [14] should be tested for improved results. In conclusion it is quite evident that a powerful tool for high temperature component life assessments has been created and that advanced multiaxial creep modelling can now be performed with only a minimum amount of actual strain data. This feature will be especially handy for modelling structures with new materials with limited data and for pinpointing critical locations in components in service, thus improving inspection targeting. The new FEA tools will in the near future also be used for assessing large components made of P91 and X20 steels.

ACKNOWLEDGEMENT

The support of the Academy of Finland, decision nr. 117700 (Prof. Kim Wallin) is gratefully acknowledged. Fortum Power & Heat is also gratefully acknowledged for all support related to the steam mixer case study.

REFERENCES

[1] Holmström S, Laukkanen A, Calonius K, Weldment matching for creep life of P22 and P91 girth welds. Conf. on Integrity of high temperature welds, 24-26 April 2007, London UK

[2] Hayhurst D. The use of computational creep continuum damage mechanics to optimise materials selection for high temperature weldments, Modelling Simul. Mater. Eng. 2, 1994, p.421-438.

[3] Perrin I, Hayhurst D, A method for the transformation of creep constitutive equations, Int. J. Pres. Ves. & Piping 68, 1996, p299-309.

[4] Perrin I, Hayhurst D, Ainsworth A, Approximate creep rupture lifetimes for butt welded steel pressurised pipes. Eur. J. Mech. a/Solids 19, 2000, p.223-258.

[5] Law M, Payten W, Weld performance under creep using finite element modelling, Int. J. Pres. Ves. & Piping 72, 1997, p45-49

[6] Law M, Payten W, Snowden S, Creep Modeling of welded joints using the theta projection concept and finite element analysis, Journal of Pressure Vessel Technology, ASME transactions Vol. 122, 2000, p. 22-26.

[7] Hyde T.H, Sun W, Life prediction of repair welds in pressurised CrMoV pipe with incorporation of initial damage, Int. J. Pres. Ves. & Piping 81, 2004, p1-12

[8] Wu R, Sandström R, Seitisleam F, Influence of extra coarse grains on the creep properties of 9 percent CrMoV (P91) steel weldment, Journal of engineering and technology, Transactions of ASME Vol. 126, p. 87-94.

[9] Becker A, Hyde T, Sun W, Andersson P, Benchmark for finite element analysis of creep continuum damage mechanics, Comp. Mat. Sci. 25, 2002, p 34-41.

[10] Law M, Payten W, Small R, Modelling the creep behaviour of reheat header longitudinal weld, Int. J. Pres. Ves. & Piping 77, 2000, p.99-103.

[11] Hurst R.C, Rantala J.H. Influence of multiaxial stresses on creep and creep rupture of tubular components, ASM Handbook, Vol. 8, 2000 p. 405-411

[12] Webster G., Holdsworth S., Loveday M., Nikbin K., Perrin I., Purper H., Skelton R., Spindler M., Fatigue & Fracture of Engineering Materials & Structures, Volume 27, Number 4, April 2004 , pp. 319-342(24), Publisher: Blackwell Publishing

[13] Andreas, W. Evaluation of creep damage due to woid growth under traxial stress states in the design of steam turbine components. JSME. IntJ. Ser A 45, p. 72-77.

[14] Spindler M.W. The multiaxial creep ductility of austenitic stainless steels. Fatigue Fract Engng Mater Struct 27, 2004. p. 273-281.

[15] R5 (2001) Assessment procedure for the high temperature response of structures. British Energy, Glouchester UK.

[16] ASME (2000) Section III Div. 1. Sub-Section NH, ASME, New York, USA

[17] RCC-MR (1987) Design and construction rules for mechanical components of FBR nuclear islands, Paris France.

[18] Holmström S, Auerkari P, Robust prediction of full creep curves from minimal data and time to rupture, submitted to Energy Materials; Materials Science and Engineering for Energy Systems. doi:10.1179/174892406X173594, 2006, Vol 1. p249-255

[19] Holmström, S., Auerkari, P., Holdsworth S. Predicting creep strain response from rupture data and robust creep curve model. International Conference on Life Management and Maintenance for Power Plants. Helsinki-Stockholm-Helsinki, 12-14 June 2007. Vol 1.

[20] Holmström, S., Laukkanen A., Calonius, K., Visualising creep exhaustion in a P22 girth weld. International Conference on Life Management and Maintenance for Power Plants. Helsinki-Stockholm-Helsinki, 12-14 June 2007. Vol 2. pp.208-221

[21] Webster G.A. High Temperature Component life assessment. Department of Mechanical Engineering, Imperial Collage of Science, ISBN 0-412-58520-0, Chapman & Hall. 1994, p.37-38

[22] EN 10162, 2002. Seamless steel tubes for pressure purposes. Technical delivery conditions. Part 2: Non-alloy and alloy steel tubes with specified elevated temperature properties. CEN, Brussels.

[23] Holdsworth, S.R., 1996b. ECCC-WG1 Recommendations, Volume 5, Guidance for the Assessment of Creep Rupture, Creep Strain and Stress Relaxation Data, ECCC Document 5524:MC:38 Issue 3.

[24] Holdsworth S., Davies R., A recent advance in the assessment of creep rupture data Nuclear Engineering and Design, Volume 190, Issue 3, 2 June 1999, Pages 287-296

[25] DIN 17243. 1987. Weldable heat resisting steel forgings and rolled or forged steel bars; Technical delivery conditions. Deutche Institut für Normung E.V.

[26] Rantala, Juhani; Salonen, Jorma; Auerkari, Pertti; Holmström, Stefan; Lehtinen, O.; Pitkänen, M.; Nikkarila, R. Life extension of hot steam piping after 200 000 h of service. Energy Materials: Materials Science & Engineering for Energy Systems. Vol. 2 (2007) No: 2, 104-108(5)

[27] ABAQUS. 2007. ABAQUS Online Documentation: Version 6.7-1, Theory Manual [CD-ROM]. ABAQUS Inc.

[28] Holmström S., Laukkanen A., Calonius K., Finding critical damage locations by Λ-filtering in finite-elementmodelling of a girth weld, In press: Mater. Sci. Eng. A (2009), doi:10.1016/j.msea.2008.04.107

[29] Rice, J.R. and Tracey, D.M., On the Ductile Enlargement of Voids in Triaxial Stress Fields, Journal of the Mechanics and Physics of Solids, Vol. 17, Issue 3, 1969, Pages 201-217.

Series title, number and report code of publication

VTT Publications 728
VTT-PUBS-728

Author(s)
Stefan Holmström

Title

Engineering Tools for Robust Creep Modeling

Abstract

High temperature creep is often dealt with simplified models to assess and predict the future behavior of materials and components. Also, for most applications the creep properties of interest require costly long-term testing that limits the available data to support design and life assessment. Such test data sets are even smaller for welded joints that are often the weakest links of structures. It is of considerable interest to be able to reliably predict and extrapolate long term creep behavior from relatively small sets of supporting creep data.

For creep strain, the current tools for model verification and quality assurance are very limited. The ECCC PATs can be adapted to some degree but the uncertainty and applicability of many models are still questionable outside the range of data. In this thesis tools for improving the model robustness have been developed. The toolkit includes creep rupture, weld strength and creep strain modeling improvements for uniaxial prediction. The applicability is shown on data set consisting of a selection of common high temperature steels and the oxygen-free phosphorous doped (OFP) copper. The steels assessed are 10CrMo9-10 (P22), 7CrWVMoNb9-6 (P23), 7CrMoVTiB10-10 (P24), 14MoV6-3 (0.5CMV), X20CrMoV11-1 (X20), X10CrMoVNb9-1 (P91) and X11CrMoWVNb9-1-1 (E911).

The work described in this thesis has provided simple yet well performing tools to predict creep strain and life for material evaluation, component design and life assessment purposes. The uncertainty related to selecting the type of material model or determining weld strength factors has been reduced by the selection procedures and by linking the weld behavior to the base material master equation. Much of the resulting improvements and benefits are related to the reduced requirements for supporting creep data. The simplicity and robustness of the new tools also makes them easy to implement for both analytical and numerical solutions.

ISBN
978-951-38-7378-3 (soft back ed.)
978-951-38-7379-0 (URL: http://www.vtt.fi/publications/index.jsp)

Series title and ISSN	Project number
VTT Publications 1235-0621 (soft back ed.) 1455-0849 (URL: http://www.vtt.fi/publications/index.jsp)	36468

Date	Language	Pages
January 2010	English	94 p. + app. 53 p.

Name of project	Commissioned by
SA-KWAK jatko	

Keywords	Publisher
Creep, strain, damage, modeling, steel, OFP copper	VTT Technical Research Centre of Finland P. O. Box 1000, FI-02044 VTT, Finland Phone internat. +358 20 722 4520 Fax +358 20 722 4374

Julkaisun sarja, numero ja raporttikoodi

VTT Publications 728
VTT-PUBS-728

Tekijä(t)
Stefan Holmström

Nimeke

Virumismallinnuksen uudet menetelmät

Tiivistelmä

Rakenteiden suunnitteluun ja elinikäennusteisiin käytetyt kuumalujien terästen lujuusarvot ja hitsien lujuuskertoimet pohjautuvat virumiskoetuloksiin, joita on varsinkin pitkäaikaisina käytettävissä usein vain niukasti. Sen vuoksi on erityisen tärkeää, että koetuloksiin sovitetut materiaalimallit ovat taloudellisia, tarkkoja ja luotettavia erityisesti ekstrapoloitaessa pidemmille käyttöajoille.

Tässä väitöstyössä on kehitetty uusia malleja työkaluiksi virumismurtolujuuden, hitsien lujuuskertoimien ja virumisvenymän luotettavaan määrittämiseen sekä virumiseliniän ennustamiseen erityisesti tapauksissa, joissa mallinnuksen tueksi on käytettävissä niukasti virumiskoetuloksia. Uusien mallien suorituskykyä on testattu eurooppalaisessa vertailututkimuksessa, jossa ne ennustivat yksin-kertaisesta muodostaan huolimatta venymiä tarkemmin kuin aiemmat ja huomattavasti monimutkaisemmat virumismallit. Uusia malleja on työssä sovellettu OFP-kuparille ja ferriittisille teräksille 10CrMo9-10 (P22), 7CrWVMoNb9-6 (P23), 7CrMoVTiB10-10 (P24), 14MoV6-3 (0.5CMV), X20CrMoV11-1 (X20), X10CrMoVNb9-1 (P91) ja X11CrMoWVNb9-1-1 (E911). Materiaalimalleja on myös sovitettu numeerisen suunnittelun työkaluihin (COMSOL ja ABAQUS) ja verifioitu pitkään käytössä olleen hitsatun putkiyhteen elinikätarkastelulla.

Väitöstyön tuloksena kehitettyjä malleja ja menetelmiä voivat soveltaa korkean lämpötilan rakenteiden suunnittelijat ja eliniän hallinnan asiantuntijat helpottamaan ja tarkentamaan virumiskäyttäytymisen ennustamista. Työn keskeinen anti on kehitettyjen menetelmien tarjoama vähentynyt materiaalidatan tarve ja mallien yksinkertainen rakenne, joka helpottaa niiden hyödyntämistä sekä analyyttisissä että numeerisissa ratkaisuissa.

ISBN
978-951-38-7378-3(nid.)
978-951-38-7379-0 (URL: http://www.vtt.fi/publications/index.jsp)

Avainnimeke ja ISSN	Projektinumero
VTT Publications 1235-0621 (nid.) 1455-0849 (URL: http://www.vtt.fi/publications/index.jsp)	36468

Julkaisuaika	Kieli	Sivuja
Tammikuu 2010	Englanti, suom. tiiv.	94 s. + liitt. 53 s.

Projektin nimi	Toimeksiantaja(t)
SA-KWAK jatko	

Avainsanat	Julkaisija
Creep, strain, damage, modeling, steel, OFP copper	VTT PL 1000, 02044 VTT Puh. 020 722 4520 Faksi 020 722 4374

Creep models are needed for design and life management of structural components operating at high temperatures. The determination of creep properties require long-term testing often limiting the amount of data. It is of considerable interest to be able to reliably predict and extrapolate long term creep behavior from relatively small sets of creep data. In this thesis tools have been developed to improve the reliability of creep rupture, creep strain and weld strength predictions. Much of the resulting improvements and benefits are related to the reduced requirements for supporting creep data. The simplicity and robustness of the new tools also make them easy to implement in analytical and numerical solutions. Creep models for selected high temperature steels and OFP copper are presented.

ISBN 978-951-38-7378-3 (soft back ed.)
ISSN 1235-0621 (soft back ed.)

ISBN 978-951-38-7379-0 (URL: http://www.vtt.fi/publications/index.jsp)
ISSN 1455-0849 (URL: http://www.vtt.fi/publications/index.jsp)